Measurement and Modeling of Temporal Variations of the Indoor Radio Channel

A Thesis Submitted to the College of

Graduate Studies and Research

in Partial Fulfillment of the Requirements

for the Degree of

Master of Science

in the

Department of Electrical Engineering

University of Saskatchewan

Saskatoon, Saskatchewan

by

Lijuan Bai

February, 1995

UNIVERSITY OF SASKATCHEWAN

Electrical Engineering Abstract 95A425

Measurement and Modeling of Temporal Variations of the Indoor Radio Channel

Student : Lijuan Bai

Supervisor: Dr. B. L. F. Daku

Master of Science Thesis

Presented to the College of Graduate Studies and Research

University of Saskatchewan

February, 1995

ABSTRACT

The results of Doppler spread and envelope fading based on CW measurements in the indoor radio channel are presented in this work. In this work, the temporal variations in the channel are caused by a moving receiver, or moving people in the vicinity of the transmitter and receiver. The result of the channel temporal variations is signal fading. The rate of fading can be measured by the Doppler spread.

CW measurements were taken at different carrier frequencies from 14 to 14.5 GHz with an increment of 50 MHz. Different locations, antenna separation distances and positions (LOS or NLOS) were selected to collect the data. Each measurement consists of 2.5 seconds of temporal variations of the channel.

The autoregressive spectral estimation method is used as a tool to estimate the Doppler spread using CW measurements in the indoor radio channel. Results demonstrated that this method provided good estimates of the Doppler spread with a reasonable resolution and smoother spectrum than traditional spectrum estimation methods. The values of the Doppler spread under different measurement conditions are compared.

Statistical analysis of envelope fading distributions based on the K-S and Chi-Square goodness tests and level crossing rates are presented. Those results can be used in future designs of wireless communication systems.

PERMISSION TO USE

In presenting this thesis in partial fulfillment of the requirements for a Postgraduate degree from the University of Saskatchewan, I agree that the Libraries of this University may make it freely available for inspection. I further agree that permission for copying of this thesis in any manner, in whole or in part, for scholarly purposes may be granted by the professor or professors who supervised my thesis work or, in their absence, by the Head of the Department or the Dean of the College in which my thesis work was done. It is understood that any copying or publication or use of this thesis or parts thereof for financial gain shall not be allowed without my written permission. It is also understood that due recognition shall be given to me and to the University of Saskatchewan in any scholarly use which may be made of any material in my thesis.

Requests for permission to copy or to make other use of material in this thesis in whole or part should be addressed to:

Head of the Department of Electrical Engineering
University of Saskatchewan
Saskatoon, Saskatchewan, Canada
S7N 0W0

ACKNOWLEDGEMENTS

I am sincerely grateful to Dr. Brian L. F. Daku for his invaluable and timely advice. His constant support and encouragement during the course of my study and this work have made my experience here significant and meaningful.

I would like to thank Mr. Garth Wells of Telecommunication Research Laboratories (TRLabs) for his guidance and help on the use, care and setup of the measurement equipment. I thank TRLabs for the financial support provided in the form of a Scholarship from 1993 to 1994.

I wish to thank my husband for his heartful support and help during measurement taking periods while he is pursuing his Ph.D degree.

Table of Contents

List of Figures

List of Tables

Abbreviations

AIC Akaike information criterion

AR autoregressive

BPSK binary phase shift keying

CAT criterion autoregressive transfer function

cdf cumulative distribution function

CW continuous wave

dBi the gain of antennas in dB to an isotropic radiator

dBm relative power in dB to 1 mW

EIR external interrupt request

FFT fast Fourier transform

FIR finite impulse response

FPE final prediction error

GPIO general-purpose input/output interface

iid identically and independently distributed

K-S Kolmogorov-Smirnov

LAN local area network

LNA low noise amplifier

LOS line of sight

MDL minimum description length

NLOS non line of sight

pdf probability density function

PN pseudo-noise

PSD power spectrum density

SSPA solid state power amplifier

1. Introduction

Wireless communications is one of the fastest growing areas in the communications industry with an annual growth rate of 40% [1]. Some types of wireless communication systems presently used, include cellular telephone, cordless telephone, paging and data transmission. The integration of these systems will eventually lead to a single portable radio telephone or terminal for both speech and data communications. At the present time an integrated system is not feasible mainly because of the severe problems with indoor wireless communications. This is because indoor communications experiences severe fading due to the multiple propagation paths that exist in such a confined structure. It is important that wireless radio communications is not only convenient but also effective for providing the integrated services in the indoor environment because of its inherent advantages. Some advantages of using such systems are [2]:

- Elimination of wiring in buildings.
- Potential in providing services for a large number of users.
- Flexibility of shifting terminals and equipment around.
- More immunity to natural and man made disasters.
- Relatively easy maintenance.

Cordless phone systems, which are very popular, are good examples of the problems that can be encountered in the indoor environment. These problems include fading and interference from other users. This simple example indicates that systems must be designed to overcome these problems and meet new challenges in the future.

An important factor in designing future indoor wireless communications systems is the comprehensive knowledge about propagation characteristics in the indoor environment. Propagation studies are essential for such systems. This means that channel models and statistical parameters can be used to design these systems.

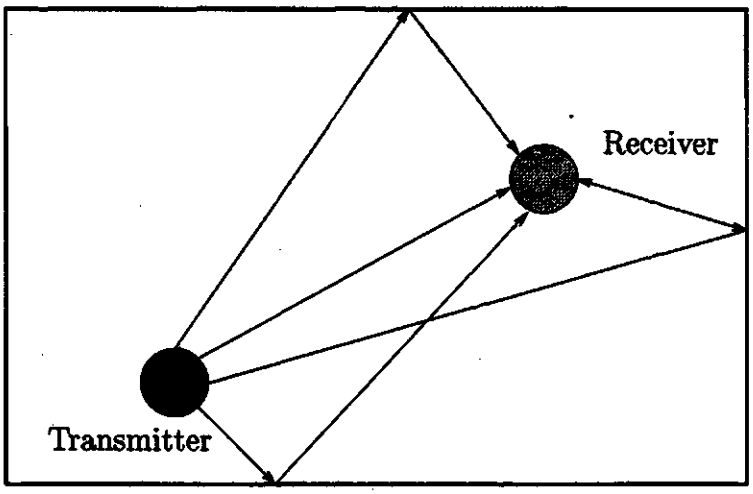

Figure 1.1 Multipath propagation

1.1 Definition of the Problem

The indoor radio channel exhibits wave interference fading associated with time-varying multipath propagation. The multipath signals are caused by reflection, refraction, and scattering of the RF signals in the building. The signal components arriving from different paths as illustrated in Figure 1.1 combine at the receiver and produce a distorted version of the transmitted signal. This distortion is referred to as multipath fading and an artificial example can be seen in Figure 1.2 for a stationary system. In general, the signals for each path have different time delays and phase shifts. Adding these signals together results in signal fading which causes the system performance, in terms of bit error rate, to degrade and in some instances totally fail. Figure 1.2 shows the frequency selective fading phenomenon which is indicated by the deep nulls. (The frequency response, shown in Figure 1.2, for the indoor channel

in a 500 MHz band is generated using a two-path model.)

There is another component of fading due to movements in systems. The predominant cause of this type of fading is variations in the phase of multipath signals. Small movements may cause small changes in the individual path lengths, but large phase changes for the radio frequency signal. This may result in large variations in their sum. This type of fading is associated with the Doppler effect. Fading caused by moving objects is shown in Figure 1.3 which is generated by a two-path model for an indoor channel with the carrier frequency of 14 GHz in a 100 ms time interval.

A Doppler shift in frequency occurs when the length of a path is changing with time. The change in the length of a path may be caused by motion of the transmitter and/or receiver or moving objects around them. The frequency shift is related to the spatial angle between the direction of arrival of that path and the direction of the motion. The paths arriving from ahead of the moving object contribute a positive Doppler frequency shift while those arriving from behind the moving object have a negative shift [3]. The Doppler effect is usually measured by the Doppler spread. For an unmodulated sine wave transmitted at some frequency f, the observed power spectrum at the receiver is a sum of the spectral components contributed by all the paths. This spectrum is called the Doppler spectrum of the channel, and its nominal width is referred to as Doppler spread which is the maximum differential Doppler frequency shift. Figure 1.4 is an example of the Doppler power spectrum of the received signal when a continuous sinusoid is transmitted.

In an outdoor cellular mobile telephone system, Doppler effects exist when vehicles are moving. The motion of the mobile station through the environment can result in a rapid fading process. Since the receiver does not know the velocity of vehicles, the Doppler frequency shift is unknown and it must be determined by means of a frequency tracking method [4]. The indoor radio channel is a slow time-varying channel, so the Doppler effect has been of considerably less concern in system design.

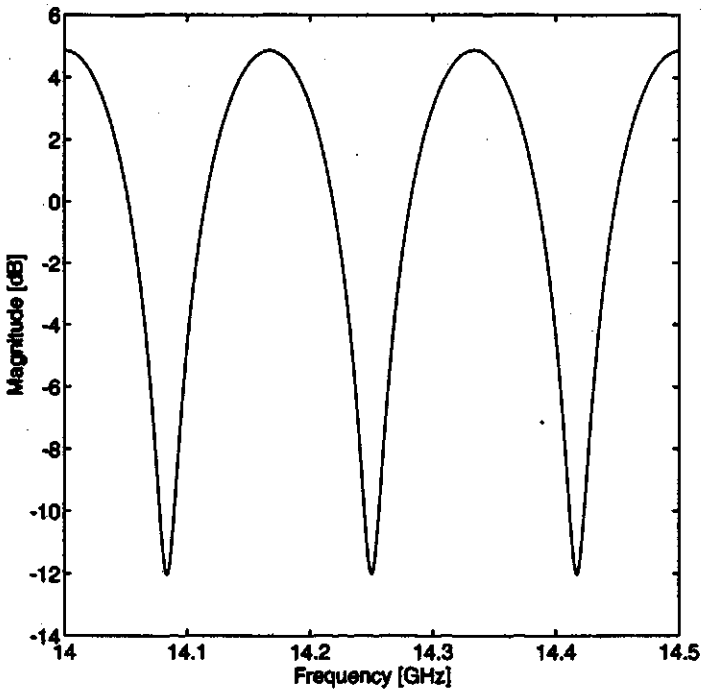

Figure 1.2 Multipath fading as a result of a sum of two paths in the channel

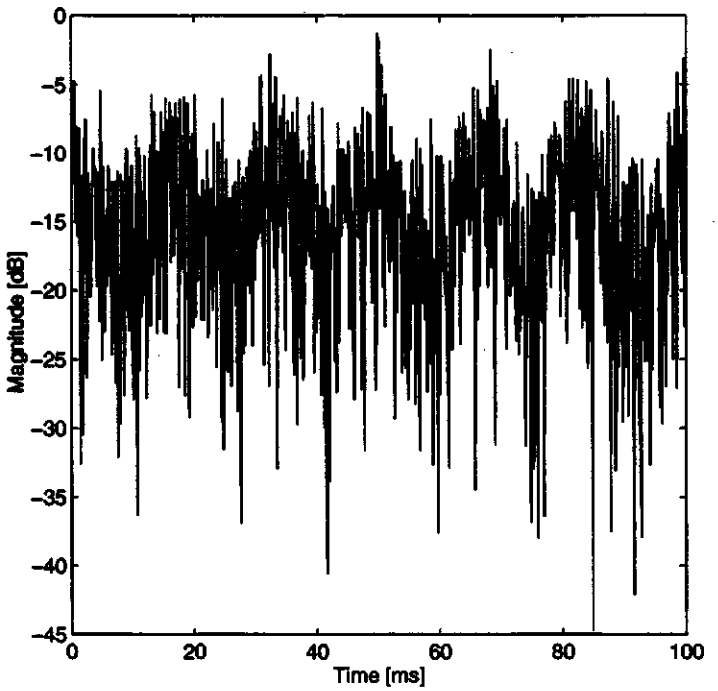

Figure 1.3 Envelope fading generated by a two-path model with moving objects in the channel

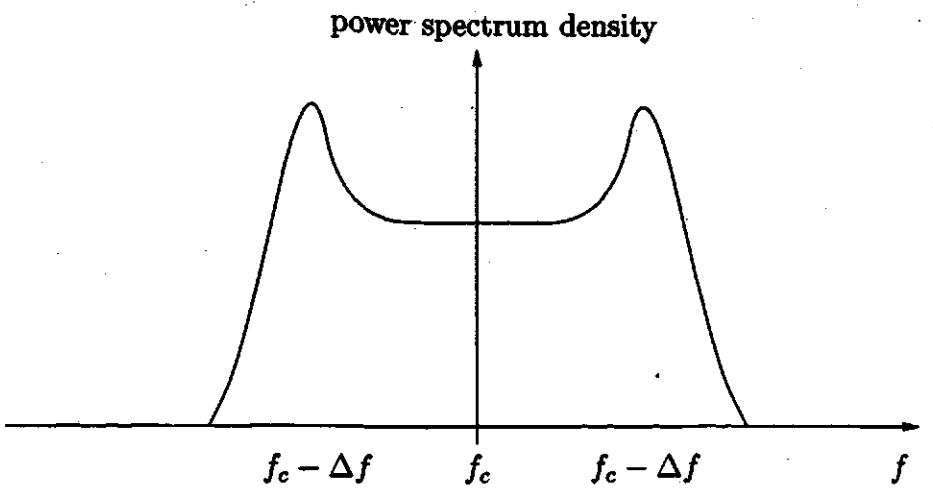

Figure 1.4 Illustration of Doppler spectrum

This is because Doppler frequency shifts in VHF and UHF frequency bands, which were caused by the moving people and equipment, can be ignored in the indoor environment. However, when the transmitted frequency is high (in SHF frequency band) even though the receiver is in slow motion, Doppler frequency shifts are the same level as the mobile phone channel in UHF band with the normal vehicle moving speed. In this case, it might be needed to compensate for overall mean Doppler frequency shift.

Statistics of the received envelope are also important from the point of view of system characterization. It is well known that an indoor channel is modeled as a Rayleigh fading or a Rician fading channel [4]. However, some other distributions were found to be better fits to empirical data in various environments [2]. In order to fully characterize the indoor channel, justifications are necessary.

1.2 Objectives

As discussed in the last section, study of Doppler frequency shifts is based on the channel transfer function. In order to carry out an analytical study on the perfor-

mance of a communication systems operating in any channel, a good mathematical description of the channel is needed. Generally a mathematical characterization of the channel is not feasible. Thus, real measurements are taken to provide accurate data which can be used to determine how the channel parameters affect the signal transmitted over it. Data obtained from the measurements can later be used to generate an analytical model for the channel.

Measurement data can be taken through either wide-band measurements or narrow-band measurements in the time domain or in the frequency domain. The way in which propagation studies should be directed depends on a particular system's specifications as well as its inherent properties. In general, the data transmission rate of a system is an important factor which is used to determine whether the statistics of the received signal envelope (narrow-band) is of concern or wide-band characteristics are of concern. But the dominant factor is the type of environment, such as the system operation range, the relative position of the transmitter and receiver, etc., in which a system is being set up. For example an integrated communication system, whose carrier frequency is high and bandwidth is narrow, may require compensations for Doppler effects. A review of the literature shows a shortage of articles characterizing Doppler effects in indoor communication channels. In order to study Doppler properties and envelope fading statistics in indoor communication systems, it is useful to:

- Determine a suitable measurement method to take the empirical data measurements.
- Obtain statistical information about the Doppler spread at different frequencies, surroundings and antenna configurations.
- Compare statistics of the Doppler spread obtained from the empirical data to theoretical calculations.

- Determine the envelope fading distribution, with possible candidates being Rayleigh, Rician, Lognormal and Weibull distributions.
- Establish a statistical model for the channel which closely fits the data.

1.3 Overview of Thesis

In the following chapter, a review of the literature regarding modeling of the indoor radio channel and some useful definitions of channel parameters are presented. In Chapter 3, the description of measurement equipment will be addressed along with the measurement plan. In Chapter 4, the mathematical theory of the Doppler spread and the methods of analyzing Doppler spectrum are given. The distribution fitting procedure performed on measured time profiles is also introduced. In Chapter 5, the analysis of the measurement results and a discussion of the Doppler spread statistics is included. Finally, conclusions are presented in Chapter 6, and some future research areas are suggested.

2. Background

Performance of a communication system relies heavily on the channel model adopted in its design. When an accurate channel model is available, a system can be designed for optimum performance.

Although modeling indoor radio propagation channels dates back to 1959, almost all measurements and modeling efforts have been reported in the last 10 years. A review of the literature shows a number of unresolved issues, and modeling efforts fall short of a full characterization of the indoor channel.

The full characterization of the channel implies determining the time-variant impulse response of the channel since in general the indoor channel is time varying. Another challenge in this area is to develop a statistical model based on empirical data with a minimum number of parameters. This model can then be used to regenerate the channel behavior accurately for computer simulations of the system.

This chapter consists of four sections. The first section describes the indoor radio channel model adopted in the study as well as some other mathematical models. In the second section, some of the multipath channel parameters are defined. A review of the statistical models of the indoor channel is presented in the third section. Finally, a summary of statistical models is given.

2.1 Channel Characterization

In this section, several mathematical models commonly used to represent the indoor channel will be introduced. It includes the impulse response model, discrete-time impulse response model, and narrow-band model. Among them the impulse

response model is the most often used model.

2.1.1 Impulse Response Model

Since the indoor radio channel is time varying, it can be viewed as a time variant linear system. Thus, the channel can be described by a linear time-variant system with the impulse response $h(\tau;t)$. The impulse response of the system is the response at time t to an impulse occurring at τ seconds in the past (or equivalently at $t-\tau$ seconds). The response $y(t)$ of this system to an input $x(t)$ is determined by an integral

$$y(t) = \int_{-\infty}^{\infty} h(\tau;t)x(t-\tau)d\tau. \tag{2.1}$$

When the system is time-invariant, $h(\tau;t) = h(\tau)$ and Equation 2.1 is the convolution integral of $h(t)$ and the input $x(t)$. Although some other forms [5] can be used to represent the impulse response of a linear time-variant system, this form is commonly used.

Both continuous and discrete multipath component representations can be used for channel modeling. In the continuous representation, the received signal is viewed as consisting of a continuum of multipath components. This received signal can be expressed in the integral form as in Equation 2.1 [4]. For the non-continuous multipath representation, a transmitted signal $s(t)$ is represented by

$$s(t) = Re[u(t)e^{j2\pi f_c t}], \tag{2.2}$$

where $u(t)$ is the low pass equivalent of the transmitted signal. Then the received signal is the sum of each component in the multipath channel. Associated with each path is an attenuation factor and a propagation delay. Both factors are time-variant. Thus the received signal is

$$y(t) = \sum_{n=1}^{N} \alpha_n(t)s[t-\tau_n(t)], \tag{2.3}$$

where $\{\alpha_n(t)\}$ and $\{\tau_n(t)\}$ are the random time-variant attenuation factor and the propagation delay for the n^{th} path, and N is the number of paths which in general is a random variable. Substituting for $s(t)$ in above Equation 2.3 results in

$$y(t) = Re(\{\sum_{n=1}^{N} \alpha_n(t) e^{-j2\pi f_c \tau_n(t)} u[t - \tau_n(t)]\} e^{j2\pi f_c t}), \tag{2.4}$$

where f_c is the carrier frequency. It is obvious from Equation 2.4 that the equivalent low pass received signal is given by

$$r(t) = \sum_{n=1}^{N} \alpha_n(t) u[\tau - \tau_n(t)] e^{-j2\pi f_c \tau_n(t)}. \tag{2.5}$$

Since $r(t)$ is the response of an equivalent low pass channel to the equivalent low pass signal $u(t)$, the equivalent low pass channel is represented by the time-variant impulse response

$$h(\tau; t) = \sum_{n=1}^{N} \alpha_n(t) \delta[\tau - \tau_n(t)] e^{-j\theta_n(t)}, \tag{2.6}$$

where $\theta_n(t) = 2\pi f_c \tau_n(t)$. An example of an impulse response of a discrete multipath channel is shown in Figure 2.1 when an impulse is transmitted at time t_0, $t_0 + \Delta t_1$, and $t_0 + \Delta t_2$.

When the impulse response $h(\tau; t)$ is modeled as a zero mean complex-valued Gaussian process, the envelope $|h(\tau; t)|$ at any instant t is Rayleigh-distributed. This multipath channel is known as a Rayleigh fading channel. On the other hand, if there exits a dominant component in the response, the channel will be a Rician fading channel. A number of other models have been used to represent the channel impulse response. Two of these models, which are discussed in the following sections, are the discrete-time impulse response model and the narrow-band model.

2.1.2 Discrete-time Impulse Response Model

If the multiple paths of the impulse response are resolvable in the time domain, then the channel can be represented by using the discrete-time impulse response. In this model the time axis is divided into small time intervals called "bins". The bin

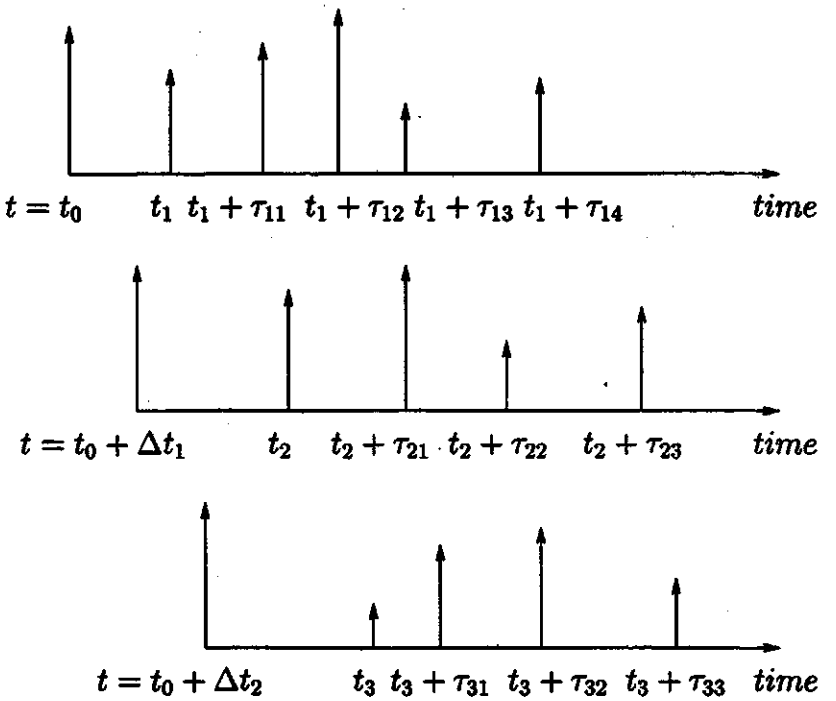

Figure 2.1 Typical time-variant impulse response of a multipath channel

size is the measurement resolution of the impulse response. Assuming that each bin can only contain one multipath component, the impulse response can be described by a sequence of "1"s and "0"s. This sequence is called the path indicator sequence. Each "1" represents a path in a given bin, and a magnitude and a phase value are associated with it. Each "0" indicates no path in that bin. Some modeling and simulation results using this model were given by [6, 7, 8]. The comparison of this method with a continuous-time model shows that it simplifies simulation and analysis of the system.

2.1.3 Narrow-band Model

When a signal at a certain frequency is transmitted, the multipath effects will cause a rapidly fluctuating CW (continuous wave) envelope at the receiver due to the motion of the receiver and movements in the environment. The CW envelope and

phase, denoted by R and Θ for a single point in space is thus given by

$$Re^{j\Theta} = \sum_{n=0}^{\infty} \alpha_n e^{j\theta_n}. \tag{2.7}$$

The narrow-band CW fading results can be generated using the wide-band impulse response model if the channel's impulse response is sampled frequently enough. A different approach could be used to produce the narrow-band CW waveforms which could be obtained directly from the wide-band frequency measurements. The CW fading statistics and temporal variations in the received signal envelope, which were caused by the movement of personnel and machinery in any fixed receive location were also reported in [9, 10].

Among these three mathematical models of the channel, the impulse response representation is used widely because of its well accepted theoretical explanations and practical justifications. The rest of the models are useful in some special circumstances. For example, if only the magnitude and phase of a single point in space are concerned, the narrow-band model will be very useful.

2.2 Definitions of Channel Parameters and Functions

Several parameters which are commonly used to represent the channel are defined prior to a discussion of the statistical characterization of the indoor channel [4].

1. Multipath intensity profile (delay power spectrum) – $\phi(\tau)$:

It is assumed that $h(\tau; t)$ is the lowpass equivalent impulse response of the band-pass channel which is wide-sense stationary, and thus the autocorrelation function of $h(\tau; t)$ is

$$\phi(\tau_1, \tau_2; \Delta t) = \frac{1}{2} E[h^*(\tau_1; t) h(\tau_2; t + \Delta t)]. \tag{2.8}$$

Equation 2.8 can be simplified, assuming the uncorrelated scattering at the delays τ_1

and τ_2 [4],

$$\frac{1}{2}E[h^*(\tau_1;t)h(\tau_2;t+\Delta t)] = \phi(\tau_1;\Delta t)\delta(\tau_1-\tau_2). \tag{2.9}$$

If $\Delta t = 0$ and $\tau_1 = \tau_2 = \tau$, the resulting autocorrelation function is simply $\phi(\tau)$, which is called the multipath intensity profile or the delay power spectrum. In practice, the multipath intensity profile can be measured by transmitting very narrow pulses (or equivalently a wide-band signal) and cross-correlating the received signal with a delayed version of itself. Typically, the measured function $\phi(\tau)$ is depicted as in Fig 2.2. The range of values of the time delay τ over which the multipath intensity profile, $\phi(\tau)$ is nonzero is called the multipath spread of the channel T_m. The reciprocal of the multipath spread is a measure of the coherence bandwidth of the channel [4]. If the coherence bandwidth is smaller than the bandwidth of the transmitted signal, the channel is said to be frequency-selective, otherwise the channel is frequency-nonselective.

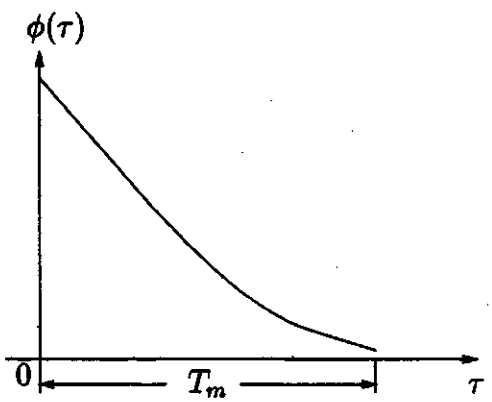

Figure 2.2 Multipath intensity profile

2. Doppler spread – B_d:

Taking the Fourier transform of Equation 2.8 with respect to τ_1 and τ_2 leads to the spaced-frequency and spaced-time correlation function of the channel,

$$\phi(\Delta f;\Delta t) = \int_{-\infty}^{\infty}\int_{-\infty}^{\infty}\phi(\tau_1;\Delta t)\delta(\tau_1-\tau_2)^{j2\pi(f_1\tau_1-f_2\tau_2)}d\tau_1 d\tau_2, \tag{2.10}$$

where $\Delta f = f_2 - f_1$. This function can be measured by transmitting a pair of sinusoids separated by Δf and cross-correlating the two separately received signals with a relative delay Δt.

From Equation 2.10 with Δf set to zero, the Fourier transform of the spaced-frequency and spaced-time correlation function, $\phi(\Delta t)$, results in the delay-Doppler spread function (the Doppler power spectrum),

$$S(\lambda) = \int_{-\infty}^{\infty} \phi(\Delta t) e^{-j2\pi\lambda\Delta t} d\Delta t, \tag{2.11}$$

where λ is called the Doppler frequency. This function represents the channel output as a sum of Doppler shifted elements. The range of values of λ, over which $S(\lambda)$ is essentially nonzero, is called the Doppler spread B_d. Figure 2.3 illustrates the relationship between $S(\lambda)$ and B_d.

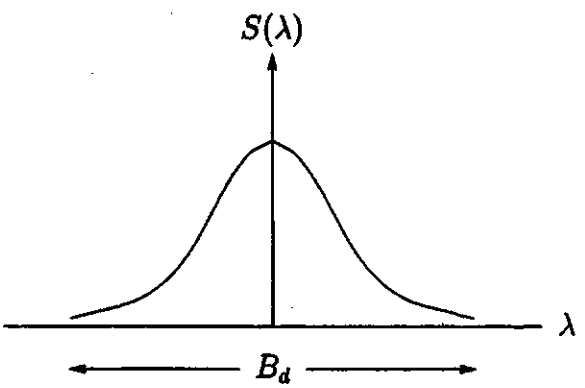

Figure 2.3 Doppler power spectrum

3. Coherence time – T_d:

Since $\phi(\Delta t)$ and $S(\lambda)$ are Fourier transform pairs, the reciprocal of B_d is referred to as the coherence time of the channel, which is denoted by T_d. Obviously, a slowly varying channel has a large coherence time or, equivalently, a small Doppler spread. This type of channel is referred to as slow fading channel. This corresponds to a Doppler spread that is much smaller than the baseband bandwidth of the channel

[11]. Fast fading implies that the channel is changing rapidly compared to one symbol interval.

4. Transfer function – $H(f;t)$ and time profile $H(f_c;t)$:

By taking the Fourier transform of $h(\tau;t)$ with respect to τ, the time-variant transfer function $H(f;t)$ is obtained, where f is the frequency variable. Thus the transfer function of the channel is

$$H(f;t) = \int_{-\infty}^{\infty} h(\tau;t)e^{-j2\pi f\tau}d\tau. \tag{2.12}$$

$H(f;t)$ has the same statistics as the time-variant impulse response $h(\tau;t)$. $H(f;t)$ at frequency f_c, $H(f_c;t)$, is referred to as the time profile of the channel, which can be measured by sending a sine wave over the channel and by comparing the received wave at time t with it to get the magnitude and phase. Note that the spaced-time and the spaced-frequency correlation function of the channel (Equation 2.10) can be determined from the transfer function of the channel. That is,

$$\phi(\Delta f;\Delta t) = \frac{1}{2}E[H^*(f;t)H(f+\Delta f;t+\Delta t)]. \tag{2.13}$$

5. Scattering function – $S(\tau;\lambda)$:

The scattering function can be determined by taking the double Fourier transform of the spaced-time and spaced-frequency function, namely,

$$S(\tau;\lambda) = \int_{-\infty}^{\infty}\int_{-\infty}^{\infty} \phi(\Delta f;\Delta t)e^{-j2\pi\lambda\Delta t}e^{-j2\pi\tau\Delta f}d\Delta t d\Delta f. \tag{2.14}$$

The scattering function gives a measure of the average power output of the channel as a function of the time delay τ and the Doppler frequency λ.

There are several other Fourier transform pairs. For example, $\phi(\Delta f;\Delta t)$ and $\phi(\tau;\Delta t)$ are Fourier transform pairs, given by

$$\phi(\tau;\Delta t) = \int_{-\infty}^{\infty} \phi(\Delta f;\Delta t)e^{j2\pi\tau\Delta f}d\Delta f. \tag{2.15}$$

The previous two equations show that the scattering function $S(\tau;\lambda)$ and $\phi(\tau;\Delta t)$ are Fourier transform pairs.

$$S(\tau;\lambda) = \int_{-\infty}^{\infty} \phi(\tau;\Delta t) e^{-j2\pi\lambda\Delta t} d\Delta t. \tag{2.16}$$

If $\tau = 0$, then $S(0;\lambda)$ is the Doppler spectrum.

2.3 Statistical Model and Analysis of the Channel

Statistical models for propagation in indoor channels are based on various measurements. A number of different empirical and theoretical channel models have been proposed for describing the statistics of multipath fading in indoor and outdoor environments [8, 9, 12, 13]. In this section, three types of models (based on measurement data) for the indoor radio channel will be briefly discussed.

Indoor radio communications covers a wide variety of situations ranging from communications with individuals walking in buildings, to fixed stations sending messages to objects in motion. The signal transmitted from the base reaches the portable receivers via multiple paths. The paths may include line of sight (LOS), and/or non-line of sight (NLOS) paths. The studies have shown that channel characteristics differ in LOS and NLOS environments.

The performance of indoor radio systems are dependent on the building architecture and surroundings of the portable antenna. Based on relative locations between the base and the portable and surroundings, there are four types of variations in channel statistics [9, 10, 14].

1. Small-scale variations: The base antenna is fixed, the portable site is moved in spatially-adjacent points in the same "local area".

2. Midscale variations: The separation distance between the base and portable antennas is same, but the surroundings of antennas in the building are different,

for example, in a room or in a hallway.

3. Large-scale variations: When the base-portable distance increases, the channel characteristics may exhibit great differences. As an example, increasing the antenna separation distance normally results in an increase in path loss.

4. Temporal variations: Variations are caused by moving objects in the channel, such as moving people and/or a moving portable which is carrying by a person.

These variations in indoor channels can be characterized by using either one of the following three methods. The first type of model is based on wide-band frequency measurements of the channel, and the second type is based on the impulse response of the channel which can be obtained directly or indirectly from measurements. Finally, a channel model using ray tracing techniques will be introduced.

2.3.1 Autoregressive Model

Autoregressive (AR) modeling has been extensively used for spectral estimation of time domain data [15, 16, 17]. This method has also been applied to the frequency domain to model the indoor channel [18, 19]. The parameters of an AR model are determined from measured channel responses. A time series $u(n), u(n-1), \ldots, u(n-M)$ is an autoregressive process of order M if it satisfies the equation

$$u(n) + a_1 u(n-1) + \ldots + a_M u(n-M) = v(n), \tag{2.17}$$

where $\{v(n)\}$ is a complex white noise process and $\{a_k\}$ $(k = 1, 2, \ldots, M)$ are the AR parameters. Equation 2.17 can be rewritten as

$$u(n) = \sum_{k=1}^{M} b_k u(n-k) + v(n), \tag{2.18}$$

where $b_k = -a_k$. The variable $u(n)$, a set of independent variables $u(n-1), u(n-2), \ldots, u(n-M)$ plus an error term $v(n)$ is often referred to as an autoregressive model. The $u(n)$ is said to be regressed on $u(n-1), u(n-2), \ldots, u(M)$.

The wide-band frequency response measurements of the indoor radio propagation channel can be interpreted as the output of an autoregressive model. The frequency response at each location is modeled by an AR process of order M given by

$$H(f_n, x) + \sum_{k=1}^{M} a_k H(f_{n-k}, x) = V(f_n), \tag{2.19}$$

where $H(f_n, x)$ is the n^{th} sample of the complex frequency domain measurements at location x. Taking the z-transformation of Equation 2.19, the AR process can be viewed as the output of a linear filter, whose transfer function is given by

$$G(z) = \frac{1}{1 + \sum_{k=1}^{M} a_k z^{-k}} \tag{2.20}$$

$$= \prod_{k=1}^{M} \frac{1}{1 - p_k z^{-k}}, \tag{2.21}$$

where p_k $(k = 1, 2, \ldots, M)$ is the k^{th} pole of $G(z)$. The above expression indicates that the channel frequency responses can be characterized by the poles of the transfer function $G(z)$. There are several methods that can be used to obtain the AR parameters, $\{a_k\}$, such as the Yule-Walker method (correlation method), the cross correlation method, the modified cross correlation method, Burg's method, and a geometric lattice method. These techniques are described in detail in reference [16].

Once the AR parameters are obtained, some characteristics could be studied. First, the frequency responses of the channel can be generated by these parameters. Using those frequency responses, the channel statistics such the rms delay spread can be obtained and compared to the rms delay spread of the empirical data. An example of AR modeling, based on the frequency measurement at 900 MHz with 200 MHz bandwidth, is given in [18]. The cumulative distribution function of the rms delay spread and the 3 dB width of the frequency correlation function with measurements performed in global, local, and mixed indoor radio propagation environments were compared, and showed a close match between the empirical data and the regenerated data. The statistics of the poles showed that the second order model was sufficient

to represent the channel both in the time domain and in the frequency domain where each pole identified the arrival of a cluster of paths and the angle of the pole represented the arrival time. The randomness of the magnitude of the first pole proved to be the dominant parameter in regenerating frequency responses with close statistical fits to the empirical data. For local movements of people around the transmitter and receiver, or small movements of the transmitter and receiver, the location of the poles remained relatively unchanged indicating that the arrival of clusters was associated with the location of terminals.

2.3.2 Impulse Response Model

A number of investigators have adopted the impulse response approach to characterize the indoor radio propagation channel. The impulse response of the indoor channel $h(\tau;t)$ is specified by Equation 2.6. The purpose of characterizing the channel's impulse response is to determine the statistical properties of time-variant variables $\{\alpha_n(t)\}$, $\{\tau_n(t)\}$ and $\{\theta_n(t)\}$. However, the rate of their variations at VHF and UHF bands, with both the base and portable being static, is very slow compared to any useful signaling rates. Thus, these parameters can be treated as virtually time-invariant random variables. A number of other parameters associated with these variables, such as the distributions of the number of multipath component and the magnitude of multipath, path losses, rms delay spread, and some frequency statistics were studied by many researchers.

1. Distribution of the number of arriving path, N

The number of arriving path, N, is determined from the impulse response, by locating all the paths which exceed a certain threshold. Some results show that the distribution of N was a Beta distribution for a factory environment, and a Gaussian distribution for an office building [6, 13].

2. Distribution of multipath magnitude

The envelope of the impulse response, $|h(\tau;t)|$, is a random variable at any time instant t in a multipath environment. Envelope fading depends on the area covered by measurements, LOS or NLOS path and some other conditions. Based on the empirical data and the distribution fitting process, several envelope fading distributions were reported in [10], they include Rayleigh, Rician, Weibull, Lognormal and Nakagami distributions.

(a) The Rayleigh and Rician distributions: A widely-accepted model for describing multipath fading in absence of a strong path is the Rayleigh fading. The Rician distribution occurs when a strong path which may be a LOS path or a path that has a large gain compared to other channel paths exists. Wide-band and CW measurements in different environments (for example, in a office building or in a factory) have shown that the distributions of envelope fading are either Rayleigh or Rician. The Rayleigh distribution is a useful approximation to the small-scale fading statistics that occurs in CW measurements [10].

(b) The Lognormal distribution: This distribution is often used to represent large scale variations of the envelope in a multipath environment. But, in some cases a good Lognormal fit can be used to describe local data. The empirical justification for using this distribution in the indoor environment has been reported in [10, 20] for both local and global data.

(c) The Weibull and Nakagami distributions: The Rayleigh distribution and the exponential distribution are as two special cases of the Weibull distribution. Besides these two special cases, the Weibull distribution is used in [21]. The Nakagami distribution (also called the m-distribution) contains many other distributions as special cases, such as the Rayleigh, Rician, one-sided Gaussian and Lognormal distribution. The envelope fading was the Nakagami distribution using the ray tracing technique reported in [22].

3. The mean excess delay and rms delay spread

The mean excess delay is the first moment of the power delay profile with respect to the first arriving path. The rms delay spread τ_{rms} is related to the variance of the power delay profile. Usually, the power delay profile is normalized so that the area beneath the curve is unity. Then taking the second central moment (variance) produces a measure of the spread of the power delay spectrum. Thus, the square root of this moment is called the rms delay spread. It is a good measure of the multipath spread and an indication of the potential intersymbol interference.

The performance of communication systems in a multipath environment is related to the value of τ_{rms}. Both the rms delay spread and the mean excess delay have been estimated in many indoor propagation measurements. The values of the rms delay spread depend on the type and size of the building and presence or absence of a clear LOS path. A comparison of τ_{rms} for different environments was presented in [10].

4. Path loss

Path losses in indoor channels are usually measured by the relationship between the received power P_r and the distance d from a transmitter with fixed power, as $P_r(d) = Ad^{-\eta}$, where η is the exponent of the power-distance relationship and A is a constant determined by the transmitted power, the measurement system gains, frequency and antenna heights. The path loss information in indoor environments is essential for determination of the coverage range for radio communication systems [18].

In summary, this section covers the impulse response model of the indoor channel. Channel parameter statistics given in some papers were presented. As it can be seen, the impulse response model is very useful to characterize the indoor channel.

In addition to the parameters mentioned above, some other channel parameters

also were discussed such as temporal variations of the indoor channel and frequency statistics. As described before, the channel is time-variant due to the motion of people and equipment or the receiver. Temporal variations make it difficult to analyze the channel, thus most channel propagation measurements had assumed some form of stationarity while taking the measurement data. The data was later supplemented by CW temporal fading measurements.

CW temporal fading measurements were taken under some circumstances in which the channel was wide-sense stationary for short intervals of time. The assumption of a stationary channel in a time span of a few seconds may be reasonable for office buildings where a large degree of movement is not expected [10]. The dynamic range of fading and the fading distributions have been studied by several investigators [6, 14, 23]. An important measure of the channel's temporal variations is the width of its spectrum, i.e. the Doppler frequency spread when a single sinusoid (constant envelope) is transmitted. A Doppler spread of about 4 Hz and a maximum value of 6.1 Hz at transmit frequency of 900 MHz has been reported in [9, 24].

2.3.3 Ray Tracing Model

The AR model and the impulse response model of the indoor radio channel are derived from a large measurement database. These two approaches may not be appropriate in some situations where it is difficult to take measurements. Specifically in a mobile channel where acquiring a large measurement database is unfeasible, the ray tracing technique is an alternative method.

The ray tracing technique is a new method of channel modeling and is based on the building characteristics. The ray tracing model is designed using the properties of reflection, refraction and scattering for a wave incident on an obstacle. Ray tracing is a stationary phase technique which relies on the quasi-optical properties of radio waves in regions where obstacles are large compared to a wavelength. For simplicity,

it is assumed that obstacles are smooth walls. When a ray is reflected, the angle of reflection equals the angle of incidence as expected. At present, all reflections are assumed to be specular and the appropriate reflection coefficient is determined from a knowledge of the bulk electrical properties of the wall on which the reflection takes place. This assumption is consistent with any surface perturbations in the building being greatly less than one wavelength.

The received signal level at a particular location is the sum of the signal components of the rays that can be traced between the transmitter and receiver. The model has been found to give a fair representation of the real environment [22]. The model is quite simple since only reflections are concerned. A more complex model was developed in [25]. In this model each edge in the building is capable of supporting a diffraction, and the power associated with each of these rays is modified by an appropriate diffraction coefficient. Scattering effects have not been considered in any of those models because of the significant computational requirements.

2.4 Summary

In this chapter, papers presented by many researchers were reviewed and channel modeling methods in indoor radio propagations were discussed briefly. Based on some assumptions, the indoor channel model was derived from the statistical analysis of the measurement data. The impulse response model and the autoregressive model are this type of model.

The impulse response model describes the channel directly. From this model, the indoor channel can be characterized as a Rayleigh, a Rician fading channel etc. The rms delay spread can predict whether intersymbol interference will be problem. The intersymbol interference limits the usable digital signaling rate for a given error rate. Typically, the rms delay spread is less than 100 ns in the indoor environment. The impulse response approach can be used to fully characterize the channel propagation

based on a number of its statistical parameters. As mentioned in [10], any realistic channel model should take as many factors as possible into accounts. The model should derive its parameters from actual field measurements rather than base them on simplified theory. Even though the impulse response model is able to characterize all kinds of variations of the channel, it is difficult to obtain $h(\tau; t)$.

A new method used to estimate the impulse response of indoor radio channels in [26] is the signal subspace techniques. This technique is based on the use of information criteria, a high resolution spectral analysis technique, and principal component analysis. The results showed that the new technique could overcome difficulties existing in conventional methods and produce more accurate estimates of the channel parameters.

Compared with the impulse response model, the AR model is relatively simple. The AR model is based on wide-band frequency measurements. The poles of the AR model are used to model the indoor channel propagation. There are fewer parameters in this model than in the impulse response model. The impulse response regenerated by this statistical model shows a good fit to the measured impulse response of the channel. So the AR model is a parametric model in the frequency domain and is often referred to as the super resolution modeling technique. In reference [19], FIR (Finite Impulse Response) filter matching produced a parametric model that could be more compact and more accurate in terms of matching the frequency response of the channel than the conventional super resolution techniques. In fact, this type of model is suitable to characterize the variations of the indoor channel when the channel is stationary.

Another modeling approach discussed in this chapter, is the ray tracing model. This technique is based on the knowledge of the detailed building geometry and construction. It has been shown that it is useful tool for designing indoor communication systems. It can be used to predict the channel behavior such as path losses, the time-

invariant impulse response, and the rms delay spread. Even though this technique needs a large amount of computational work, it is still attractive with the speed of existing workstations.

3. Measurement Procedure

The indoor channel can be characterized by measuring the response of the channel. Measurements can be taken either in the frequency domain or in the time domain. Measurements can be classified as wide-band or CW (narrow-band) measurements. Wide-band and CW measurements have been carried out at frequencies as low as 35 MHz and as high as 60 GHz by many researchers [2, 10].

In this chapter, the measurement method will be discussed. Then the description of the measurement system follows. Finally, the controlling software will be addressed.

3.1 Measurement Method

There are many different ways to take measurements. Basically, two wide-band measurement techniques will be discussed here.

One method uses sliding correlators to measure the impulse response of the channel. This system, which is complex, includes two PN (pseudo-noise) code generators, a modulator and demodulator, filters, and amplifiers on both the transmitter and the receiver sides. Usually, a PN coded signal is BPSK (binary phase shift keying) modulated and transmitted at a carrier frequency. On the receiver side, the signal is demodulated by cross-correlating this signal with a replica of the transmitted signal. Thus, the output of the receiver is the impulse response of the channel. Figure 3.1 is a simplified system block diagram which illustrates this system [27].

A frequency domain technique using a swept carrier has also been used to measure the wide-band channel response. The disadvantage, for general usage, is that the measurement must be done while the receiver is stationary to avoid the possibility of

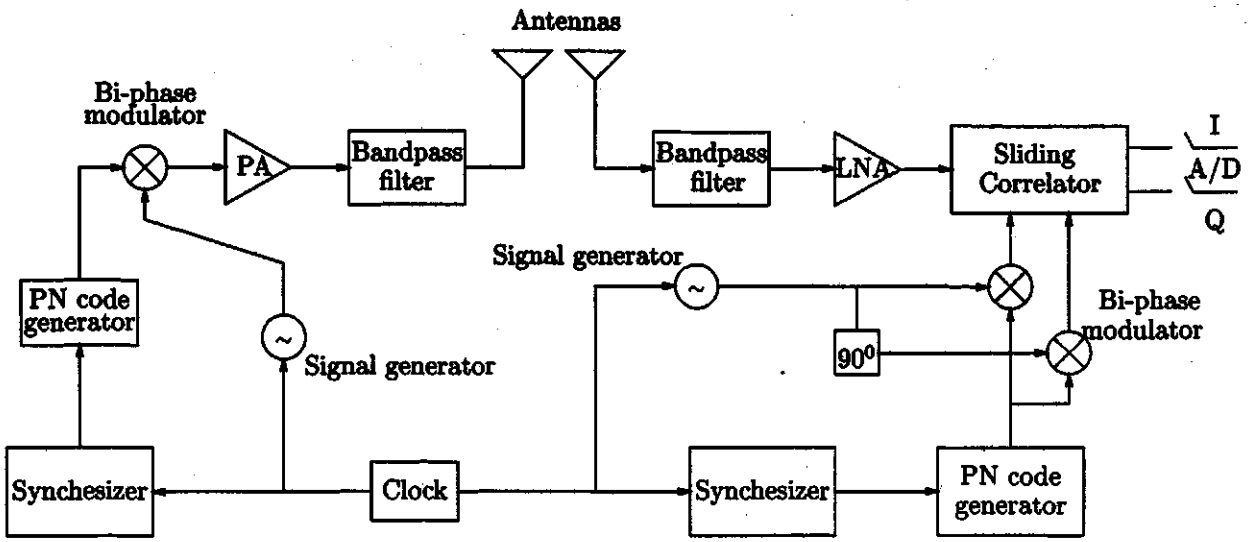

Figure 3.1 Sliding correlator system block diagram

the frequency response varying. However, the availability of network analyzers makes this technique attractive for indoor wide-band measurements. A network analyzer is widely used as a frequency measurement system. Magnitude and phase information can be directly obtained from the network analyzer. A disadvantage particular to the network analyzer technique is that both the transmitter and receiver must be connected to the analyzer by coaxial cables. This limits the mobility of this system. The main difficulty encountered in the use of the analyzer is the calibration to remove the effects of the antennas, cables, and power amplifiers which must be done in a clutter-free environment [28]. Although the sliding correlator provides the time domain impulse response directly, the frequency response of the channel can be easily converted to the impulse response in time domain through the inverse Fourier transform. The frequency domain measurements using a network analyzer have been reported by some researchers. Wide-band measurements have been presented with bandwidth ranges of 200 MHz [18], 400 MHz [19], and 500 MHz [29] respectively. Equivalent resolutions in the time domain are 5 ns (nanoseconds), 2.5 ns, and 2 ns. Actually, these resolutions are not achievable since the data is windowed before taking

the inverse Fourier transform. Windowing decreases the resolution due to the main lobe width of the window function. For example, a Hamming window which has a 6 dB main lobe width of 1.81 bins was used to window the data in [19], this decreased the resolution from 2.5 ns (nanosecond) to about 4.7 ns.

A comparison of these two radio propagation channel impulse response determination techniques (the sliding correlator and network analyzer) was reported in the literature [27]. In this paper, the impulse responses which were obtained by these two techniques are very similar.

The CW (narrow-band) measurement technique is usually used to characterize the temporal variations of the channel. A network analyzer can be used to compare the magnitude and phase between the transmitted sinusoid and the received signal. If the received signal can be sampled fast enough, then a network analyzer can be used to take the CW measurement. The measurement system using a network analyzer will be described in Section 3.3.

3.2 Measurement Plan

The measurement plan is divided into two parts. The goal of the measurement in part I is to investigate the Doppler spread at a single transmit frequency when the receiver is moving. The time variations in the indoor channel cause Doppler shifts. Therefore, when there are no time variations in the channel, there is no spectral broadening observed in the transmission of a pure frequency tone. If the receiver is in motion, the Doppler spread will not be zero because of the changes in the length of multipaths with time. It is very useful to study Doppler effects for different channel conditions.

Measurements in part I involved moving the receiver in a straight line at a low speed while the transmitter was fixed. Figure 3.2 shows this configuration. The

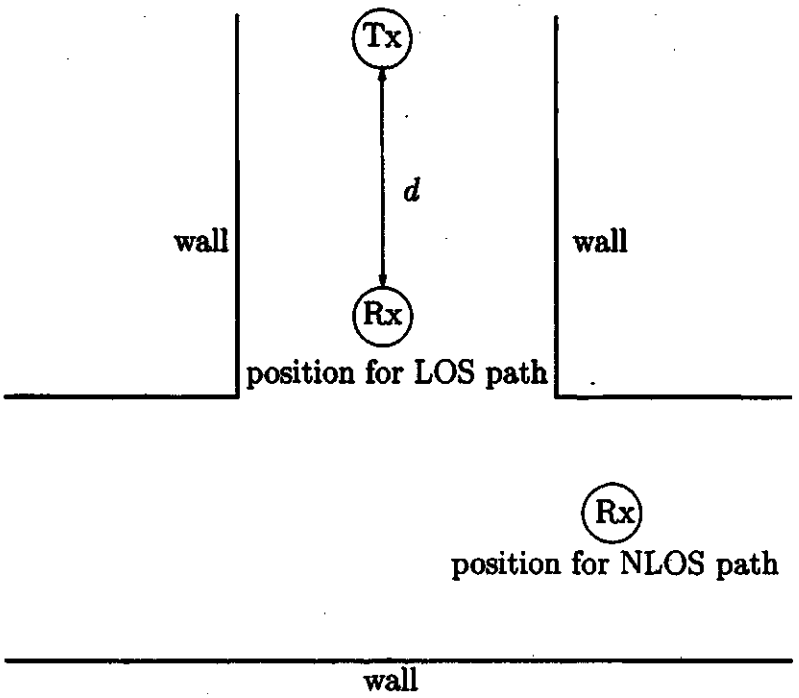

Figure 3.2 Measurement configuration

measurements were carried out while keeping a constant receiver speed.

The initial antenna separation distance, d, was 5, 7.5 or 10 meters. The CW frequency was varied from 14 GHz to 14.5 GHz with an increment of 50 MHz. At each antenna separation distance 22 individual time profiles were obtained at 11 frequencies with the receiver moving at a speed of 1.36 m/s or 1.09 m/s. There is a total of 308 time profiles. Each time profile corresponds to 2.5 seconds of temporal variations of the channel.

For each antenna separation, several locations were selected so as to cover as many different areas as possible, for example, a hallway, and an open area. The selection was made on the basis of what was considered to be typical positions in future wireless indoor communications systems. For each configuration the transmitter and receiver antennas were placed in their positions which include both line of sight (LOS) and non line of sight (NLOS) topographies which can be seen in Figure 3.2.

Measurements of the indoor radio channel were performed on the second floor of the Agricultural building and all three floors of the Engineering building at the University of Saskatchewan, Saskatoon, Canada. In order to eliminate effects of moving people around the antennas, measurements were made late at night or on weekends. There were only a few people in the building, so as to minimize the moving objects which also cause Doppler shifts in the channel.

The part II measurements were carried out to study the temporal variations caused by moving people. Motion of people results in distortions in the channel and fading phenomenon. The measurements were taken when both antennas were stationary, and only a few people were moving around.

The data was obtained at three antenna separation distances and two positions. The motion of people was limited around the receiver only. The number of persons around the receiver was zero, one, or two.

As in part I, each recording corresponds to 2.5 seconds of channel's temporal variations. People were moving throughout the whole 2.5 seconds, and followed the same moving pattern. There is a total of 18 time profiles at the transmit frequency 14 GHz.

3.3 Measurement Setup and Technique

In this section, the measurement system using a network analyzer is described in detail. It includes operations of the network analyzer, instrument connections, and the receiver transporting system.

3.3.1 Measurement System Description

The measurement system for the indoor radio channel is given in Figure 3.3. The main component of this measurement system is a Hewlett-Packard 8510B network

analyzer with a frequency synthesizer and a S-parameter test set. The signal generator provides a trigger signal to the network analyzer as part of the data acquisition system. The frequency of the signal from the signal generator controls the sampling interval in the measurement.

Two ports of the network analyzer are connected to the transmitter antenna and receiver antenna. A pre-amplifier and a power amplifier are used on the transmitter side, and a low noise amplifier is used on the receiver side.

The measurements are controlled by a controller over a HP-IB bus. It controls the network analyzer during the measurements and also serves as a temporary storage device for the measurement data. The controller also has a GPIO (HP98622) interface built in. The interface is known as the General-Purpose Input/Output Interface (GPIO). This interface is a very flexible parallel interface that allows communication with a variety of devices. It sends and receives up to 16 bits of data with a choice of several handshake methods. External interrupt and user-definable signal lines are provided for additional flexibility. A microswitch, which was placed on the track used by the receiver transporting system, is connected to the interrupt line, so the data is automatically taken by the controller when the microswitch is touched by the receiver cart, and sends a logic low signal to the controller through the GPIO interface.

Finally, the data stored in the controller is transferred to a Sun workstation via RS 232C utilizing the Kermit protocol for ASCII data transfer. This process requires about 7 minutes for each profile. Data is stored permanently on the workstation for further analysis.

The actual components used in the measurement system are:

1. Hewlett-Packard 8510B Network Analyzer.

2. Hewlett-Packard Series 9000/300 Desktop Controller.

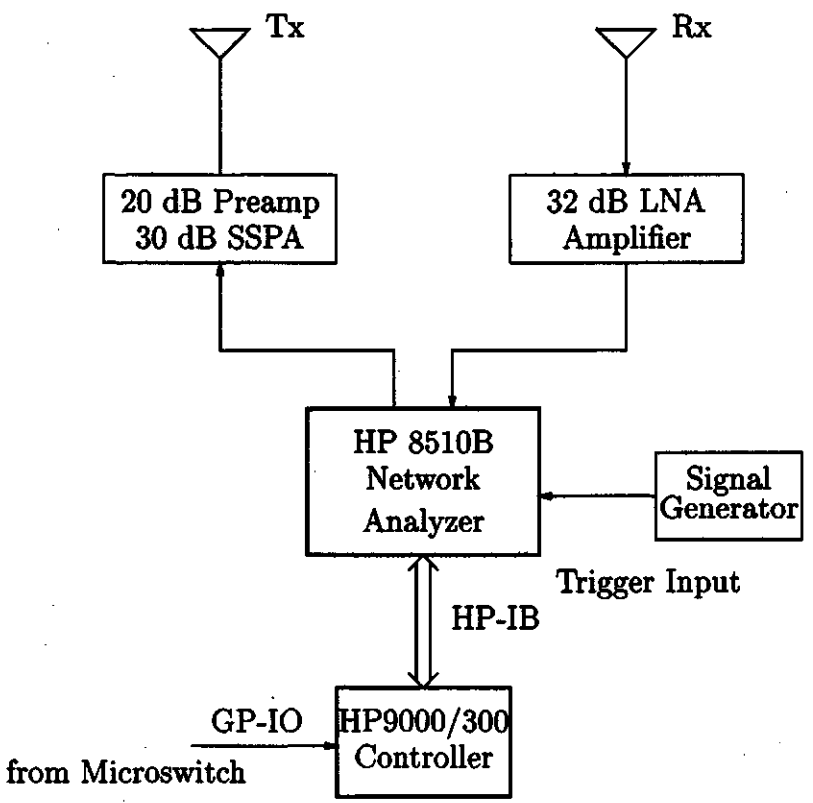

Figure 3.3 Measurement system

3. Philips PM5134 Function Generator.

4. Two WJ 4856 Wide-band Antennas.

5. A Pre-amplifier and a Ga As FET Amplifier.

6. A M/N AMF-4s-140145020 Low Noise Amplifier.

7. Marathon Electric AC Motor.

3.3.2 Network Analyzer

The CW temporal narrow-band measurements are made with the HP 8510B network analyzer set to operate in "FASTCW" data acquisition mode. In this mode the network analyzer takes a measurement at a single transmit frequency, when it receives a pulse at its rear trigger port. FASTCW mode provides synchronized data acquisition at rates of less than 1 millisecond/sample (1 ms/sample) which includes the time required to acquire the measurement data and transfer the data over the HP-IB bus to the controller. A rear panel hardware trigger input is used to precisely control when data acquisition occurs.

The network analyzer took the measurements using S-parameter S21, which is the through loss of the channel in this case. This gives the magnitude and phase of the channel response at each sample (actually, the network analyzer compares the phase difference of the received and transmitted signals). A TTL trigger signal (falling edge) is generated by the function generator. The function generator controls the sampling frequency of the measurements. The sampling frequency used in the measurements is 1000 Hz to meet the resolution requirement of the Doppler spread.

The network analyzer must be calibrated before any measurement is undertaken. The whole calibration process involves measuring the through loss of each piece of the measurement system. The frequency responses of amplifiers and cables were measured

and stored in a data file by David Donald [29]. The correction data can be used later to eliminate effects of these components.

3.3.3 Instrument Connections

The antennas used in the measurements are omni-directional Watkins - Johnson WJ 4856 wide-band antennas with vertical polarization. The frequency range of the antennas is between 4 and 26 GHz. The gain of the antennas is 0 dB or zero dBi with respect to an isotropic radiator. The maximum voltage standing wave ratio of the antennas is 3:1 [29].

The two antennas are placed at two different heights so that the measurement condition will be similar to the actual condition of antennas in use for a wireless local area network (LAN). The transmit antenna is set close to the roof level at a height of 2.45 m. The receiver antenna is placed at a height of 1.4 m.

Three amplifiers are used to improve the signal quality. On the transmitter side, there are two amplifiers. One is a 20 dB gain pre-amplifier which was designed by SED Systems of Saskatoon. The second one is a 1.0 Watt (or 30 dBm) solid state power amplifier (SSPA) with 30 dB of gain. These two amplifiers are connected via a very short piece of 0.141 inch semi-rigid coaxial copper cable.

The receiver side of this system is equipped with a low noise amplifier (LNA) with 32 dB gain and a noise figure of 1.5 dB. This gives a very good signal-to-noise ratio for the measurements. An Andew Corporation LDF4-50 heliax Cable (14 meters long) is connected from the network analyzer to the receiver antenna. This cable has an average loss of 1.2 dB/m between 14 and 14.5 GHz.

All other connections between the network analyzer and the transmitter, the transmitter and the amplifiers, and the amplifier and the receiver were made by using 0.141 inch semi-rigid cable. The semi-rigid cable has an average loss of 0.67 dB/m in the

same frequency band. The network analyzer has a dynamic range of 70 dB with input levels varying from -50 dBm to +20 dBm. Some details such as the frequency responses of the amplifiers, the cables and the antennas can be found in [29].

3.3.4 The Receiver Transporting System

The temporal measurements of the indoor radio channel were performed when the receiver was moving at a constant speed v. In this section, the receiver moving system will be briefly described.

The receiver transporting system consists of a 0.51 m $\times$ 0.51 m cart with wheels, which supported a pole. The receiver was mounted at the top of this pole. The receiver cart was placed on a 5.0 m long wooden track which was fixed to the floor. The receiver cart was pulled by a steel cable along this track using an AC motor and a belt-pulley system. Combinations of different sizes of pulleys gives the desired moving speed for the receiver. The motor is a $1/2$ *hp*, 1725 *rpm* AC motor made by Marathon Electric. The motor was manually started using a switch. It was automatically turned off using a microswitch which was placed at the end of the track when the receiver cart activated this microswitch.

3.4 Controlling Software

From the setup of the network analyzer to storing the data into a disk, the measurement process was automatically executed by a controlling program. It is made up of the interrupt service and the data acquisition program which plays a key role in the measurement.

The External Interrupt Handling Software:

The GPIO Interface can sense the External Interrupt Request line (EIR) being driven to logic low by a peripheral. When an EIR event occurs, the interrupt is

logged by the operating system. After logging the occurrence, any further interrupts from the GPIO interface are automatically disabled until specifically enabled by a program.

The state of the EIR line can be read by the program. Note that the interrupt is a level-sensitive event, not edge-triggered. If the EIR line's state is not held low long enough, the interrupt will be missed.

The interrupt is triggered by a microswitch which is placed at the beginning of the track. It sends a logic low signal to the EIR line of the controller when the moving receiver hits it. After the controller receives the interrupt signal, the measurement will be automatically taken. A BASIC program referred to as the data acquisition program is used to record the measurement.

The Data Acquisition Program in FASTCW mode:

The measurements are automatically taken when the program is started by the interrupt. There are four parts in the program which was written in HP-BASIC 5.0. HP-BASIC has many HP-IB control commands built in, and as a result the controlling program is simplified. First, the network analyzer is calibrated to get ready for the measurements. The EIR line is checked and waits to accept the interrupt signal in the second part of the program. Thirdly, the data is collected and stored in the controller. Finally, the data is transferred into a file.

The BASIC program controls the measurement system. The HP 8510B is initialized and set to the FASTCW mode, the analyzer phase-locks the receiver to the current CW frequency and waits for a HP-IB trigger from the controller. A delay has to be introduced here in order to give the operator time to get into position for the measurement. In the measurements the network analyzer waits until the AC motor goes through the accelerating period and is moving at a constant speed. Once the network analyzer is ready, it acquires a data point each time a TTL level trigger is

received from the function generator. The measured data is then placed into a first-in, first-out buffer. If an ENTER or TRANSFER statement occurs in the program, the data is transferred immediately to the controller in a binary format. If the controller removes data from the buffer as fast as it is being acquired, data acquisition can continue indefinitely with no limitations on the number of measured points. Because the data taken from the network analyzer is binary, a converting process is needed to convert the binary data into a decimal format. This complex decimal data format is then converted into magnitude in dB and phase in degrees. The magnitude and phase information from the measurement are plotted on the screen for verification of the measured results. Finally, the file has to be written to the disk, which has proved to be a fairly time-consuming task.

4. Doppler Spread and Envelope Fading

4.1 Introduction

In the fading channel modem design, sequences of symbols and side-by-side channel frequency allocations result in two concerns related to the signaling rate: with the time smear (the multipath delay spread T_m) that may cause intersymbol interference or the frequency smear (the Doppler spread B_d) that may cause increase of the bit error rate in a given signal to noise ratio and limit the minimum signaling rate. If there is essentially no loss of coherence over the symbol as received, a simple symbol waveform of duration T to be processed coherently requires $T \leq 1/B_d$. Meanwhile, if there is essentially no intersymbol interference, $T \geq T_m$.

On the other hand, two kinds of fadings in a channel have been encountered. The first kind of fading is associated with the coherence bandwidth of the channel (approximately $1/T_m$), which is the frequency-selective fading when the bandwidth of the transmitted signal is larger than the coherence bandwidth of the channel. Otherwise, the fading is called frequency-nonselective. The second kind of fading is related to the Doppler spread of the channel. The channel is referred to as the fast fading channel when the signaling interval, T, is greater than the coherence time of the channel (approximately $1/B_d$). Otherwise, the channel is slow fading. The fading results in poor communication quality, and requires additional transmitter power to overcome the fades. For example, in a mobile telephone network, for a portable moving at a velocity of 20 m/s (about 45 mph) and a carrier frequency of 800 MHz (the wavelength $\lambda_c = 0.375$ m), the peak frequency shift is about 50 Hz. In terms of

fading, this fading is typically as fast as one fade per second per mile per hour of the portable speed. The similar peak Doppler shift can be reached in SHF band indoor channels even though the receiver moving speed is low. Hence, the fading caused by the moving receiver in an indoor channel must be concerned and studied in order to use some techniques to overcome it.

From the above discussion, the Doppler frequency shift is directly related to the receiver speed. Thus selections of the receiver speed should reflect a potential use of such systems. To meet this requirement, the receiver speed is around 1.33 m/s which is approximately normal human walking speed. This measurement condition would duplicate the actual condition of the receiver for a wireless indoor system, which is carried by someone who is walking. To eliminate the effects of moving people around, the measurements were taken late at night or on weekends. Under this condition, random movements of a few people around two antennas do not have significant effects on the channel.

In addition to the Doppler spread issue, statistics of envelope fading in a multi-path environment will be discussed. The distribution fitting procedure is performed on the measured time profiles. Envelope fading may follow different distributions which depend on whether a LOS path exists or not, and some other conditions. Possible candidates are Rice, Rayleigh, Lognormal, and Weibull distributions. Statistical testing methods are introduced to determine the best fit of envelope fading.

4.2 Doppler Spread

In this section, the mathematical representation of the Doppler spread will be presented. Then a comparison of a number of different analysis methods will be given.

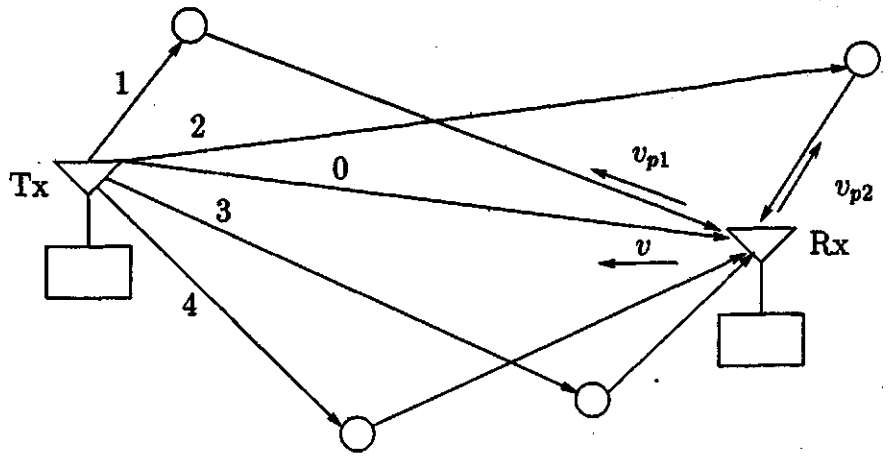

Figure 4.1 Illustration of Doppler frequency shifts

4.2.1 Mathematical Representation

Doppler frequency shifts are caused by the path length changes with time. This would result from a receiver moving towards a stationary transmitter. In a multipath environment the Doppler frequency shift will be different for each path because the velocity component for each path is different. Figure 4.1 illustrates how the receiver in motion causes Doppler frequency shifts in multipath environments. As can be seen in this figure, path 1 and path 2 have different velocity components. Thus, they will produce different Doppler frequency shifts.

For a single path, lengthening this path results in a frequency decrease (path 2) while shortening it results in a frequency increase (path 0, 1, 3, and 4). The Doppler frequency shift is only dependent on the radial component of the velocity of the receiver with respect to the objects. The Doppler frequency shift of a single path, denoted by f_d, is given by the following Equation 4.1 when there is only one moving source (either the receiver or objects) [11].

$$f_d = \frac{v_r}{\lambda_c} = \frac{v_r f_c}{c}, \tag{4.1}$$

where λ_c is the wavelength of the transmitting frequency f_c, c is the velocity of

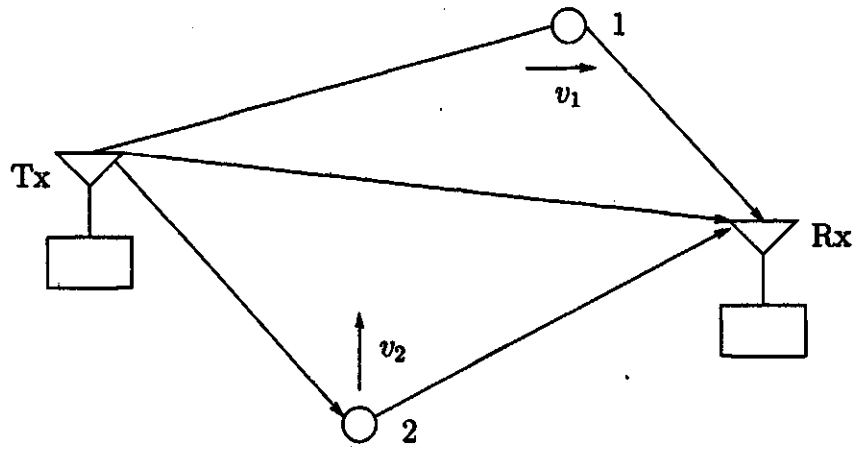

Figure 4.2 Effects of the position of a scatterer on the Doppler spread

propagation, and v_r is the radial velocity of the moving source.

The Doppler frequency shift due to the movement of an object in the environment is position dependent. An object can have a greater or lesser effect, which depends on its position and moving speed. The maximum effect occurs when the position of the object allows for the motion to either shorten or lengthen both distances to the transmitter and receiver. Figure 4.2 shows that the position of a object affects Doppler frequency shifts. Object 2 has a greater effect because it shortens both distances to the transmitter and receiver when it moves at a speed v_2.

The Doppler frequency shift for all paths in Figure 4.1 can be plotted as a function of frequency. The width of the distribution of Doppler frequency shifts in the plot is referred to as the Doppler spread, B_d. The absolute maximum value of the Doppler spread is given by

$$B_{d\,max} = \frac{2v_r f_c}{c}. \tag{4.2}$$

Since this value is the absolute maximum, in general B_d will be less than this value. This expression is usually used in the analysis of active sonar or radar signals where the transmitter and receiver are located at the same position. In active sonar or radar

the intent is to measure the speed of the object using Equation 4.2. For the indoor radio channel at 14 GHz where the receiver is moving at the approximate human walking speed of 1.3 m/s, the maximum Doppler spread will be

$$\begin{aligned} B_{d\,max} &= \frac{2v_r f_c}{c} \\ &= \frac{2 \times 1.3 \times 14 \times 10^9}{3 \times 10^8} \simeq 121Hz. \end{aligned}$$

In Chapter 2, the time profile $H(f_c;t)$ of the indoor radio channel for an unmodulated sine wave of frequency f_c was described. A sample time profile is shown in Figure 4.3. The autocorrelation of one time profile at f_c can be obtained by setting $\Delta f = 0$ in the complex autocorrelation function, $\phi(\Delta f;\Delta t)$ of $H(f_c;t)$. This gives,

$$\phi(0;\Delta t) = \frac{1}{2}E[H(f_c;t+\Delta t)H^*(f_c;t)]. \tag{4.3}$$

Figure 4.4 shows the sample autocorrelation function (of the sample time profile in Figure 4.3). The Doppler power spectrum is defined as the Fourier transform of $\phi(0;\Delta t)$, which is given by

$$S_d(\lambda) = \int_{-\infty}^{\infty} \phi(0;\Delta t)e^{-j2\pi\lambda\Delta t}d\Delta t. \tag{4.4}$$

Since $S_d(\lambda)$ is the Fourier transform of the complex autocorrelation function of $H(f_c;t)$, the Doppler power spectrum is equal to the magnitude squared of the transfer function of $H(f_c;t)$, that is, $S_d(\lambda) = |H(f_c;\lambda)|^2$, where

$$H(f_c;\lambda) = \int_{-\infty}^{\infty} H(f_c;t)e^{-j2\pi\lambda t}dt \tag{4.5}$$

is the Fourier transform of $H(f_c;t)$.

The Doppler spread B_d is the range of frequency λ over which the Doppler power spectrum $S_d(\lambda)$ is nonzero. $|H(f_c;\lambda)|$ is never zero in real measurements, and a threshold is used to determine B_d. Figure 4.5 illustrates a Doppler spectrum calculated from a time profile of length $N = 2501$. A more specific measure of the Doppler

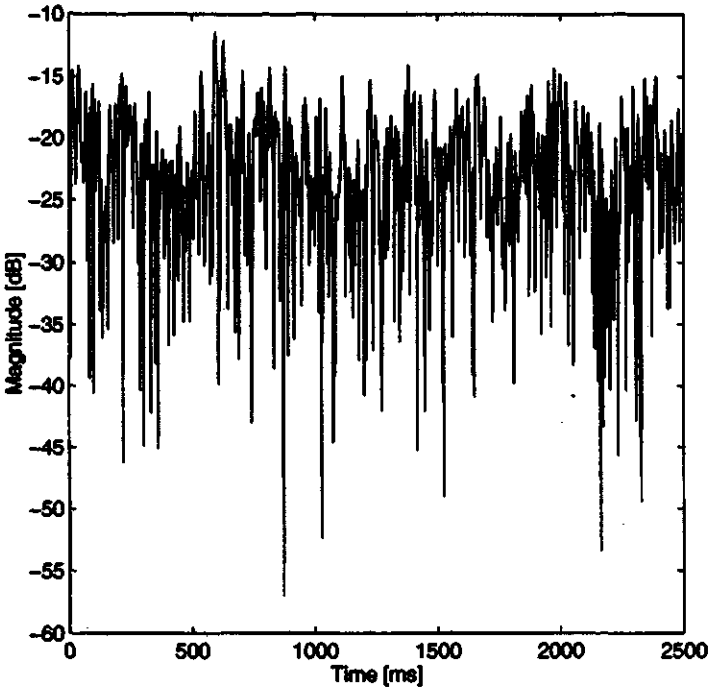

Figure 4.3 A sample time profile at a carrier frequency of 14 GHz with the moving receiver

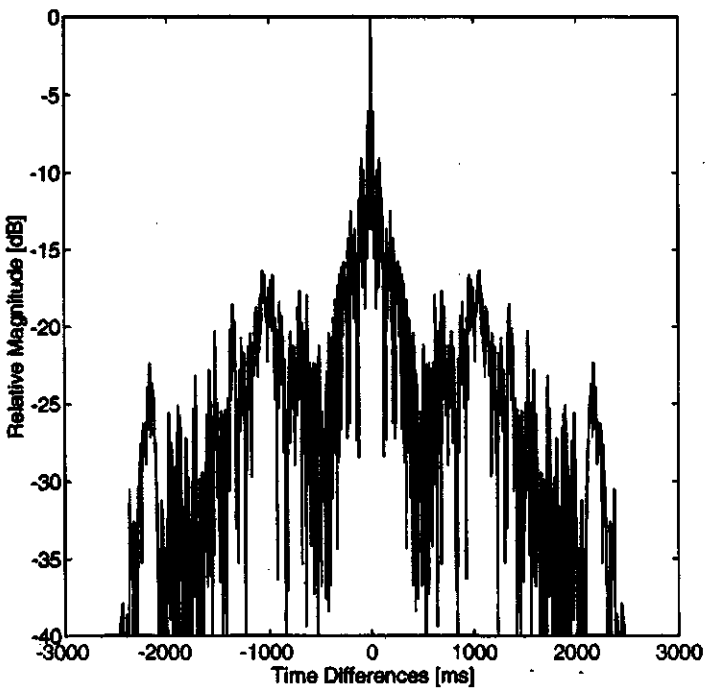

Figure 4.4 The corresponding autocorrelation function to the time profile in Figure 4.3

spread is the rms Doppler bandwidth, given by

$$f_n = [\frac{\int \lambda^2 S_d(\lambda) d\lambda}{\int S_d(\lambda) d\lambda}]^{\frac{1}{2}}, \tag{4.6}$$

which is a measure of the distribution of the power rather than the width of the power distribution [11].

4.2.2 Analytical Method

As mentioned before, the Doppler spread is a measure of the width of the Doppler spectrum. An example of a Doppler spectrum calculated using the FFT (Fast Fourier Transform), is given in Figure 4.5. The FFT method is a consistent estimation of the PSD (power spectrum density) for $N \rightarrow \infty$, where N is the data length [16]. Because finite length N is used, random fluctuations in power spectrum are inevitable. This is evident in Figure 4.5 for a data length of $N = 2501$. The Doppler spectrum for a data length of $N = 1001$ is shown in Figure 4.6 (the resolution of Doppler frequencies will decrease from 0.4 Hz to 1 Hz). The data length N and the data sampling frequency f_s determine the resolution of the Doppler frequency.

It is not easy to calculate Doppler spread B_d from these figures due to random fluctuations. The PSD can be smoothed by windowing the data. Also this can be done by running the data through a moving average filter. Data windowing can reduce the magnitude of the PSD at frequencies not near the peak of the Doppler spectrum. Windowing data also decreases the resolution of Doppler spectrum. Comparison of different spectral estimation methods based on the Fourier transform is given in [16]. These kinds of methods are referred to as classical techniques.

A popular parametric method of time series modeling to estimate the spectrum of a signal is called autoregressive (AR). This technique is often referred to as a modern spectral estimation method. In Chapter 2, the AR model was used to model the static indoor wide-band frequency domain measurements. Here it is used to model the time variations of the frequency domain measurements at a particular frequency.

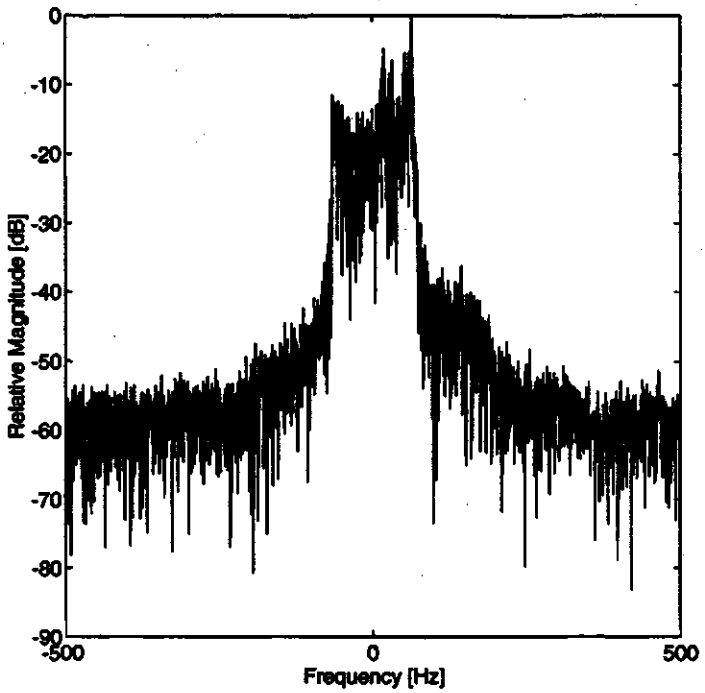

Figure 4.5 Doppler spectrum using the FFT method with $N = 2501$

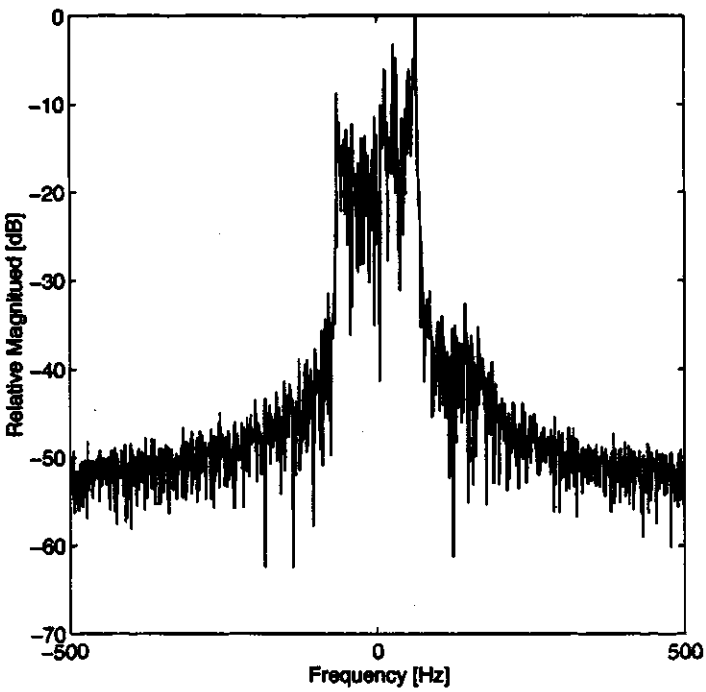

Figure 4.6 Doppler spectrum using the FFT method with $N = 1001$

The purpose here is to use the AR model to estimate the Doppler spread B_d. When the AR modeling assumption is valid, spectral estimators have a lower variability than conventional Fourier based spectral estimators [16]. A rule of thumb for applying the AR model to time series data is that the power spectral density of the time series contain sharp peaks. This is generally the case for the Doppler power spectrum and thus the AR model is a reasonable model.

Estimating the Doppler spectrum using the AR model requires an estimate of the model parameters. In the following section, the mathematical representation of the AR spectral estimator is introduced and the technique to determine the AR parameters is briefly discussed.

4.2.3 AR Spectral Estimation Method

The system transfer function $G(z)$ between the input $v(n)$ and the output $u(n)$, for an AR model of order M given in Equation 2.17 (page 17),is the rational function

$$G(z) = \frac{U(z)}{V(z)} = \frac{1}{1 + \sum_{k=1}^{M} a_k z^{-k}}. \tag{4.7}$$

It is well known that the power spectrum of the output of a linear filter is the power spectrum of the input multiplied by the square of the magnitude of its transfer function, which is given by

$$S_u(\lambda) = |G(\lambda)|^2 S_v(\lambda) \tag{4.8}$$

where $S_v(\lambda)$ is the PSD of the white noise process $v(n)$ with zero mean and variance σ_v^2. σ_v^2 has units of power. This power spectrum of the AR process, $u(n)$ is

$$S_u(\lambda) = \sigma_v^2 |G(\lambda)|^2. \tag{4.9}$$

$G(\lambda)$ can be obtained by evaluating $G(z)$ around the unit circle, $z = e^{j2\pi\lambda}$ for $-\frac{1}{2} \leq \lambda \leq \frac{1}{2}$, where λ is normalized Doppler frequency. If the sampling frequency, f_s, of the time series is 1000 Hz then the actual Doppler frequency range is -500 to 500 Hz.

Substituting $z = e^{j2\pi\lambda}$ into Equation 4.7 gives

$$G(\lambda) = \frac{1}{1 + \sum_{k=1}^{M} a_k e^{-j2\pi\lambda k}} = \frac{1}{\sum_{k=0}^{M} a_k e^{-j2\pi\lambda k}}, \tag{4.10}$$

where $a_0 = 1$ and taking the magnitude squared gives

$$|G(\lambda)|^2 = \frac{1}{|\sum_{k=0}^{M} a_k e^{-j2\pi\lambda k}|^2}. \tag{4.11}$$

Equation 4.11 can be simplified using matrix notation to give

$$|G(\lambda)|^2 = \frac{1}{|\mathbf{A}^T \mathbf{S}_e(\lambda)|^2} \tag{4.12}$$

where $\mathbf{A}^T$ is a $1 \times M+1$ vector with $\mathbf{A}^T = [a_0, a_1, \ldots, a_M]$, $\mathbf{S}_e$ is a $M+1 \times 1$ vector with $\mathbf{S}_e^T(\lambda) = [1, e^{-j2\pi\lambda}, \ldots, e^{-j2\pi\lambda M}]$. So the PSD of the AR process is

$$S_u(\lambda) = \frac{\sigma_v^2}{|\mathbf{A}^T \mathbf{S}_e(\lambda)|^2}. \tag{4.13}$$

The next step is to estimate the AR parameters and the variance of the white noise process. There are many methods to estimate the AR parameters, but here only the modified covariance method will be introduced. Because the properties of poles of the AR process are not a major concern in this discussion, it may be used to obtain perfect estimates of the frequencies despite the possibility of poles obtained by using the modified covariance method may be outside the unit circle. In general, the modified covariance method produces AR parameters that give statistically stable estimates of the spectrum with reasonable high resolution. It is really desirable and effective when the process is composed of a number of sinusoids in white noise. As a result, it is highly effective in estimations of the Doppler power spectrum.

The modified covariance method is based on the maximum likelihood estimation criterion, which estimates the parameters by minimizing the estimate of the prediction error power. The details of the derivation of this method is omitted here and only the final results are given [16].

The AR parameters $\{\hat{a}_k\}$ for $k = 1, 2, \ldots, M$ are given by solving the following set of linear equations

$$\begin{bmatrix} C_{xx}(1,1) & C_{xx}(1,2) & \ldots & C_{xx}(1,M) \\ C_{xx}(2,1) & C_{xx}(2,2) & \ldots & C_{xx}(2,M) \\ \vdots & \vdots & \ldots & \vdots \\ C_{xx}(M,1) & C_{xx}(M,2) & \ldots & C_{xx}(M,M) \end{bmatrix} \begin{bmatrix} \hat{a}_1 \\ \hat{a}_2 \\ \vdots \\ \hat{a}_M \end{bmatrix} = - \begin{bmatrix} C_{xx}(1,0) \\ C_{xx}(2,0) \\ \vdots \\ C_{xx}(M,0) \end{bmatrix}$$

where

$$C_{xx}(j,n) = \frac{1}{2(N-M)} \left(\sum_{i=M}^{N-1} u^*(i-j)u(i-n) + \sum_{i=0}^{N-1-M} u(i+j)u^*(i+n) \right). \quad (4.14)$$

In this equation, $\{u_i\}$, $i = 1, 2, \ldots, N$, is the time series, N is the data length, and M is the order of the AR model. The estimate of the white noise variance σ_v^2 is given by

$$\hat{\sigma}_v^2 = C_{xx}(0,0) + \sum_{k=1}^{M} \hat{a}_k C_{xx}(0,k). \quad (4.15)$$

Once the AR parameters $\{\hat{a}_k\}$ and the white noise variance $\hat{\sigma}_v^2$ are estimated, the AR spectral estimator (4.13) can be used to estimate Doppler spectrum. The computational efficiency and speed are about the same level as the FFT method, but the AR method has a higher resolution. It is relatively easy to find the Doppler spread, B_d, from the AR derived PSD since there are no random fluctuations as observed in the FFT method shown in Figure 4.5. Figure 4.7 shows the AR Doppler spectrum for the indoor channel with the receiver moving. Actually, the time series used to determine Figure 4.7 is the same as the one used in the FFT method which is illustrated in Figure 4.5.

4.2.4 Model Order Selection

It is important to determine the correct model order, M, for the AR model. If the model order is too large, the resultant Doppler spectrum will have spurious peaks and if the model order is very low, the spectrum will be smoothed. As a result, it

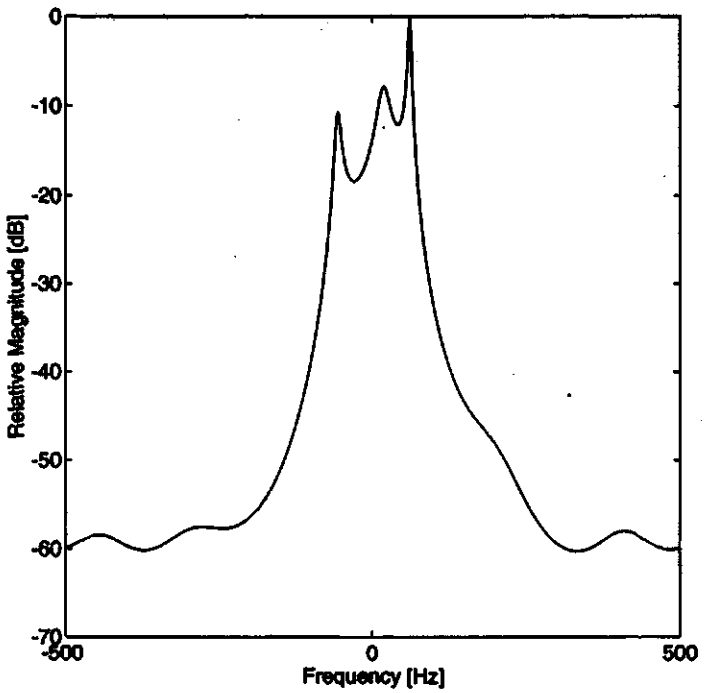

Figure 4.7 Doppler spectrum using the AR method for a 5 meter antenna separation distance, receiver moving speed of 1.36 m/s, and the AR model order $M = 8$

would be difficult to get accurate information about the Doppler spread. There are many techniques proposed to estimate the model order, some of which are presented here.

Four different methods are proposed by Akaike, Parazen and Rissanen [16]. The first one is called the *final prediction error* (FPE). The model order is selected as the value that minimizes

$$FPE(M) = \frac{N+M}{N-M}\hat{\rho_M}, \tag{4.16}$$

where $\hat{\rho_M}$ is the estimation of the prediction error power (white noise variance) for the M order AR model and N is the data length.

A second criterion is the *Akaike information criterion* (AIC). It has the form

$$AIC(M) = N\ln(\hat{\rho_M}) + 2M. \tag{4.17}$$

The model order selected is the one that minimizes the AIC. The performance of the FPE and AIC are similar, and as $N \rightarrow \infty$, the FPE and AIC are equivalent. The model orders selected by these two methods are considered to be too low [16, 17]. For practical use, the FPE , AIC and the third method termed the *criterion autoregressive transfer function* (CAT) will be all used to determine the model order M.

The CAT method was introduced by Parazen [16, 17]. The CAT is derived for AR spectral estimation based on an arbitrary data set, and not just a pure AR process unlike the FPE which is based on a pure AR process. It is defined as

$$CAT(M) = \frac{1}{N}(\sum_{i=1}^{M} \frac{N-i}{N} \frac{1}{\hat{\rho}_i} - \frac{N-K}{\hat{\rho_M}}). \tag{4.18}$$

Again minimizing (4.18) leads to the estimated model order. This criterion takes estimation errors in the prediction coefficients into account and has similar performance as the FPE and AIC have.

The fourth method was developed by Rissanen, which is called the *minimum description length* (MDL) process, given by

$$MDL(M) = N \ln(\hat{\rho_M}) + M \ln(N). \tag{4.19}$$

It is considered to be a consistent estimator compared to the AIC method in [17].

4.3 Estimation of Envelope Fading Distribution

Envelope fading in a multipath environment can be characterized statistically by fitting a density function to the envelope value, which and be considered a random variable. For CW fading measurements the following distributions are possible fits to the measurement data: Rayleigh, Rician, Lognormal and Weibull distributions.

4.3.1 Candidate Distributions

Rayleigh distribution

The Rayleigh model is widely used in indoor communications systems in absence of a strong received component. The theoretical explanation is based on the joint distributions of $x = \sqrt{I^2 + Q^2}$, where I and Q are the quadrature components of the received signal which are independent Gaussian random variables with zero mean. The Rayleigh distribution is given by its probability density function (pdf)

$$f(x) = \frac{x}{\sigma^2} e^{-\frac{x^2}{2\sigma^2}} \quad x \geq 0, \tag{4.20}$$

and its corresponding cumulative distribution function (cdf) is

$$F(x) = 1 - e^{-\frac{x^2}{2\sigma^2}} \quad x \geq 0,$$

where σ^2 is the variance of fading components. The pdf and cdf of a Rayleigh distribution are shown in Figure 4.8, where $\sigma^2 = 0.6316$.

Rician distribution

The Rician distribution is used when a strong path exists. This strong path may be a LOS path or a path that goes through much less attenuation compared to other paths. The Rician distribution can be considered to be the sum of two components: the strong path component which is deterministic, and a Rayleigh distributed component representing the rest of the paths. Rice [10] has shown the pdf to be

$$f(x) = \frac{x}{\sigma^2} e^{-\frac{x^2+\alpha^2}{2\sigma^2}} I_0\left(\frac{\alpha x}{\sigma^2}\right) \quad x \geq 0, \tag{4.21}$$

where I_0 is the zeroth-order modified Bessel function of the first kind, α is the magnitude of the strong component, and σ^2 is proportional to the power of the Rayleigh component. No mathematical representation of the Rician cdf is given. Figure 4.9 shows the Rician pdf and cdf with $\alpha = 0.7$ and $\sigma^2 = 0.6859$.

Lognormal distribution

The Lognormal model has often been used to fit large scale variations of signal envelopes in a multipath fading environment. The pdf is given by

$$f(x) = \frac{1}{\sqrt{2\pi}\sigma x} e^{-\frac{(\ln x - \mu)^2}{2\sigma^2}} \quad x \geq 0,$$

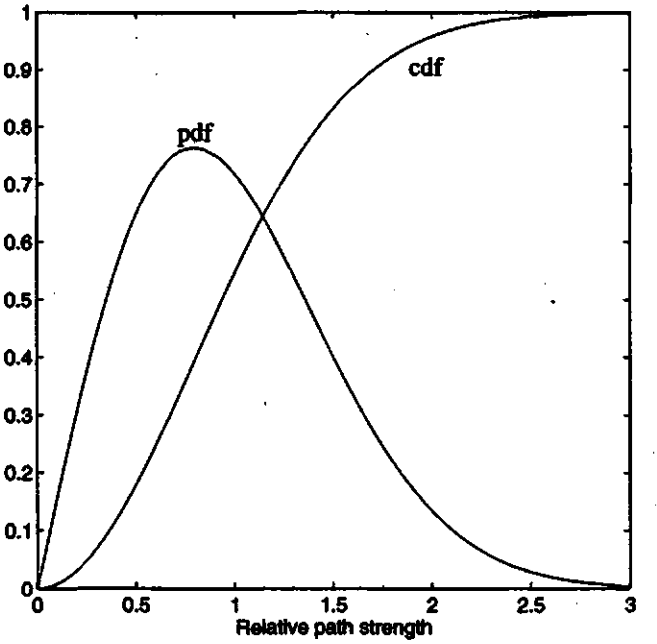

Figure 4.8 Rayleigh distribution

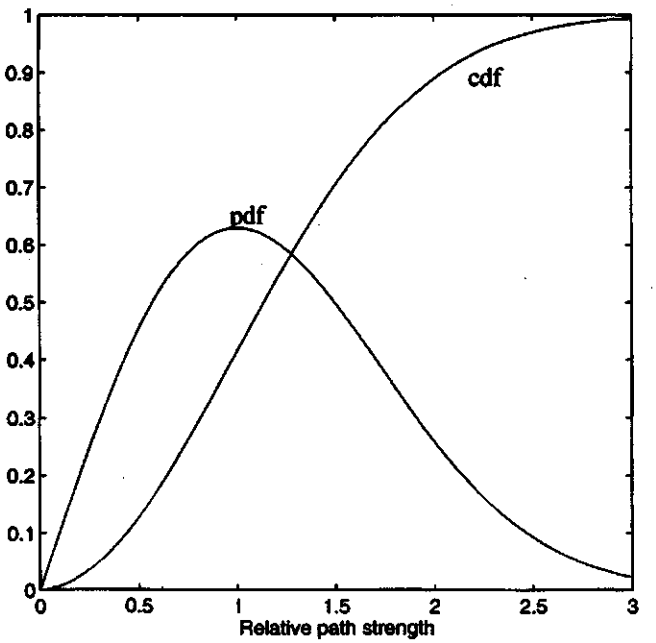

Figure 4.9 Rician distribution

where μ is the mean and σ^2 is the variance of multipath components. Note that $\log x$ has a Gaussian (normal) distribution. The Lognormal distribution can be characterized as a multiplicative process. Its pdf and cdf with $\mu = -0.1681$ and $\sigma^2 = 0.4172$ are shown in Figure 4.10.

Weibull distribution

The Weibull distribution is given by its pdf and cdf

$$f(x) = \begin{cases} \alpha\beta x^{\beta-1} e^{-\alpha x^\beta} & x \geq 0 \\ 0 & x < 0 \end{cases} \quad \alpha > 0,\ \beta > 0$$

and

$$F(x) = 1 - e^{-\alpha x^\beta} \quad x \geq 0.$$

The pdf and cdf of a Weibull distribution are plotted in Figure 4.11, where $\alpha = 0.7818$ and $\beta = 2.0393$.

4.3.2 Estimation of Statistical Distribution Parameters

In a multipath environment the envelope of the sum of the multipath received signals is observed. The envelope value at some time, t, can be represented by a random variable X. The pdf of X is $f(x;\Phi)$, where the form of the pdf or cdf is assumed known but there are some unknown parameters, represented by the parameter vector Φ. For example, the Rayleigh pdf may fit the measurement data very well thus the single parameter $\varphi = \sigma$ in (4.20) must be estimated. This estimation process is referred to as parametric point estimation. Parametric point estimation involves using the measured data to estimate the unknown parameter vector Φ to obtain an estimate of its value $\hat{\Phi}$.

The estimation method used here, which will now be described, is referred to as the maximum likelihood estimation. First the terminology must be defined. Let $X_1, X_2, \ldots, X_n$ be a random sample from a pdf $f(x;\Phi)$, where the X_i are independent

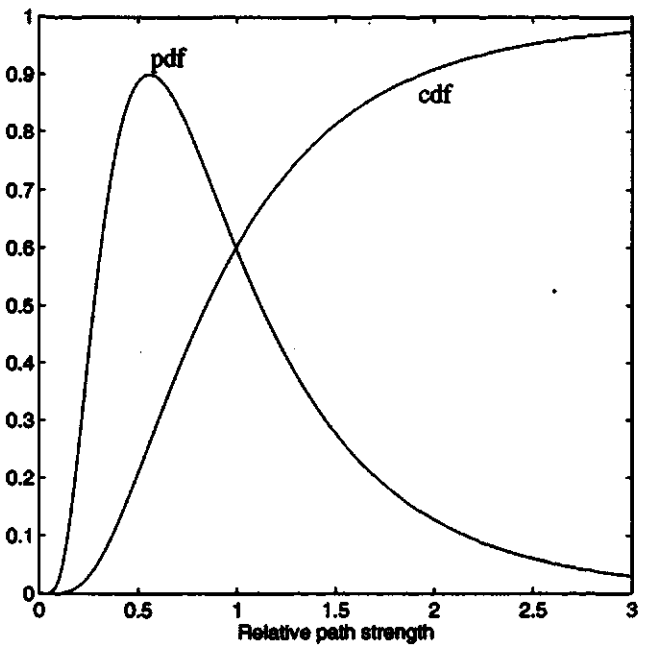

Figure 4.10 Lognormal distribution

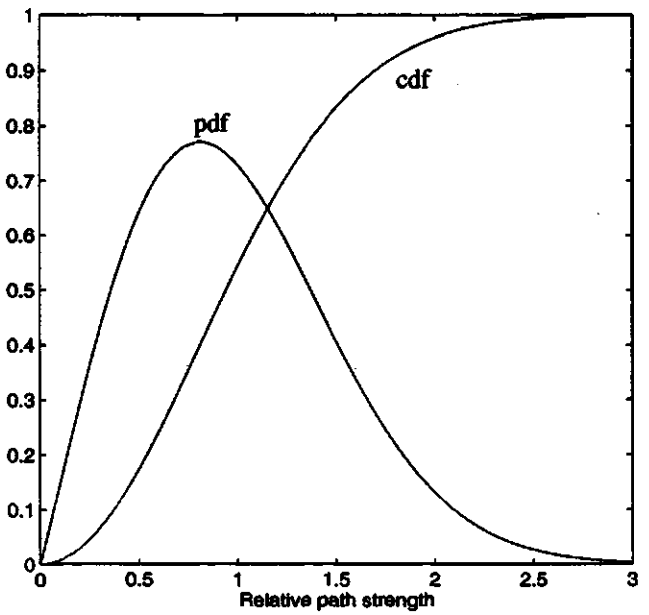

Figure 4.11 Weibull distribution

and identically distributed (iid). The maximum likelihood technique is developed using the joint probability density function of $X_1, X_2, \ldots, X_n$ which is given by [30]

$$L(\varphi_1, \varphi_2) = f(x_1; \varphi_1, \varphi_2) f(x_2; \varphi_1, \varphi_2) \ldots f(x_n; \varphi_1, \varphi_2) \tag{4.22}$$

$$= \prod_{i=1}^{n} f(x_i; \varphi_1, \varphi_2) \tag{4.23}$$

where the parameter vector, Φ, consists of two elements φ_1 and φ_2, and $L(\varphi_1, \varphi_2)$ is called the likelihood function. The values which maximize $L(\varphi_1, \varphi_2)$ are maximum likelihood estimators of φ_1 and φ_2, denoted by $\hat{\varphi}_1$ and $\hat{\varphi}_2$, respectively.

In practice, it is easier to deal with a sum instead of a multiplication. Thus, the natural logarithm of $L(\varphi_1, \varphi_2)$ is used to solve for the estimation parameters. The natural logarithm form is

$$\ln L(\varphi_1, \varphi_2) = \ln \prod_{i=1}^{n} f(x_i; \varphi_1, \varphi_2) \tag{4.24}$$

$$= \sum_{i=1}^{n} \ln f(x_i; \varphi_1, \varphi_2). \tag{4.25}$$

The maximum likelihood estimators, $\hat{\varphi}_1$ and $\hat{\varphi}_2$ are determined by solving the set of the first order partial derivatives

$$\frac{\partial \ln L(\varphi_1, \varphi_2)}{\partial \varphi_1} = 0, \tag{4.26}$$

$$\frac{\partial \ln L(\varphi_1, \varphi_2)}{\partial \varphi_2} = 0, \tag{4.27}$$

for the maximum value of φ_1 and φ_2.

An alternate approach for selecting estimations is the the method of moments. The basic idea is to match the first moment of X to the sample mean $E(X)$ and the second moment to the sample variance $E[(X - E(X))^2]$. In general, if there are m parameters which have to be estimated, the first m moments are set equal to the first m moments of the sample that are given in terms of the unknown parameters. Solving for $\varphi_1, \varphi_2, \ldots, \varphi_m$, the moment estimators are obtained. Usually, the moment

method is needed to solve nonlinear equations, the mathematical representations of estimator $\tilde{\varphi_1}, \tilde{\varphi_2}, \ldots, \tilde{\varphi_m}$ are difficult. Some examples can be found in [30]. For simple cases, the method that has the smallest mean square error is selected. For example, if

$$E[(\hat{\varphi} - \varphi)^2] < E[(\tilde{\varphi} - \varphi)^2]$$

,

then $\hat{\varphi}$ is selected. This means that if $E(\hat{\varphi}) = E(\tilde{\varphi}) = E(\varphi)$, then the one with the smallest variance would be selected. Further discussion about selecting the estimation method can be found by using Cramer-Rao bound in [30]. In practice, the variance of the maximum likelihood estimator $\hat{\varphi}$ is closer to the Cramer-Rao lower bound, so the maximum likelihood method is used in this work.

4.3.3 Mathematical Representations of Estimators

Based on the probability density functions given in section 4.3.1, the estimation for the parameters $\hat{\sigma^2}$ for the Rayleigh distribution, $\hat{\alpha}$ and $\hat{\sigma^2}$ for the Rician distribution, $\hat{\mu}$ and $\hat{\sigma^2}$ for the Lognormal distribution, and $\hat{\alpha}$ and $\hat{\beta}$ for the Weibull distribution are presented here.

Using the Rayleigh distribution as an example the following gives the derivation of the estimation parameters. The detailed derivations for the cases of the Lognormal distribution and the Weibull distribution are not given here, only the results are presented. The log likelihood function of the Rayleigh pdf is

$$\begin{aligned} \ln L(\sigma) &= \ln \prod_{i=1}^{n} f(x_i;\sigma) \\ &= \sum_{i=1}^{n} \ln f(x_i;\sigma). \end{aligned}$$

Substitute the expression of $f(x_i;\sigma)$ into above equation

$$\ln L(\sigma) = \sum_{i=1}^{n} \ln(\frac{x_i}{\sigma^2} e^{-\frac{x_i^2}{2\sigma^2}}) \tag{4.28}$$

$$= \sum_{i=1}^{n} (\ln x_i - 2\ln\sigma - \frac{x_i^2}{2}\frac{1}{\sigma^2}). \tag{4.29}$$

Take the first order derivative respect to σ

$$\frac{d\ln L(\sigma)}{d\sigma} = \sum_{i=1}^{n}(-\frac{2}{\sigma} + \frac{x_i^2}{\sigma^3}) = 0. \tag{4.30}$$

The solution for σ^2 is found by solving the equivalent equation

$$-\frac{2n}{\sigma} + \frac{1}{\sigma^3}\sum_{i=1}^{n} x_i^2 = 0. \tag{4.31}$$

It is easy to see that

$$\hat{\sigma^2} = \frac{1}{2n}\sum_{i=1}^{n} x_i^2 \tag{4.32}$$

can be used to generate a value of the estimation for σ^2.

Similarly, the mathematical formulas of the estimated parameters of the rest of the distributions can be derived from their corresponding maximum likelihood functions.

For the Lognormal distribution, the mean μ and variance σ^2 can be estimated by

$$\begin{cases} \hat{\mu} = \frac{1}{n}\sum_{i=1}^{n}\ln x_i \\ \hat{\sigma^2} = \frac{1}{n}\sum_{i=1}^{n}(\ln x_i - \hat{\mu})^2. \end{cases}$$

In the Weibull distribution, the nonlinear equation must be dealt with. The $\hat{\alpha}$ and $\hat{\beta}$ parameters follow as

$$\begin{cases} \hat{\alpha} = \frac{n}{\sum_{i=1}^{n} x_i^{\hat{\beta}}} \\ \frac{n}{\hat{\beta}} - \hat{\alpha}\sum_{i=1}^{n} x_i^{\hat{\beta}}\ln x_i + \sum_{i=1}^{n}\ln x_i = 0 \end{cases}$$

Solving these two equations, the estimation value of $\hat{\beta}$ can be decided by adding some restrictions because the solution for $\hat{\beta}$ is not unique (β is around 2).

It is not easy to find the estimators of the Rician distribution using the maximum likelihood method. Here the moment method is used to find mathematical expressions of these estimators. Matching the first moment and the second moment of the random variable X with its sample mean and variance gives [21]

$$E[x] = \sqrt{\frac{\pi}{2}}\sigma e^{-\frac{\alpha^2}{2\sigma^2}} H(\frac{3}{2}, 1, \frac{\alpha^2}{2\sigma^2}), \tag{4.33}$$

and

$$E[x^2] = \alpha^2 + 2\sigma^2, \tag{4.34}$$

where H is the confluent hyper-geometric function given by

$$H(\frac{3}{2}, 1, \gamma^2) = 1 + \frac{3}{2}\gamma^2 + \frac{\frac{3}{2}\frac{5}{2}}{2!}\frac{\gamma^4}{2!} + \frac{\frac{3}{2}\frac{5}{2}\frac{7}{2}}{2!}\frac{\gamma^6}{2!} + \ldots \tag{4.35}$$

The parameter γ^2 is equal to $\frac{\alpha^2}{2\sigma^2}$. The estimators of the Rician distribution can be described in terms of γ^2.

$$\begin{cases} E[x] = \frac{1}{2}\sqrt{\frac{\pi E[x^2]}{1+\gamma^2}}e^{-\gamma^2}H(\frac{3}{2}, 1, \gamma^2) \\ \hat{\sigma^2} = \frac{E[x^2]}{2(1+\gamma^2)} \\ \hat{\alpha} = \sqrt{2\hat{\sigma^2}\gamma^2} \end{cases}$$

The estimators $\hat{\alpha}$ and $\hat{\sigma^2}$ can be obtained by solving these non-linear equations.

4.4 Tests of Fit

The estimation of pdf parameters is one step in the distribution fitting procedure. The next step is to determine which distribution has the closest fit to the empirical data.

Two types of testing methods are employed to determine the distribution of envelope fading. The theoretical distribution (cdf or pdf) will be tested against the corresponding empirical distribution using each of the two statistical testing methods described below.

1. The Kolmogorov-Smirnov Test

The Kolmogorov-Smirnov (K-S) Test is the goodness fit test between a theoretical cumulative distribution function (cdf) and an empirical cdf. Based on the closeness of the empirical and the theoretical cumulative distribution functions, $F_N(x)$ and $F(x)$. The K-S goodness fit test is defined by

$$D_N = Max_x[|F_N(x) - F(x)|]. \tag{4.36}$$

The distribution of D_N depends on N, the size of the samples, and is independent of $F(x)$. If the empirical cumulative distribution $F_N(x)$ is sufficiently close to $F(x)$, that is, the value of D_N is sufficiently small, $F(x)$ can be accepted.

Another application of the K-S statistic is in forming a confidence band for an unknown distribution $F(x)$. To form a confidence band based on a sample of size N, select a number d such that

$$P(D_N > d) = \alpha. \tag{4.37}$$

Then

$$\begin{aligned} 1-\alpha = &\ P(D_N \leq d) \\ = &\ P(Max_x|F_N(x) - F(x)| \leq d) \\ = &\ P(|F_N(x) - F(x)| \leq d \ for\ all\ x) \\ = &\ P(F_N(x) - d \leq F(x) \leq F_N(x) + d \ for\ all\ x). \end{aligned}$$

The relationship between D_N and α is given in Table 4.1. If D_N is smaller than d, with a confidence level of $(1-\alpha)\%$ the hypothesis $F(x) = F_N(x)$ passes the K-S test.

Table 4.1 The Kolmogorov-Smirnov Acceptance Limits

α	0.20	0.10	0.05	0.01
D_N *for large* n	$\frac{1.07}{\sqrt{n}}$	$\frac{1.22}{\sqrt{n}}$	$\frac{1.36}{\sqrt{n}}$	$\frac{1.63}{\sqrt{n}}$

2. The Chi-Square Test

The Chi-Square Test is a very adaptable test statistic and can be used for many different types of tests. In particular, one application of it allows us to test the appropriateness of different probabilistic models and, in this sense, is a competitor of

the K-S test. First, look at a random variable X which has a chi-square distribution with n degrees of freedom. The pdf of random variable X is

$$f(x) = \frac{1}{\Gamma(\frac{n}{2})2^{\frac{n}{2}}} x^{\frac{n}{2}-1} e^{-\frac{x}{2}}, \quad x \geq 0.$$

Then X is $\chi^2(n)$, which stands for a chi-square distribution with n degrees of freedom.

Considering the basic chi-square statistic, let random variable B_1 be the binomial distribution with the pdf, $b(n, p_1)$, where $0 < p_1 < 1$. According to the central limit theorem,

$$Z = \frac{(B_1 - np_1)^2}{\sqrt{np_1(1-p_1)}} \tag{4.38}$$

has an approximate normal distribution $N(0,1)$ for large n. Thus it is not surprising that $Q_1 = Z^2$ is approximately $\chi^2(1)$, a chi-square distribution with one degree of freedom. If $B_2 = n - B_1$ and $p_2 = 1 - p_1$, Q_1 may be written as

$$Q_1 = \frac{(B_1 - np_1)^2}{np_1(1-p_1)} = \frac{(B_1 - np_1)^2}{np_1} + \frac{(B_1 - np_1)^2}{n(1-p_1)} \tag{4.39}$$

Since $(B_1 - np_1)^2 = (n - B_2 - n + np_2)^2 = (B_2 - np_1)^2$, Q_1 has the following form

$$Q_1 = \frac{(B_1 - np_1)^2}{np_1} + \frac{(B_2 - np_2)^2}{np_2}. \tag{4.40}$$

In a sense, Q_1 measures the closeness of the observed numbers B_1 and B_2 to the corresponding expected numbers $np_1 = E(B_1)$ and $np_2 = E(B_2)$.

To generalize, let an experiment have k mutually exclusive and exhaustive outcomes, say $A_1, A_2, \ldots, A_k$. Let $p_i = P(A_i)$ and thus $\sum_{i=1}^{k} p_i = 1$. The experiment is repeated n independent times, and B_i represent the number of times the experiment results in $A_i, i = 1, 2, \ldots, k$. A statistic that measures the closeness of the observed number B_i of occurrences A_i to the expected value $e_i = np_i, i = 1, 2, \ldots, k$, is

$$q_{k-1} = \sum_{i=1}^{k} \frac{(b_i - np_i)^2}{np_i}. \tag{4.41}$$

The corresponding random variable,

$$Q_{k-1} = \sum_{i=1}^{k} \frac{(B_i - np_i)^2}{np_i} \tag{4.42}$$

for large n, can be shown to have an approximate chi-square distribution with $k-1$ degrees of freedom, namely, $\chi^2(k-1)$.

From Equation 4.42, actually, the chi-square test is based on the comparison between the histogram of the data and the pdf of the theoretical distributions. The data is first put in bins. The number of data points that are in the i^{th} bin is denoted by B_i (integer), the corresponding number for the theoretical distribution is denoted by n (experiment times) $\times p_i$ (the theoretical probability in this bin).

A large value $\chi^2(k-1)$ indicates a bad fit between the theoretical and empirical distributions. The distribution with the smaller χ^2 is selected to represent the best fit, passing the chi-square goodness fit test.

5. Analysis and Discussion of Results

In this chapter, the results will be presented and discussed. These include the Doppler spread and the rms Doppler bandwidth calculations in different environments, and the statistics of envelope fading of the time profiles.

5.1 Data Correction Procedure

The components in the measurement system, such as amplifiers and cables have a non-ideal frequency response. The effects of these components, as previously discussed, must be removed from the measured data in order to obtain accurate results. These frequency dependent components are: the transmit pre-amplifier and power amplifier, the receive low noise amplifier, the heliax cable, and the semi-rigid 0.141 inch coaxial copper cable. Note that the various lengths of semi-rigid cable that interconnect the components of the system are not dealt with individually. Their effects are included in the components connected to them.

As previously mentioned in chapter 3, each component in this system was measured in the frequency band ranging from 14 to 14.5 GHz. The data was then stored in the workstation. A correction file was formed by adding or subtracting the frequency dependent factors of each of the components in decibels (dB). Detailed procedure for this operation can be found in [29].

A set of time profiles $H(f_i;t)$ is obtained by measuring $H(f_i;t)$ over time, t, for a constant frequency f_i. Measurements are made at 11 different frequencies which are equally spaced in the 14 to 14.5 GHz band. The magnitude and phase of the correction factor for each of these frequencies are shown in Figure 5.1. At each of

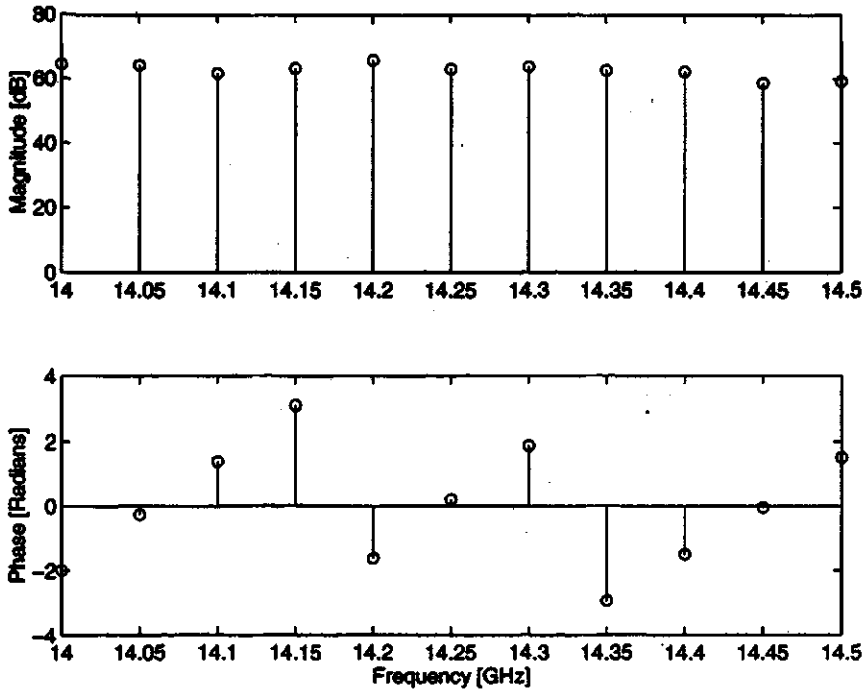

Figure 5.1 Magnitude and phase of correction factor at 11 frequencies

these frequencies the time profile was corrected by subtracting the corresponding correction factor in dB at that frequency. The corrected time profiles reflect the actual signal levels by eliminating the non-ideal amplifier and cable effects.

5.2 Comparison of Spectral Estimation Methods

5.2.1 Selecting of Model Order

The AR spectral estimation method is used as a tool to calculate the Doppler spread of the indoor channel. It is necessary to determine a suitable AR model order from the point of view of computational efficiency and accurate results. Discussions of required techniques to select model order were outlined in chapter 4. Basically, the four criteria used here are the Final Predictor Error (FPE), the Alaike Information Criterion (AIC), the Criterion Autoregressive Transfer function (CAT), and the Minimum Description Length method (MDL).

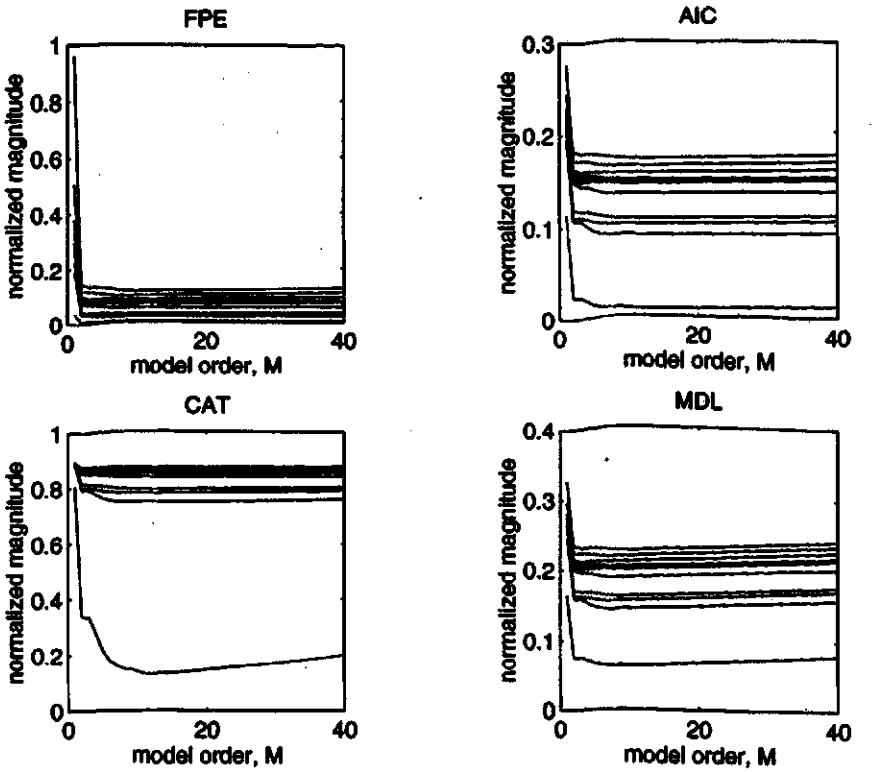

Figure 5.2 Normalized magnitude vs. model order using the FPE, AIC, CAT, and MDL method

Each method uses a set of data with 11 different frequencies for one location and a specified speed. The plots of those methods can be seen in Figure 5.2. The FPE, AIC, and CAT method shows when M around 10 minimizes them. The MDL is minimized at about 8. Hence, it was determined that an eighth order model would be used to compute the Doppler spread at different frequencies and receiver moving speeds. Selection of this model order also takes into account some other reasons. The main concern is that if the model order is too high, it will result in spurious peaks in the Doppler spectrum. So a moderate model order would be suitable.

5.2.2 Comparisons Between AR and FFT Spectral Estimation Methods

With the model order now selected, the spectrum of each time profile can be generated. Using the $ar(.)$ function (the modified covariance method is the default method used to solve for the AR model parameters) in the System Identification

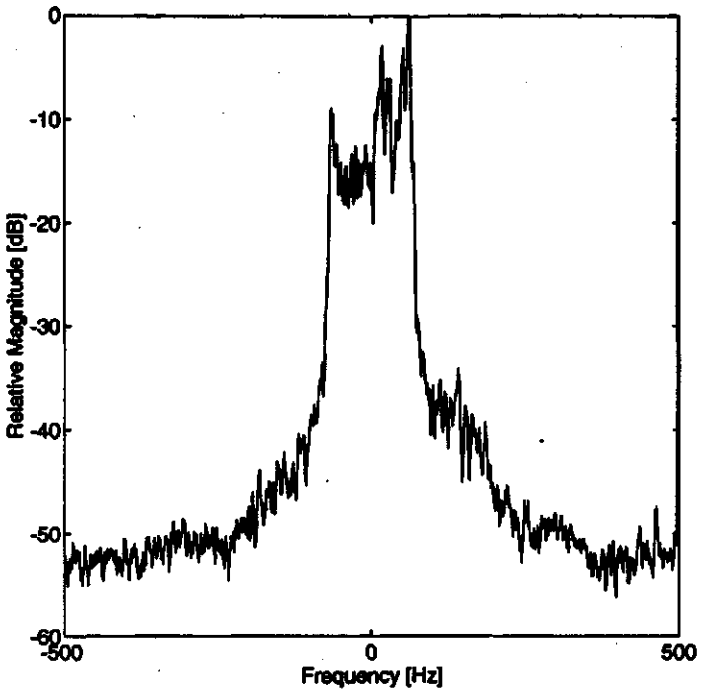

Figure 5.3 Doppler spectrum in Figure 4.5 filtered by a moving average filter

Toolbox of MATLAB, the parameters of the AR model are easily calculated, and a short program can be used to obtain the Doppler spectrum.

The Doppler spectrum can be directly obtained by the FFT method, but it is difficult to calculate the Doppler spread even though the spectrum can be smoothed by filtering the spectrum through a moving average filter. Figure 5.3 shows the filtered spectrum, but there are still random fluctuations in the spectrum compared to Figure 4.7.

These two methods can both be used to estimate the Doppler spread, but the random fluctuations in the FFT method may cause some difficulties in finding the value of the Doppler spread. Hence, the AR method will be used to determine the Doppler spread.

In the AR spectral estimation method, the poles are indications of spectral peaks. A pole close to the unit circle represents significant power at the frequency related to

the angle of the pole. The frequency is given by

$$f = \frac{angle(pole)}{2\pi} f_s \tag{5.1}$$

where f_s is the sampling frequency. The sampling frequency combined with the length of each time profile gives the resolution of the Doppler spread. In this case the resolution of the Doppler Spread is 0.4 Hz.

The pole plots can be seen in Figure 5.4. Note the two poles which are close to the unit circle. One has a positive angle, and the other has a negative angle. These two poles correspond to the spectral peaks in the Doppler spectrum, one corresponds to the positive shift and the other is associated with the negative shift. The corresponding shifts can be seen in Figure 5.5. For example, the positive shift and negative shift calculated using (5.1) are 59.1728 Hz and 62.2440 Hz, respectively.

However, the Doppler spectrum is almost vertical around the peaks. This can be observed in the spectrum obtained by both the FFT method and AR method. It is easier to calculate frequencies at the peaks based on such a large data base. So, the values of the Doppler spread used in this chapter will be the difference value between the negative frequency peak and the positive one. In general, based on the poles and the relation between frequencies and angles of the poles the Doppler spread B_d can be calculated. For the last example, the Doppler spread is 121.4 Hz. In practice, the Doppler spread will be calculated directly from the spectrum plot through finding the peak shift value difference. In Figure 5.5, the Doppler spread is 121.6 Hz.

5.3 Statistical Analysis of the Doppler Spread

In this section, the Doppler spread for different measurement conditions will be presented and discussed. Comparison results will be given for different frequencies, receiver moving speeds, antenna positions and environments.

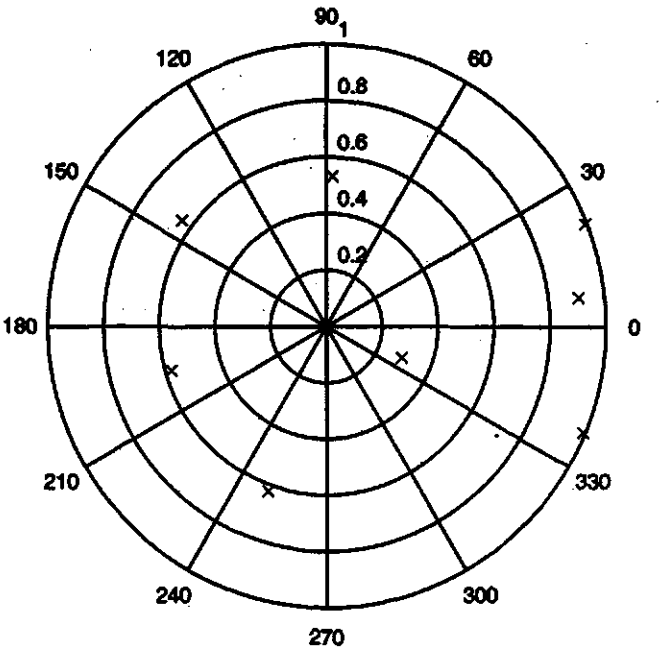

Figure 5.4 Poles of AR model

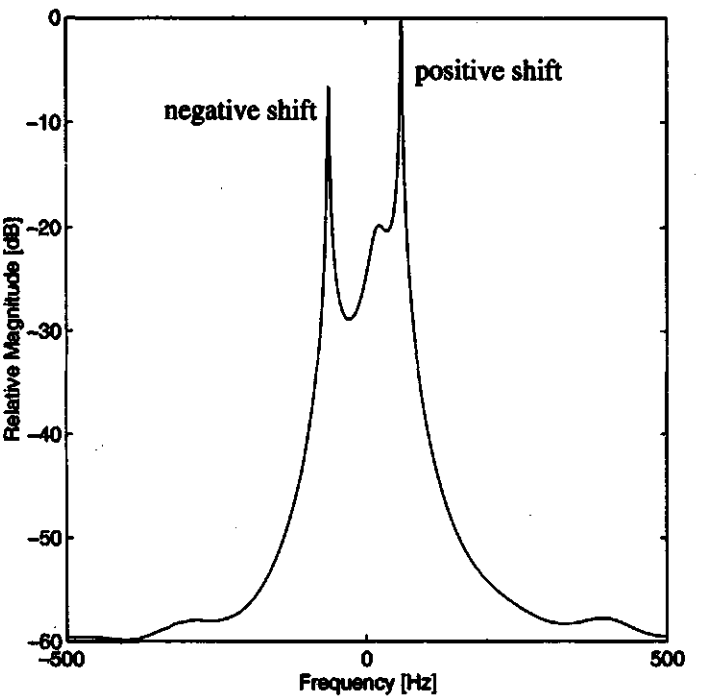

Figure 5.5 Doppler spectrum using the AR method (poles in Figure 5.4) for a carrier frequency of 14 GHz, and a 5 meter antenna separation distance with LOS path

5.3.1 Statistics of Doppler Spread at Different Frequencies and Speeds

In a mobile radio channel, the rapidly changing signal is essentially a spatial phenomenon, but a receiver moving through the field experiences a time related change which causes a Doppler shift. However, even though the receiver is moving at a low speed in an indoor channel, it will produce a noticeable Doppler shift at a transmit frequency of 14 GHz.

The time profiles at each frequency were measured in different environments, receiver moving speeds, and antenna positions (LOS or NLOS). The maximum Doppler spread is directly related to the receiver moving speed and the transmit frequency, as expressed in (4.2). In this section, some results will be presented to show the dependence of Doppler spread on the transmit frequency and the receiver speed.

Table 5.1 shows Doppler spreads for a receiver moving speed of 1.36 m/s with the antenna separation distance being 5 meters and a LOS path existing. In Table 5.1, the Doppler spread is a measure of width of the power distribution. The rms Doppler bandwidth is a measure of the distribution of the power. The value of Doppler spread varies from 121.6 to 126.8 Hz, and the corresponding coherence time is between 7.9 and 8.2 ms.

Comparing the theoretical and measured Doppler spreads in Table 5.1 shows that the measured Doppler spread is less than the theoretical. This is to be expected since the theoretical values obtained by using (4.2) are the maximum values.

Table 5.2 is a list of Doppler spreads at the receiver moving speed of 1.09 m/s while other conditions are the same as in Table 5.1. Comparing these values in this table to those listed in Table 5.1, it can be seen that the Doppler spread increases with the receiver moving speed, so does the rms Doppler bandwidth because the fade rate is directly related to the speed of the moving receiver. Appendix A shows figures

Table 5.1 Doppler Spread at Different Frequencies for a 5 meter antenna separation distance and a receiver moving speed of 1.36 m/s with LOS path in a hallway

Frequency $[GHz]$	*Theoretical* $B_d[Hz]$	*Measured* $B_d[Hz]$	*rmsDoppler bandwidth*$[Hz]$
14.00	126.9	121.6	57.3090
14.05	127.4	123.2	58.8102
14.10	127.8	122.8	58.1300
14.15	128.3	125.6	59.2832
14.20	128.7	123.2	58.7431
14.25	129.2	124.4	59.0266
14.30	129.7	123.2	58.5474
14.35	130.1	126.0	59.1354
14.40	130.6	124.4	59.0245
14.45	131.0	126.4	59.8107
14.50	131.5	126.8	60.2472

Table 5.2 Doppler Spread at Different Speeds for a 5 meter antenna separation distance with LOS path in a hallway

Frequency $[GHz]$	*Theoretical* $B_d[Hz]$	*Measured* $B_d[Hz]$	*rmsDoppler bandwidth*$[Hz]$
14.00	101.7	92.0	43.1122
14.05	102.1	93.2	44.3651
14.10	102.5	94.0	44.5533
14.15	102.8	95.2	45.2690
14.20	103.2	94.4	44.8501
14.25	103.6	94.8	44.7418
14.30	103.9	95.6	45.1022
14.35	104.3	95.2	44.9843
14.40	104.6	95.6	44.8220
14.45	105.0	96.4	45.4353
14.50	105.4	97.2	45.5031

of the Doppler spectrum at different speeds.

5.3.2 Doppler Spread at Different Antenna Separation Distances and Positions

The antenna separation distance is 5, 7.5 and 10 meter, respectively. There are two types of measurements, one is line of sight (LOS) where there is an unobstructed path between the antennas. The other is non line of sight (NLOS) where the LOS path does not exist. Most of NLOS measurements were taken at corners of hallways. Figure 3.2 shows this measurement configuration.

In a mobile communication system, the fading is a very strong function of the physical position of the mobile station. A small change in position, even a few cen-

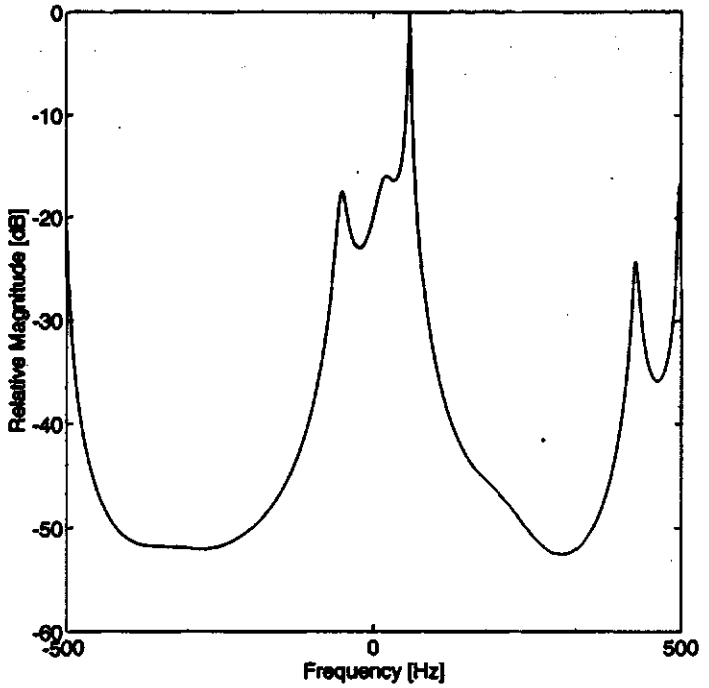

Figure 5.6 Doppler spectrum for a carrier frequency of 14 GHz, a 10 meter antenna separation distance, and a receiver moving speed of 1.36 m/s with NLOS path

timeters (at 14 GHz), changes the delays of all of the paths and results in a different phase for each path. This means that the Doppler spread will also change because the velocity in the direction of each path will change.

After the results at the three distances are analyzed, the values of Doppler spread increase slightly, approximately $2 \sim 3$ Hz as the antenna separation distance increases. The rms Doppler bandwidth also increases. This is true when a line of sight path exists. No significant changes are observed for a non line of sight path though the rms Doppler bandwidth increases a little bit. Particularly in one case (distance is 10 meters), it increases dramatically. The rms Doppler bandwidths at two different receiver moving speed are about same. Figure 5.6 shows the Doppler spectrum for a 10 meter antenna separation distance with non line of sight path. From this figure, except for the main spectral peaks around 60 Hz there are two peaks around ± 500

Table 5.3 Doppler Spread for a 5 meter antenna separation distance with NLOS path at a receiver moving speed of 1.36 m/s in a hallway

Frequency $[GHz]$	*Theoretical* $B_d[Hz]$	*Measured* $B_d[Hz]$	*rmsDoppler bandwidth*$[Hz]$
14.00	126.9	107.2	48.1782
14.05	127.4	108.4	50.3202
14.10	127.8	107.2	51.1664
14.15	128.3	105.2	47.7548
14.20	128.7	106.4	49.6176
14.25	129.2	106.0	50.4177
14.30	129.7	109.2	51.6594
14.35	130.1	106.4	49.5023
14.40	130.6	106.0	49.2339
14.45	131.0	106.0	51.1096
14.50	131.5	108.4	51.8348

Hz and one around +420 Hz with relative strong powers. This phenomenon can be explained as the signal reflects back to the transmitter, which then reflects it to the receiver as explained in [31]. The power of reflected signal is relative strong compared to the power of signal which is directly received by the receiver when the transmitter and receiver separation distance increases to 10 meters. If the path losses of reflected signal are fairly large, these surplus peaks will not be seen in Doppler spectrum.

The data listed in Table 5.3 presents the results of the 5 meter antenna separation with NLOS path. The Doppler spread when there is a line of sight path is larger than the one when there is no line of sight path. The wider NLOS spectrum shown in Figure 5.7 is caused by many reflections arriving from different angles. Intuitively, this is to be expected since NLOS propagation is measured at the corners of hallways

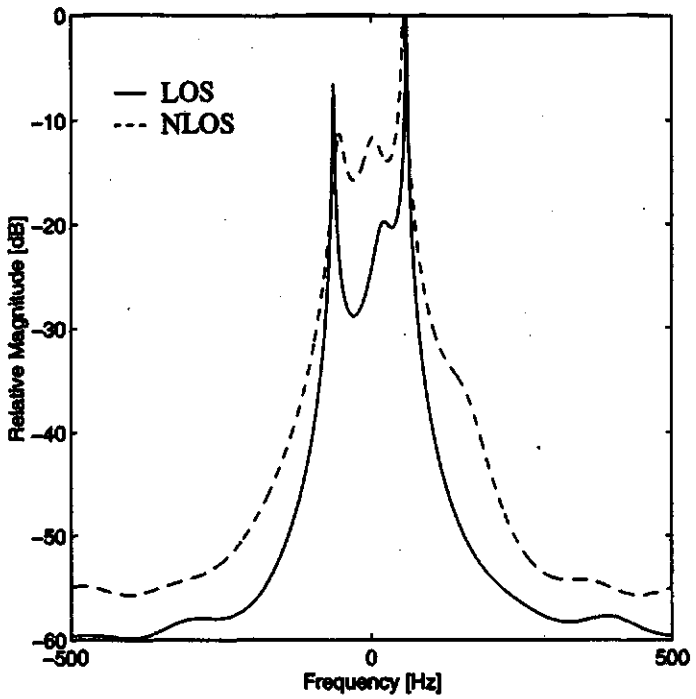

Figure 5.7 Doppler spectrum for LOS path and NLOS path at a carrier frequency of 14 GHz, a 5 meter antenna separation distance, and a receiver moving speed of 1.36 m/s in a hallway

where one of hallway walls is made of steel. There are some variations which are discussed in the next section.

5.3.3 Dependence of Doppler Spread on Environments

The materials of the walls such as brick, metal, wood and concrete have different reflection coefficients, therefore the Doppler spread also depends on the materials of wall. But the materials of wall are not concerns here. Different environments are referred to the structure of the measurements where they were taken. For example, the measurements were taken in a hallway or in an open area.

Table 5.4 lists the Doppler spread and the rms Doppler bandwidth in an open area (the second floor of Agricultural Building) where the ceiling is high and only metal railings are near the measurement equipment. There are no big differences between

Table 5.4 Doppler Spread for a 5 meter antenna separation distance with LOS path in an open area

$B_d[Hz]$ $v = 1.36m/s$	f_n $[Hz]$	$B_d[Hz]$ $v = 1.09m/s$	f_n $[Hz]$
117.6	48.8431	88.8	34.6108
122.0	50.3590	94.0	39.3111
119.2	44.7804	90.0	35.0508
116.8	46.8924	91.6	35.3090
119.6	45.3285	91.6	35.0052
117.6	43.1218	90.0	33.2928
115.2	41.9531	88.8	32.7300
117.2	41.4734	88.8	31.4840
122.0	41.9108	92.8	32.4293
124.4	43.4723	91.6	32.4242
125.2	47.2476	92.4	35.3120

the Doppler spread of a hallway in Table 5.1 and Table 5.2 and the Doppler spread of an open area in Table 5.4, but a large difference is observed in terms of the rms Doppler bandwidth f_n. About 10 Hz difference exists in terms of f_n between these two environments. This can also be seen from their spectrum in Figure 5.8.

The spectrum in an open area is not as peaky as one in a hallway. This may be explained as the number of multipaths in an open area is relatively small. In order to verify this result, the measurements were taken in the Tractor Lab which has high ceilings and fairly open spaces. The Doppler spread and the rms Doppler bandwidth obtained in this case are consistent with those in Table 5.4.

It is worthwhile to mention that the Doppler spread heavily depends on antenna positions and environments. As discussed in the last three sections, the measurements

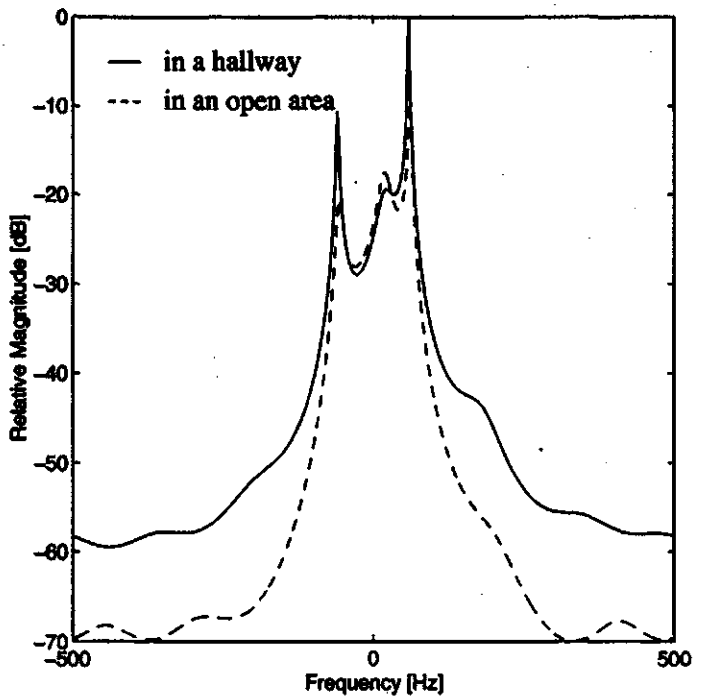

Figure 5.8 Doppler spectrum in different locations for LOS at a 5 meter antenna separation distance and a receiver moving speed of 1.36 m/s at 14 GHz

were carried out at the corners of hallways when there was no line of sight path. In these measurements, the transmitter antenna faced walls which are not far from it. This is one of typical positions of antennas in an indoor environment. However, measurements should be taken at as many different areas as possible so that better statistics of the Doppler spread could be obtained.

Measurements were also taken at an intersection of a very long hallway where there was no line of sight path. Only a small room separated the transmitter and the receiver with a 10 meter separation distance. The Doppler spread is smaller than the one with line of sight path, but the difference is also small. The rms Doppler bandwidths at two different receiver moving speeds tends to be close even though the Doppler spreads for these two situations depend on their own speeds. Again the surplus perks are observed in their spectrum. These peaks are around ± 350 Hz and

+450 Hz.

5.3.4 Effects of Moving People on Doppler Spread

In part two of the measurement goals, the measurements were taken when moving people were around the receiver. Motion of people causes fading in the indoor channel. It is also referred to as temporal variations of the indoor channel. The data can be used to supplement impulse responses which were taken under assumptions of some forms of stationarity of the channel. When no moving objects are around the transmitter and receiver, only noise will be present in the channel.

Moving people may have greater or lesser effects on the Doppler spread, which depends on the distance from people to the receiver and some other factors. Also, the number of people around the receiver is one of the factors which is related to the Doppler spread. Examples of CW temporal envelope fading are shown in Figure 5.9 and Figure 5.10. Magnitudes are normalized to their mean values. In these two figures, random movements of people around the receiver antenna cause variations even though both antennas are stationary.

Obviously, the more the people around the receiver antenna, the greater are the variations. The results presented in the literature [21] shows that temporal variations increase when the number of people around the receiver increases from 1 to 2, and from 2 to 3. However, changes were less noticeable for increase from 3 to 4 persons. Comparing Figure 5.9 to Figure 5.10 reveals that temporal variations increase when the number of people increases from 1 to 2. The corresponding Doppler spread increases from 2.4 $\sim$ 5.2 Hz to 6.8 $\sim$ 7.6 Hz with LOS path. This is also true when there is no line of sight path. The Doppler spread varies from 5.2 $\sim$ 12 Hz to 6.4 $\sim$ 16 Hz when the number of people increases. Figure 5.11 shows the Doppler spectrum when there are one or two persons around the receiver with LOS path.

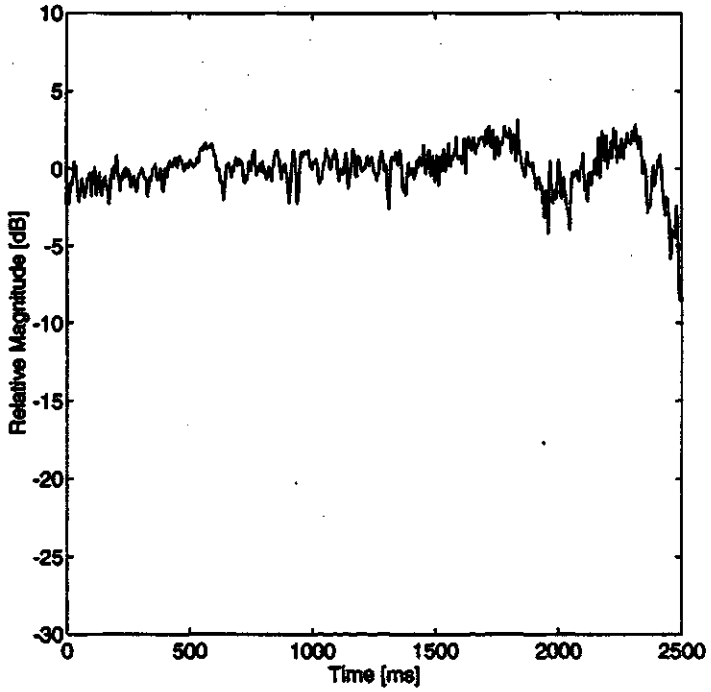

Figure 5.9 Temporal CW envelope fading for a hallway at a carrier frequency of 14 GHz, 5 meter antenna separation distance, and LOS path, one person around the receiver

5.4 3 dB Doppler Spread Bandwidth

The Doppler spread is important in determining the minimum signaling rate for coherent detections [11]. The 3 dB width of the time correlation function is related to the coherence time of the channel. The time correlation function was given in (4.3). Figure 5.12 shows the autocorrelations for even numbered frequencies in Table 5.1 and Table 5.2. The correlation function is normalized so that the value at the zero lag will be 1. Before performing the complex autocorrelation on time profiles, the DC component of each profile has been removed.

The simplest way to obtain the 3 dB width of the time correlation function is to find the corresponding time at the correlation value of 0.707. Thus, the 3 dB width of the time correlation function is around 4 ms for the high receiver moving speed and

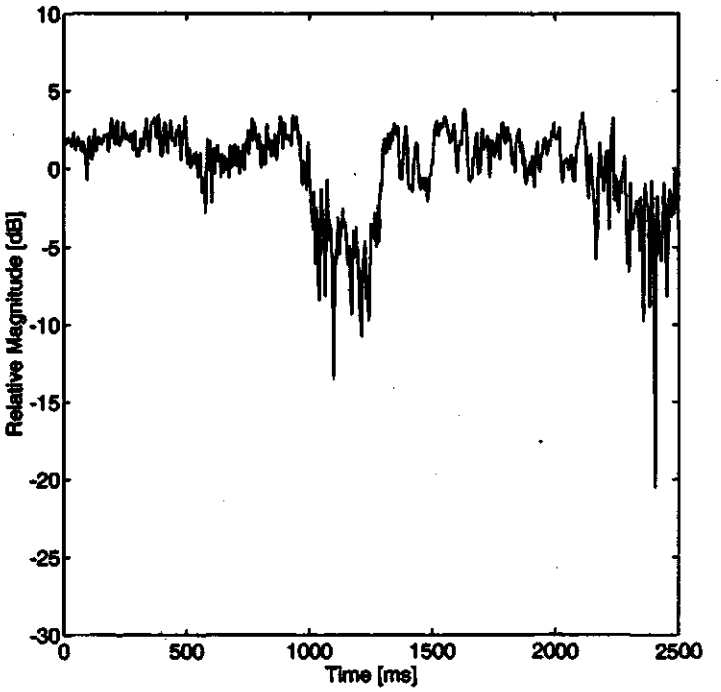

Figure 5.10 Temporal CW envelope fading for a hallway at a carrier frequency of 14 GHz, 5 meter antenna separation distance, and LOS path, two persons around the receiver

5 ms for the low speed. Then, the coherence time of the channel can be estimated by doubling the 3 dB width, that is, about $8 \sim 10$ ms. The theoretical calculations are 8.3 ms and 10.7 ms at the frequency 14 GHz [4].

5.5 Results of Distribution Fittings

In this section, the distribution fitting results of the measured data are presented and compared in different measuring conditions. The goodness fit testing results will be discussed, and the best fit distribution will be determined.

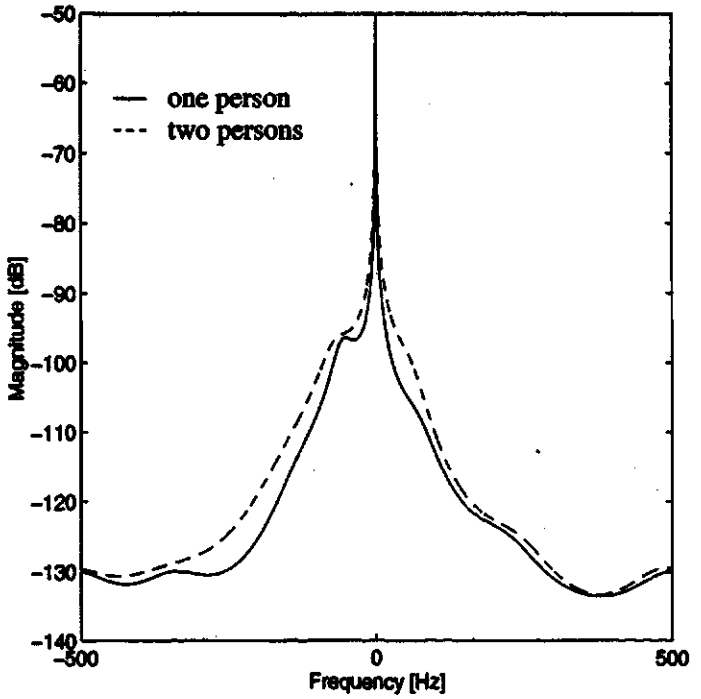

Figure 5.11 Doppler spectrum at a carrier frequency of 14 GHz for different number of people around the receiver in a hallway

5.5.1 Estimated Distribution of Envelope Fading for LOS Path

The distribution fitting procedure was performed on all the measurement data. Based on a review of the literature, the distributions used here are Rician, Rayleigh, Lognormal, and Weibull. Their theoretical cumulative distribution functions (cdf) and probability density functions (pdf) were presented in chapter 4, as well as the estimation methods.

If a strong signal component exists in the channel, the distribution can be modeled as Rician. Otherwise, this multipath channel is well known as a Rayleigh fading channel. As mentioned in chapter 2, for rapid fading, the Rayleigh distribution provided a good fit to the data. But, if the power fluctuations are small, the Rayleigh distribution is no longer a close fit. It has been suggested that the Suzuki distribution

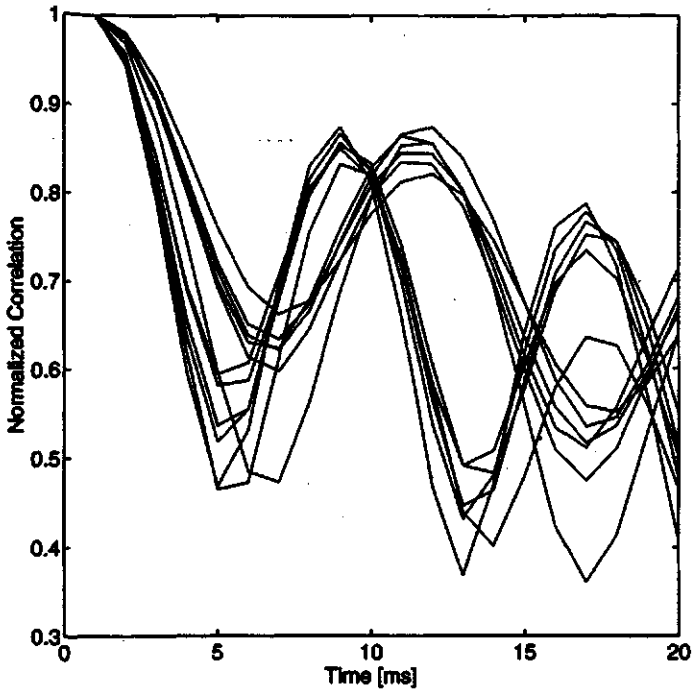

Figure 5.12 The 3 dB width of the time correlation function for a 5 meter antenna separation distance with LOS path in a hallway

is the best fit for VHF and UHF mobile communications in built-up areas and forests while the Weibull distribution is appropriate when a line of sight path exists [3]. It may be appropriate that a certain distribution or a combination of two distributions is the best fit to a particular propagation behavior. Also, the geometry and layout of the measuring area have a strong influence on the distribution of the envelope fading.

The distribution fitting was performed on all measurements on a linear scale. The processing programs were written using MATLAB. The procedure is as follows:

Step one: Normalize each envelope fading to its mean value on a linear scale.

Step two: Sort the magnitudes in each profile in ascending order.

Step three: Use the above data which stands in an ascending order to calculate the practical cumulative distribution function. For the n^{th} magnitude value, the

probability of the magnitude less than this value will be $\frac{n}{N}$, where N is the total number of points in a profile.

Step four: Utilize the estimators for Rician, Rayleigh, Lognormal and Weibull distributions described in Chapter 4 to estimate their parameters.

Step five: Plot the cdfs for visual inspection.

Step six: Perform goodness of fit tests to each distribution, and determine which one is the best fit to the data.

Following this procedure, the parameters of each distribution were calculated. The cumulative distribution and probability distribution of each candidate along with the empirical distribution are plotted in Figure 5.13 and Figure 5.14, respectively. The relative path strength on a linear scale is used in these figures. The K-S test values are also listed in Figure 5.13.

The testing results from these figures shows that the best fit distribution is Rician although Rayleigh and Weibull also pass the K-S test with the confidence level of 90%. The Chi-Square test will be used and combined with the K-S test to determine which one is the best fit for the empirical data when more than one distribution passes the K-S test. The Rician distribution has the smallest K-S value among them. It also gives the smallest value of the Chi-Square test. But this is not always true.

The K-S critical values are 0.0244, 0.0272 and 0.0326 for the confidence level of 90%, 95% and 99%, respectively. Such a confidence level is not easy to achieve due to the large number of points in a sample time profile ($N = 2501$). If the data is first binned to reduce the number of points, it will definitely be much easier to reach this goal [21] because the K-S critical value is related to the sample points. However, the unbinned data was used here to perform the distribution fitting procedure on the envelope fading of time profiles in the indoor environment while the receiver is

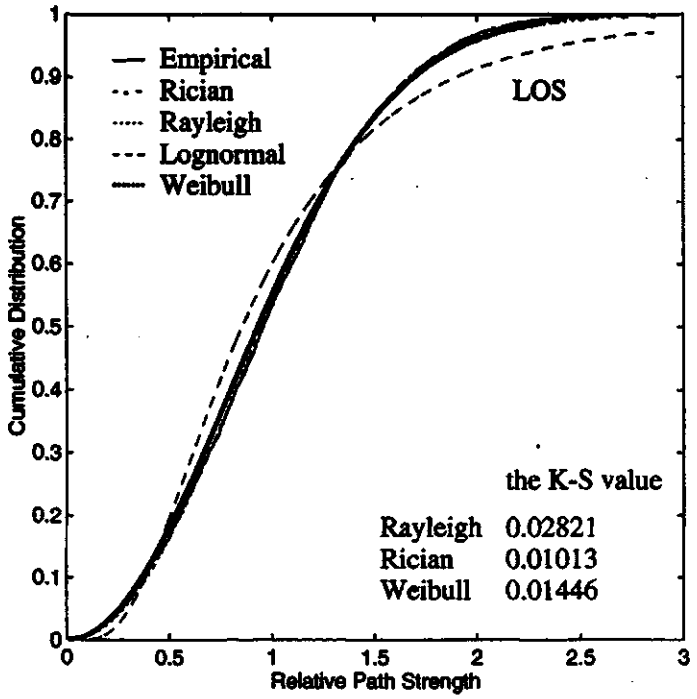

Figure 5.13 Theoretical and practical distributions (cdf) on a linear scale for a carrier frequency of 14.1 GHz and a 5 meter antenna separation distance with LOS path in a hallway

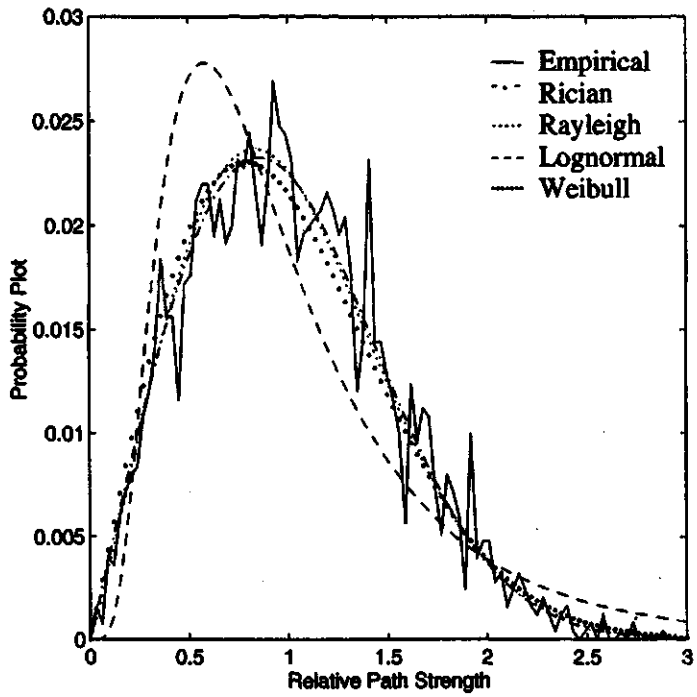

Figure 5.14 The pdfs corresponding to Figure 5.13

moving with LOS and NLOS paths.

After the distribution fitting results are examined, the statistics reveal that the Weibull distribution provides the best fit for the data for almost all LOS cases, that is, over 95% of the data passes the K-S test with the confidence level of 90%. With the same confidence level, 75% of cases are good fit for the Rician distribution. The Rayleigh distribution shows the best fit for only 54.5% of cases. It should be mentioned that a few cases pass the K-S test with a higher confidence level for Rician and Rayleigh distributions. If the distribution with the smallest K-S value is selected as the best fit for the data, then 48.3%, 39.8% and 9.7% are good fits for the Rician, the Weibull and Rayleigh distributions, respectively. Only 2.3% of the cases have not passed the K-S test at any of three confidence levels. If the Weibull distribution is eliminated from the candidate distributions, 71.5% of the cases are good fit for the Rician distribution, and about 21% for the Rayleigh distribution. The remaining cases have not passed any level of K-S test. The Lognormal distribution provides the poorest fit for all data using the K-S test, not even a single case passes the K-S test.

Using the Chi-Square test, 37.5% of the envelopes follow the Rician distribution, and the Weibull distribution provides good fit to 53.4% of the cases. Only 9.1% of the data is a good fit for the Rayleigh distribution. If the Weibull distribution were not a candidate, Rician and Rayleigh would split the percentage of the Weibull distribution, and end up with about 70% of the cases for the Rician distribution and 30% for the Rayleigh distribution. Then 74.5% of the cases fits to the Rician distribution, and 26.5% for the Rayleigh distribution. The Rayleigh distribution is a special case of Weibull distribution with $\beta = 2$. From Table B.3 in Appendix B, the value of β is around 2 between 1.8 and 2.3. The variance of β varies from 0.01 to 0.04. These differences are very small. This is the reason that these three distributions can not be easily distinguished by visual inspections as shown in Figure 5.13 and Figure 5.14.

The parameters of each distribution are listed in Appendix B. The α (the nor-

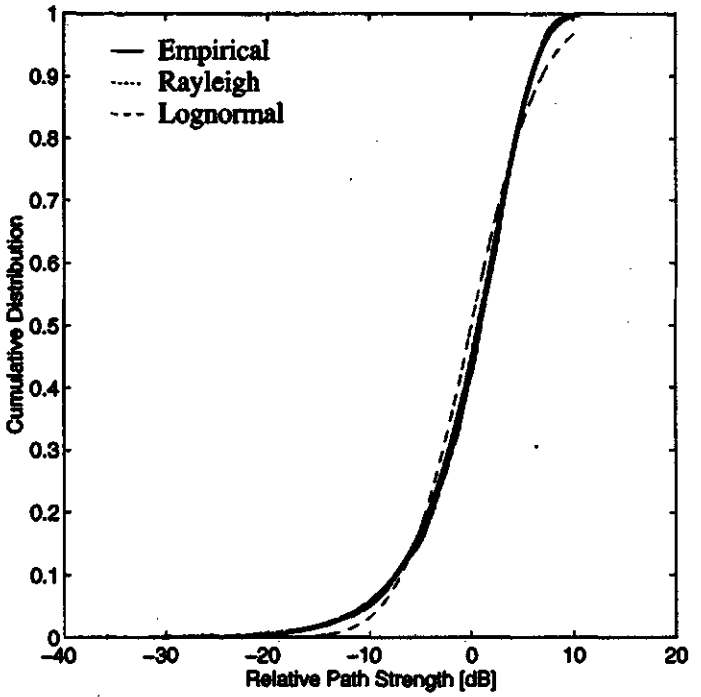

Figure 5.15 Theoretical and practical distributions (cdf) on a log scale corresponding to Figure 5.13

malized magnitude of the strong component) in the Rician distribution is about 0.7. The corresponding test results using the K-S and Chi-Square test are also included in Table B.1 and Table B.2 of Appendix B.

Based on the above analysis, the distribution fitting results depend on the goodness of fit testing methods. Using the K-S test method, the Rician distribution provides the best fitting results for the data. Using the Chi-Square test, the best fitting distribution is the Weibull distribution. Overall the results show that the Rician distribution fits the data more closely than the Rayleigh distribution. It concludes that the Rician distribution is the best fit. The distribution fitting discussed above is performed on a linear scale. If the procedure is performed on a log scale, the candidates will only be the Rayleigh and Lognormal distributions due to the mathematical complexity of the Rician and Weibull distributions. Figure 5.15 shows the cumulative distribution on a log scale for the same set of data used in Figure 5.13.

5.5.2 Estimated Distribution of Envelope Fading for NLOS Path

The cellular mobile station channel typically consists of the Rayleigh faded components if there are no line of sight received signal components. In an indoor environment, the CW measurements taken by some investigators [21] showed the fading statistics was Rayleigh while the transmission path was obstructed by human bodies.

In the last section, the results showed that the Rician distribution was a good fit for the measurements in an indoor environment with presence of a line of sight path. It is expected based on the literature that the Rayleigh distribution should be the best fitting distribution for NLOS. This is not the case for this data, the results of which are presented now.

The K-S test results of the distribution fitting of the data which was taken while there was no line of sight path in the channel shows that 84.8%, 50.9% and 25.8% of the cases pass the K-S test with any one of three confidence levels for the Weibull, Rayleigh and Rician distributions, respectively. Comparing with their counterpart LOS data, these numbers are quite low. Further analysis reveals that the Weibull distribution gives the smallest K-S value at the average percentage of 69.7. Following the Weibull distribution, the Rayleigh and Rician distributions have the smallest K-S value for about 6.8% and 10.6% of the cases. A relatively high percentage of the data, 12.9%, has not passed the K-S test at any level. This means that the Weibull distribution provides the best fit for the measurements in an indoor channel without line of sight paths. However, 30.4% of the cases which give the smallest K-S value is close to the Rayleigh distribution compared to the Rician distribution with only 17.4%. As a result, the Rayleigh distribution is better fit for the data at the measuring condition without LOS paths than the Rician distribution. Figure 5.16 presents one of the distribution fitting results under this measuring condition.

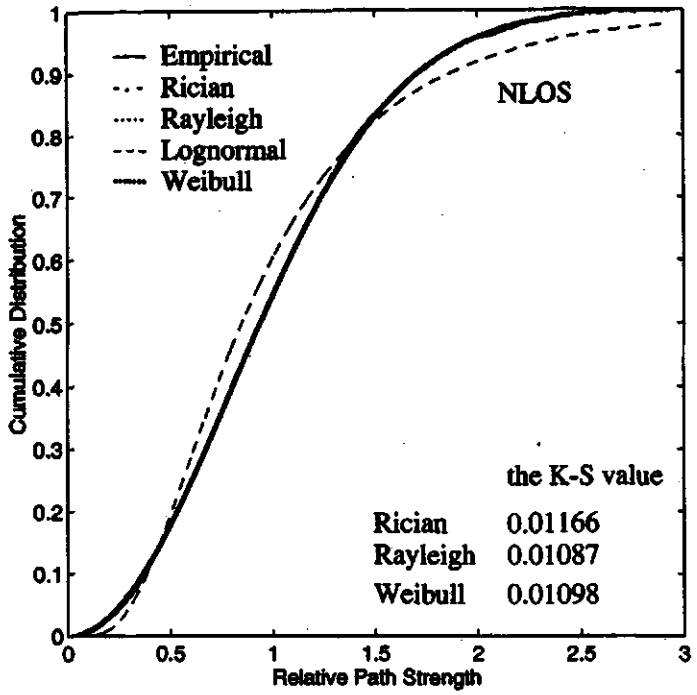

Figure 5.16 Theoretical and practical distributions (cdf) on a linear scale for a carrier frequency of 14.5 GHz and a 7.5 meter antenna separation distance with NLOS path in a hallway

The Chi-Square test gives similar results. The Weibull distribution is a good fit for 87.9% of the cases, the Rayleigh and Rician distributions are good fit for 5.3% and 6.1% of all cases. If the Weibull distribution was not considered, 92.2.8% of its cases would be a better fit to the Rayleigh distribution, 7.8% of them would be good fit to the Rician distribution. Therefore, about 86.3% of the cases are fit to the Rayleigh distribution, 13% of the cases are a close fit to the Rician distribution. Around 0.8% of the cases would be good fit for the Lognormal distribution.

Summarizing the above analysis and discussions, the Weibull distribution provides the best fit for the data which was taken when there was no line of sight path between the transmitter and receiver. The values of β of the Weibull distribution in Appendix B have a large variation range from 1.6 to 2.4 because of increasing path losses and noise levels compared to the signal levels under this measuring condition.

The Rayleigh distribution is closer fit to the data than the Rician distribution.

5.5.3 Estimated Distribution of Envelope Fading for the Temporal Variations Caused by Moving People

The statistics of the temporal envelope fading in an indoor channel were given by one researcher [21]. It was found that for linear scale distribution fittings, the Weibull distribution provides the best fit for most cases. But, different results were presented by some other investigators [10].

In this work, a small number of profiles in one location at several different antenna positions were taken. The distribution fitting results show that the Lognormal fit is the best without any exception. The test method used is the Chi-Square test. The cdfs can be seen in Figure 5.17. The Rician distribution is far away from the empirical distribution, and thus not shown in this figure.

5.5.4 Dynamic Range and Level Crossing Rate

The range of the envelope fading of each time profile will be discussed first. The mean level of the signal varies about 6 dB among the three antenna separation distances with LOS paths in a hallway. This number increase to 10 dB for NLOS cases. The magnitude variation in dB ranges from 35 to 60 dB for all LOS and NLOS measurements observed. The maximum value of fading in temporal variations data that was taken with moving people around the receiver is about 20 dB, which is relatively small compared to 60 dB. However, comparing the magnitude of 5m LOS data in a hallway to the corresponding data in an open area, path losses are bigger in an open area. This difference in dB ranges from 3 to 10 dB. This is because the lengths of paths in an open area are longer, the losses of paths increase with the length of a path.

The envelope fading is directly related to the performance of the radio receivers.

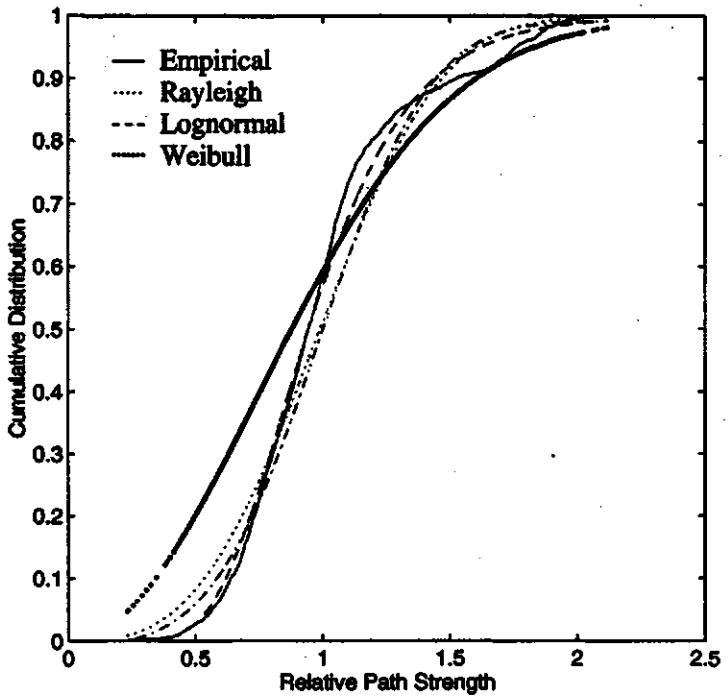

Figure 5.17 Theoretical and practical distributions (cdf) of temporal variations on a linear scale for a carrier frequency of 14 GHz, a 7.5 meter antenna separation distance with LOS path, and one moving person

The level crossing rate is often used as a parameter in envelope fading statistics to describe the average rate at which the envelope crosses a given signal level. Only the positive slopes were calculated for the number of times that the signal crosses a threshold from -25 to +10 dB. The value of a threshold is relative to the envelope mean. This number is normalized to the number of sample points. The results for one of measurements is plotted in Figure 5.18. As can be seen in this figure, at the transmit frequency f = 14 GHz, a receiver moving speed of 1.36 m/s, and the theoretical Doppler shift f_d=63.5 Hz, the level crossing rate is 148 per second at the threshold of -3 dB. This is reduced to about 2 times per second with the threshold of -25 dB. The -3 dB level crossing rates for all the data are listed in Table C.1 in Appendix C. The overall conclusion is that the level crossing rate depends on the

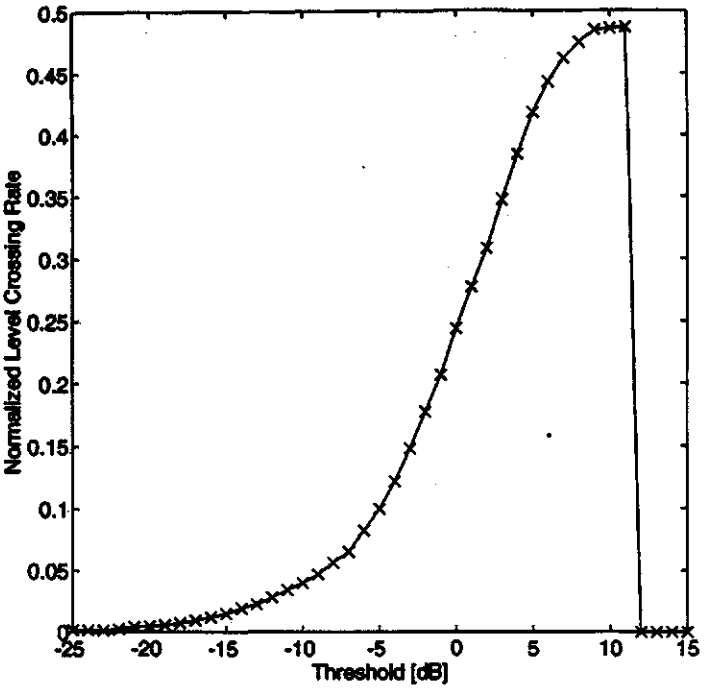

Figure 5.18 The level crossing rate for a carrier frequency of 14 GHz and a 5 meter antenna separation distance with LOS path

receiver moving speed. The bigger the speed is, the higher the level crossing rate is. This is true, as the level crossing rate is directly related to the maximum Doppler spread [3]. The maximum Doppler spread is proportional to the receiver moving speed and the transmit frequency. The level crossing rate is also sensitive to the environment. In a particular location, where the materials of one side wall of the hallway is concrete, and the other side wall is occupied by metal lockers and the wall is also metal, the level crossing rates are higher than those in other locations at the corresponding antenna separations and positions. This indicates that metal lockers make the envelope of time profiles fade more rapidly due to the different reflection coefficients.

Fading statistics of the indoor channel can be described by the fading duration, which is the duration of time that the signal is below a given level. The average

duration of fades below a specified level can be calculated by the probability of the envelope fading below this level over the level crossing rate. It is not difficult to calculate the fading duration. The average fading duration below the threshold - 3dB is 1.6 ms with LOS paths for the level crossing rate of 148 per second in Table C.3 of Appendix C

In this chapter, the analysis results based on the measurement time profiles were presented and discussed. The statistics of the Doppler spread and envelope fading are the main topics of this chapter. Those statistics can be used in modeling and characterizing the indoor channel, and the channel model is very useful in designs of indoor communications systems.

6. Conclusions

The indoor radio channel experiences two types of fadings. One is the time dispersive multipath fading, and the other is the fading caused by moving objects. In this work two issues relating to the second type of the fading were addressed: the Doppler spread and the envelope fading distribution. Some analysis results for the Doppler spread and the envelope fading were presented. Those results can be used in future designs for wireless communications systems.

The maximum Doppler spread mainly depends on the transmit frequency and the receiver moving speed when a single tone was transmitted over the channel and the receiver was the only moving source. Measurements were taken at different transmit frequencies, receiver moving speeds, antenna positions, and environments to study the effects of measurement conditions on the Doppler spread. It is found that the Doppler spread is related to not only the above two factors, but also the antenna separation distance and position (LOS path exists or not), and the environment (for example, a hallway or an open area). The value of the Doppler spread varies from 119 to 130 Hz for a receiver moving speed of 1.36 m/s and from 92 to 102 Hz for a speed of 1.09 m/s for a LOS path. For NLOS measurements, the value of the Doppler spread is less than the one for LOS by about $2 \sim 15$ Hz with the same antenna separation distance in hallways.

Based on measured time profiles, the values of the Doppler spread were obtained using the AR spectral estimation method. The AR model used here is a tool to calculate the Doppler spread of the indoor channel. Comparing this method to the FFT method, shows that it has a better resolution and smoother spectrum.

The envelope fading in an indoor channel is modeled using either a Rician or Rayleigh distribution, depending on whether a LOS path is present or not. The distribution fitting procedure was performed on all the measurement data. The best fit distribution was determined by using the K-S or Chi-Square goodness test method. The results showed that the Rician distribution was the best distribution fit to the data while there was a line of sight path in the channel, and the Weibull distribution was the best fitting distribution for NLOS data.

Compared to the effect of the moving receiver, the temporal variations caused by the moving people are not significant. The value of the Doppler spread is less than 20 Hz for two moving people around the receiver. The envelope fading distribution results showed that the Lognormal distribution is the best fit.

In this work, temporal variations in an indoor channel were measured. The rate of temporal variations is a function of the velocity and geometry of the receiver/objects and the carrier frequency. On the other hand, although many models have been used to characterize the indoor radio channel, most of these models do not take into account temporal variations in the channel. Integrated static measurements (the time-invariant impulse response $h(t)$) and temporal measurements (the time profile $H(f_c; t)$) of the channel will lead to a more accurate and realistic model of the channel, which includes the time dimension in it. However, the method for modification of the time-invariant impulse response models using temporal variations information from the CW fading measurements is unknown. If static measurements can be taken at close separations (less than 2 mm), temporal variations caused by the moving receiver can be predicted based on the quantified correlations. Quantifying correlations should be the next step in this work.

References

[1] R. Braham, "Prolog to: The indoor radio propagation channel," in *Proceedings of the IEEE*, vol. 81, pp. 941–942, 1993.

[2] D.Molkdar, "Review on radio propagation into and within buildings," *IEE Proceedings Part H*, vol. 138, pp. 61–73, February 1991.

[3] P. J. B. Clarricoats and J. R. Y. R.-S. Wait, eds., *Radiowave propagation*. London, United Kingdom: Peter Peregrinus Ltd., 1989.

[4] J. G. Proakis, *Digital Communications*. New York: McGraw-Hill Book Company, 1989.

[5] M. C. Jeruchim, P. Balaban, and K. S. Shanmugan, *Simulation of Communication Systems*. New York: Plenum, 1992.

[6] H. Hashemi, "Impulse response modeling of indoor radio propagation channels," *IEEE Journal on Selected Areas in Communications*, vol. 11, pp. 967–978, September 1993.

[7] R.Ganesh and K. Pahlavan, "Statistical modeling and computer simulation of the indoor radio channel," in *IEE Proceedings Part I*, vol. 138, pp. 153–161, June 1991.

[8] A. A. M. Saleh and R. A. Valenzuela, "A statistical model for indoor multipath propagation," *IEEE Journal on Selected Areas in Communications*, vol. SAC-5, pp. 128–137, February 1987.

[9] R. J. C. Bultitude, "Measurement, characterization and modeling of indoor 800/900 MHz radio channels for digital communications," *IEEE Communications Magazine*, vol. 25, pp. 5–12, June 1987.

[10] H. Hashemi, "The indoor radio propagation channel," in *Proceedings of the IEEE*, vol. 81, pp. 943–967, July 1993.

[11] S. Stein, "Fading channel issues in system engineering," *IEEE Journal on Selected Areas in Communications*, vol. SAC-5, pp. 68–89, February 1987.

[12] R. J. C. Bultitude, S. A. Mahmoud, and W. A. Sullivan, "A comparison of indoor radio propagation characteristics at 910 MHz and 1.75 GHz," *IEEE Journal on Selected Areas in Communications*, vol. 7, pp. 20–30, January 1989.

[13] P. Yegani and C. D. McGillem, "A statistical model for the factory radio channel," *IEEE Transactions on Communications*, vol. 39, pp. 1445–1454, October 1991.

[14] R.Ganesh and K. Pahlavan, "Statistics of short time and spatial variations measured in wideband indoor radio channels," in *IEE Proceedings Part H*, vol. 139, pp. 297–302, October 1993.

[15] S. S. Haykin, *Adaptive Filter Theory.* Englewood Cliffs, N.J.: Prentice-Hall, 1986.

[16] S. M. Key, *Modern Spectral Estimation: Theory and Application.* Englewood Cliffs, N.J.: Prentice-Hall, 1988.

[17] S. L. Marple, *Digital Spectral Analysis: with applications.* Englewood Cliffs, N.J.: Prentice-Hall, 1987.

[18] S. J. Howard and K. Pahlavan, "Autoregressive modeling of wide-band indoor radio propagation," *IEEE Transactions on Communications*, vol. 40, pp. 1540–1552, September 1992.

[19] G. Morrison and M. Fattouche, "Super resolution modeling of the indoor radio propagation channel," in *Proceedings of Wireless'93*, (Calgary, AB), pp. 383–391, July 1993.

[20] R.Ganesh and K. Pahlavan, "Statistical characterization of a partitioned indoor radio channel," in *IEE Proceedings Part I*, vol. 139, pp. 539–545, October 1992.

[21] H. Hashemi, M. McGuire, T. Vlasschaert, and D. Tholl, "A study of temporal variations of the indoor radio propagation channel," tech. rep., Telecommunication Research Laboratories, 1993.

[22] D. I. Laurenson, A. U. H. Sheikh, and S. McLaughlin, "Characterization of the indoor mobile channel using a ray tracing technique," in *1992 IEEE Int. Conf. Selected Topics in Wireless Communication*, (Vancouver, B.C), pp. 65–68, June 1992.

[23] D. M. J. Devasirvatham, "Multipath time delay spread in the digital portable radio environment," *IEEE Communications Magazine*, vol. 25, pp. 13–21, June 1987.

[24] S. Howard and K. Pahlavan, "Doppler spread measurements of indoor radio channel," *Electronics Letters*, vol. 26, pp. 107–109, January 1990.

[25] P. A. Sharples and M. J. Mehler, "Propagation modeling in microcellular environments," in *Eighth International Conference on Antennas and Propagation*, vol. 2, (Edinburgh, UK), pp. 68–71, April 1993.

[26] T. Lo, J. Litva, and H. Leung, "Estimating the impulse response of indoor radio channels using signal subspace techniques," *IEE Proceedings Part I*, vol. 140, pp. 203–210, June 1993.

[27] D.Tholl, M. Fattouche, R. C. Bultitude, P. Melancon, and H. Zaghloul, "A comparison of two radio propagation channel impulse response determination techniques," *IEEE Transaction on Antennas and Propagation*, vol. 41, pp. 515–517, April 1993.

[28] P. J. Cullen and P. C. A. M. Fannin, "Wide-band measurement and analysis techniques for the mobile radio channel," *IEEE Transactions on Vehicular Technology*, vol. 42, pp. 589–603, November 1993.

[29] D. A. Donald, "Measurement and modeling of the indoor radio propagation channel in the ku frequency band," Master's thesis, University of Saskatchewan, 1994.

[30] R. V. Hogg and E. A. Tanis, *Probability and Statistical Inference.* New York: Macmillan Publishing Co. Inc., 1983.

[31] A. R. Tharek, "Bit error rate measurements in the millimeter wave band about 60 Ghz," in *Proceedings of the Sixth International conference on wireless Communication*, vol. 1, (Calgary, AB), pp. 156–161, July 1994.

A. Doppler Spectrum

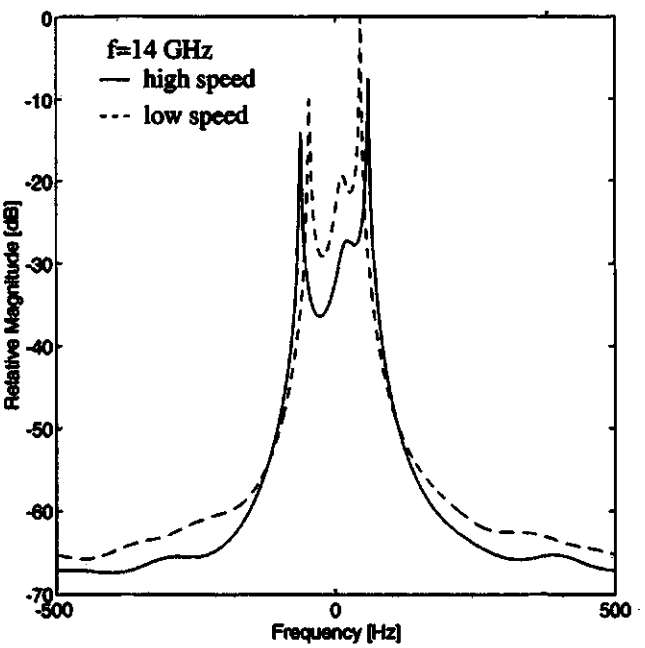

Figure A.1 Doppler spectrum for a 5 meter antenna separation distance and a carrier frequency of 14 GHz with a line of sight path at different speeds

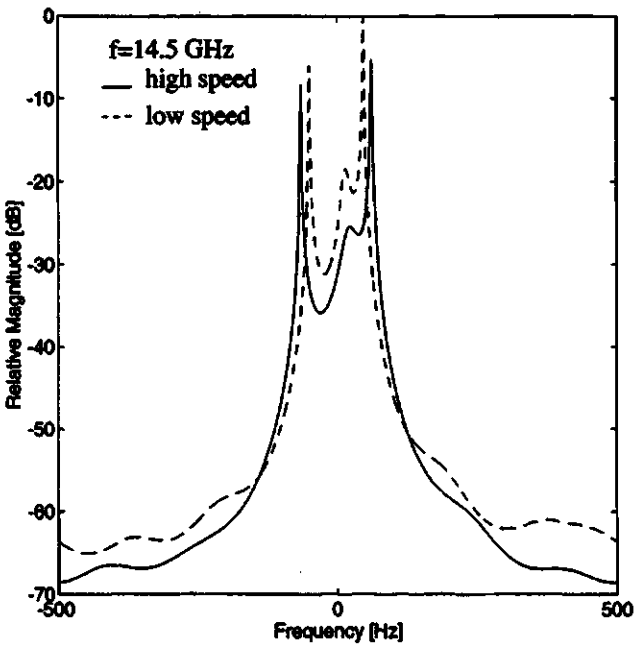

Figure A.2 Doppler spectrum for a 5 meter antenna separation distance and a carrier frequency of 14.5 GHz with a line of sight path at different speeds

B. Estimated Parameters and Test Results

Table B.1 Test results: 5m LOS path

Ray.	Rice	Wei.	Log.	Ray.	Rice	Wei.	Log.
00	10	11	00	00	10	11	00
11	11	10	00	10	11	10	00
10	11	10	00	10	10	11	00
10	11	10	00	11	10	10	00
10	10	11	00	10	10	11	00
00	11	10	00	00	11	00	00
00	00	11	00	00	11	10	00
10	10	11	00	00	11	10	00
10	10	11	00	00	10	11	00
10	10	11	00	10	11	10	00
10	00	11	00	10	10	11	00

Note that: The first number represents the K-S test and second one represents the Chi-Square test. A "1" means that this distribution passes the corresponding test. A "0" represents that it fails that test. The first four columns are the distributions of fading envelopes at the high receiver moving speed, and followed by the low speed.

Table B.2 Test results: 5m NLOS path

Ray.	Rice	Wei.	Log.	Ray.	Rice	Wei.	Log.
10	10	11	00	10	00	11	00
00	00	11	00	00	00	11	00
00	00	11	00	10	00	11	00
00	00	11	00	10	00	11	00
00	00	11	00	10	10	11	00
00	00	11	00	00	00	11	00
10	11	10	00	10	00	11	00
00	00	11	00	00	00	11	00
00	00	01	00	00	00	01	00
00	00	01	00	00	00	01	00
00	00	11	00	00	00	11	00

Table B.3 Estimated Distribution Parameters

Rayleigh	Rice		Weibull		Lognormal	
σ^2	α	σ^2	α	β	μ	σ^2
0.6124	0.7578	0.3253	0.7622	2.2339	-0.1386	0.3345
0.6316	0.5401	0.4858	0.7818	2.0393	-0.1681	0.4172
0.6227	0.6766	0.3939	0.7746	2.1166	-0.1567	0.3905
0.6303	0.5695	0.4682	0.7812	2.0481	-0.1656	0.4104
0.6309	0.5571	0.4757	0.7796	2.0500	-0.1551	0.3752
0.6222	0.6819	0.3897	0.7734	2.1263	-0.1591	0.3932
0.6594	0.8161	0.3264	0.8005	1.8525	-0.1863	0.4433
0.6264	0.6338	0.4256	0.7755	2.0909	-0.1541	0.3714
0.6291	0.5915	0.4543	0.7797	2.0599	-0.1617	0.3984
0.6308	0.5594	0.4743	0.7795	2.0516	-0.1595	0.3865
0.6437	0.8076	0.3176	0.7888	1.9551	-0.1724	0.4106
0.6167	0.7291	0.3509	0.7687	2.1782	-0.1483	0.3699
0.6258	0.6410	0.4204	0.7751	2.0971	-0.1583	0.3883
0.6288	0.5976	0.4503	0.7776	2.0698	-0.1584	0.3832
0.6449	0.8087	0.3186	0.7921	1.9387	-0.1739	0.4248
0.6289	0.5951	0.4519	0.7769	2.0710	-0.1522	0.3653
0.6157	0.7364	0.3445	0.7658	2.2000	-0.1490	0.3652
0.6085	0.7799	0.3045	0.7602	2.2735	-0.1397	0.3434
0.6162	0.7324	0.3480	0.7719	2.1679	-0.1528	0.3910
0.6217	0.6869	0.3858	0.7723	2.1307	-0.1494	0.3649
0.6314	0.5448	0.4831	0.7826	2.0370	-0.1679	0.4200
0.6312	0.5486	0.4808	0.7813	2.0427	-0.1640	0.4064
mean=0.6277	0.6632	0.4034	0.7773	2.0832	-0.1587	0.3888
var.=0.0001	0.0091	0.0042	0.0001	0.0093	0.0001	0.0007

C. Level Crossing Rate and Fade Duration

Table C.1 Level crossing rate at -3 dB threshold for all measurements at the high speed

148	146	180	147	148	151	174	159	145	152	152	138	178	148
158	153	173	156	144	156	153	156	148	165	165	143	160	152
154	150	169	157	144	154	158	171	150	155	155	153	179	164
152	148	166	170	158	160	158	166	152	150	150	154	162	159
143	139	166	149	142	152	175	146	164	152	152	152	157	151
152	142	174	160	154	147	172	162	156	152	152	157	154	147
160	147	163	161	146	151	151	148	160	156	156	156	164	152
152	157	162	152	159	139	153	170	150	152	152	150	157	135
154	160	160	170	148	140	176	164	153	151	151	153	159	138
162	161	161	150	147	152	173	154	165	164	164	146	165	152
159	141	174	152	149	155	148	156	158	154	154	144	174	154

The value in each column represents the level crossing rate of measurements in a location. The value in each row represents the level crossing rate of measurements at a frequency.

Table C.2 Level crossing rate at -3 dB threshold for all measurements at the low speed

137	138	166	148	140	157	154	141	141	137	154	147	163	147
146	148	155	158	142	149	151	143	156	150	165	142	155	151
145	134	154	153	139	150	158	161	151	138	145	148	160	160
149	146	139	155	151	140	148	157	160	152	135	152	174	144
147	130	132	134	134	157	173	143	155	152	140	151	167	138
149	143	139	153	133	143	152	151	151	149	148	152	156	140
133	142	155	141	133	143	136	130	158	141	144	155	168	144
136	146	140	149	140	142	160	145	129	159	153	152	164	124
137	152	148	151	150	139	154	142	151	149	140	154	166	130
149	141	152	143	141	135	160	150	139	150	154	158	191	138
148	145	162	145	148	146	142	147	154	152	148	161	166	138

Table C.3 Average fade duration at -3 dB threshold for all LOS measurements

1.5595	1.6913	1.3920	1.4701	1.6585	1.5968	1.4289	1.6181
1.5985	1.6214	1.4120	1.5064	1.6056	1.5630	1.4555	1.5231
1.5610	1.6117	1.5166	1.4082	1.6722	1.5755	1.3832	1.5374
1.6026	1.6226	1.4217	1.4906	1.6218	1.5675	1.3985	1.5745
1.6106	1.5948	1.4227	1.6425	1.6657	1.6457	1.4566	1.5549
1.6247	1.5887	1.3701	1.5564	1.6354	1.6240	1.3660	1.4827
1.5985	1.6332	1.4020	1.5373	1.6885	1.6349	1.4127	1.5799
1.5564	1.7526	1.4158	1.5711	1.6625	1.6628	1.3629	1.5600
1.5311	1.6625	1.4464	1.5189	1.7182	1.6610	1.2880	1.6058
1.4876	1.5856	1.3632	1.4521	1.6196	1.5722	1.3796	1.5547
1.6045	1.5710	1.4564	1.5910	1.5995	1.5891	1.4011	1.5923
1.6579	1.7507	1.5157	1.5730	1.6857	1.6199	1.5065	1.6714
1.7225	1.7601	1.6331	1.5533	1.6208	1.6515	1.5291	1.7143
1.6556	1.7113	1.6286	1.5326	1.7608	1.6489	1.4746	1.6617
1.6327	1.7088	1.5245	1.6005	1.6631	1.6848	1.4622	1.5445
1.6495	1.6554	1.4653	1.6078	1.7104	1.6735	1.5404	1.6844
1.6425	1.6723	1.5072	1.6084	1.7417	1.6145	1.4961	1.5491
1.6757	1.6958	1.5000	1.6544	1.7327	1.7059	1.4721	1.6636
1.6041	1.8324	1.5641	1.6381	1.7307	1.7163	1.5288	1.6749
1.6901	1.7342	1.4825	1.6323	1.7234	1.6839	1.4401	1.6451
1.6702	1.6997	1.5105	1.5391	1.6431	1.7604	1.5625	1.5851
1.6334	1.6022	1.5223	1.6309	1.6405	1.6274	1.5226	1.7038

Table C.4 Average fade duration at -3 dB threshold for all NLOS measurements

1.7080	1.6798	1.7139	1.7110	1.3919	1.6721
1.7378	1.6465	1.5833	1.7283	1.4525	1.6728
1.7005	1.5995	1.6572	1.7285	1.4474	1.5815
1.7474	1.6080	1.6330	1.6719	1.5246	1.6146
1.6650	1.6273	1.6388	1.5947	1.5663	1.6958
1.6240	1.6711	1.6704	1.6667	1.5078	1.7684
1.6817	1.6256	1.6114	1.6718	1.4499	1.6693
1.6835	1.6457	1.6282	1.6676	1.5995	1.6746
1.7337	1.5794	1.6605	1.6754	1.4422	1.7168
1.6320	1.6577	1.6500	1.7308	1.4393	1.7480
1.6886	1.6114	1.6762	1.7028	1.4633	1.7377
1.7139	1.6618	1.7409	1.7120	1.4570	1.6567
1.7282	1.6888	1.7046	1.7260	1.4755	1.6852
1.7434	1.7428	1.7383	1.7439	1.6209	1.6025
1.6800	1.7323	1.7219	1.7953	1.4529	1.6898
1.8454	1.6772	1.7257	1.6905	1.5287	1.6319
1.7692	1.7534	1.6981	1.7474	1.4653	1.7343
1.6768	1.6714	1.6482	1.6959	1.4071	1.7091
1.7523	1.7204	1.6606	1.7421	1.4780	1.7055
1.7719	1.7634	1.7094	1.7995	1.4155	1.7485
1.7500	1.6907	1.7195	1.7443	1.2872	1.6957
1.7195	1.7316	1.6911	1.7363	1.4227	1.7014

D. MATLAB and BASIC Programs

This appendix contains two MATLAB programs. One is used to estimate the Doppler spread B_d. The other is used to fit distributions. The BASIC program is used to control the network analyzer and the measurement process.

D.1 The Program for Calculating the Doppler Spread

```
% This program is used to estimate the Doppler spread.

% Read the .mat file to the variable man_bt.
input_path='/home/bai/data/jun9/';
k=input('Which set of data do you want to process?');
cor_chank=['cor_chan' int2str(k)];
filename=[input_path,cor_chank];
eval(['load ' filename])
man_bt=eval(cor_chank);

% Plot the magnitude of time profiles in dB.
lom_b=20*log10(abs(man_bt));
subplot(211),plot(lom_b);grid
xlabel('Time[ms]');ylabel('Magnitude[dB]')

% Using function fre_ar_est to estimate the Doppler spread. This
% function contains the ar(.) function to calculate the
% parameters of the AR model.
order=8;                          % the AR model order
```

```
x_t=fre_ar_est(man_bt,order);
x_t=10*log10(x_t);
xmax=max(x_t);

% Calculate the Doppler Spread
[ma1,mb1]=max(x_t(1:1250));      % find the negative frequency shift
[ma2,mb2]=max(x_t(1251:1600));   % find the positive frequency shift
B_spread=(mb2-mb1+1250)*.4       % the Doppler spread in Hz

f=-500:.4:500;                   % the Doppler frequency range
subplot(212),plot(f,x_t-xmax);grid
xlabel('Frequency[Hz]'),ylabel('Magnitude[dB]')
title('Doppler Spectrum')

% Calculate rms bandwidth of the Doppler Spread
x_t_n=(f.^2).*(10.0.^(x_t/10));
x_t_d=(10.0.^(x_t/10));
fn=sum(abs(x_t_n))/sum(abs(x_t_d));
fn=sqrt(fn)                      % the rms bandwidth in Hz
```

D.2 The Program for Envelope Fading Distributions

```
function [vv,mu,l_sigmas,w_beta,w_alpha,alpha,sigma]=curve_fitr(man_b)
% Fitting procedure begins.
% Sample data is normalized to its mean, then 0 - 3.0(normalized
% data range) is divided into 100 intervals.

ww=mean(man_b);                  % man_b is the magnitude
nor_mag=man_b/ww;                % step one: normalization
[n,m]=size(man_b);
```

```
r=sort(nor_mag);                % step two: sort magnitudes
y=0:1/2500:1;                   % step three: the practical distribution

% calculate the estimators of Rayleigh
vv=sum(nor_mag.^2)/(2*m);       % step four: parameter estimation
yr=cdfr(r,vv);

% Rice
save man_b man_b;
[yri,sigma,alpha]=cdR(r);

% Lognormal
mu=sum(log(nor_mag))/m;
l_sigmas=sum((log(nor_mag)-mu).^2)/m;
yl=cdfll(r,l_sigmas,mu);

% Weibull
w_beta=fzero('wei_est',2);
w_alpha=m/sum(nor_mag.^w_beta);
yw=1-exp(-w_alpha*(r.^w_beta));
!rm man_b.mat;

% step five: plot the final fitting results for visual inspection
clg;
plot(r,y,'-',r,yri,'-.',r,yr,'.',r,yl,'--',r,yw,':');grid
xlabel('Relative Path Strength');
ylabel('Cumulative Probability')

% step six: fitting tests
% Rayleigh
```

```
RDn=max(abs(y-yr));
dn=1.63/sqrt(m);
dn90=1.22/sqrt(m);
dn95=1.36/sqrt(m);
if RDn <= dn90
   fprintf('Rayleigh distribution passes the K-S test with a confidence
level of 90/100.\n');
   fprintf('the K-S value=%6.5f\n',RDn)
else if RDn <= dn95
   fprintf('Rayleigh distribution passes the K-S test with a confidence
level of 95/100.\n');
   fprintf('the K-S value=%6.5f\n',RDn)
else if  RDn <= dn
   fprintf('Rayleigh distribution passes the K-S test with a confidence
level of 99/100.\n');
   fprintf('the K-S value=%6.5f\n',RDn)
end
end
end

%lognormal
lDn=max(abs(y-yl));
if lDn <= dn
   fprintf('Lognormal distribution passes the K-S test with a confidence
level of 99/100.\n')
   fprintf('the K-S value=%6.5f\n',lDn)
end

%rician
rin=max(abs(y-yri));
```

```
if rin <= dn90
   fprintf('Rice distribution passes the K-S test with a confidence level
of 90/100.\n');
   fprintf('the K-S value=%6.5f\n',rin)
else if rin <= dn95
   fprintf('Rice distribution passes the K-S test with a confidence level
of 95/100.\n')
   fprintf('the K-S value=%6.5f\n',rin)
else if rin <= dn
   fprintf('Rice distribution passes the K-S test with a confidence level
of 99/100.\n')
   fprintf('the K-S value=%6.5f\n',rin)
end
end
end

%weibull
wDn=max(abs(y-yw));
if wDn <= dn90
   fprintf('Weibull distribution passes the K-S test with a confidence
level of 90/100.\n');
   fprintf('the K-S value=%6.5f\n',wDn)
else if wDn <= dn95
   fprintf('Weibull distribution passes the K-S test with a confidence
level of 95/100.\n')
   fprintf('the K-S value=%6.5f\n',wDn)
else if wDn <= dn
   fprintf('Weibull distribution passes the K-S test with a confidence
level of 99/100.\n')
   fprintf('the K-S value=%6.5f\n',wDn)
```

```
end
end
end

%Chi-Square tests l=50; r1=0:3/l:3; num=zeros(1,l+1); [n,m]=size(man_b);
for n=1:l
 I=0;
 I=find(r>(n-1)*3/l & r<n*3/l);
 num(n+1)=size(I,2);
end

% Rayleigh
pr=r1/vv.*exp(-r1.^2/(2*vv));
pp=sum(pr);
pr=pr/pp*m;
qr=sum(((num(2:l+1)-pr(2:l+1)).^2)./pr(2:l+1));

% rician
pr=r1/sigma.*exp(-(r1.^2+alpha^2)./(2*sigma)).*besseli(0,alpha*r1/sigma);
pp=sum(pr);
pr=pr/pp*m;
qri=sum(((num(2:l+1)-pr(2:l+1)).^2)./pr(2:l+1));

% lognormal
pr=[0(1/sqrt(2*pi*l_sigmas)./r1(2:l+1)).*exp(-(log(r1(2:l+1))-mu).^2/
   (2*l_sigmas))];
pp=sum(pr);
pr=pr/pp*m;
ql=sum(((num(2:l+1)-pr(2:l+1)).^2)./pr(2:l+1));
```

```
% weibull
pr=w_alpha*w_beta*(r1.^(w_beta-1)).*exp(-w_alpha*(r1.^w_beta));
pp=sum(pr);
pr=pr/pp*m;
qw=sum(((num(2:l+1)-pr(2:l+1)).^2)./pr(2:l+1));

if qr <=ql & qr <=qw & qr <=qri
   fprintf('\nRayleigh distribution passes the chi-square test.\n');
   fprintf('Chi-Square value=%6.5f\n',qr)
end

if ql <=qr & ql <=qw & ql <=qri
   fprintf('\nLognormal distribution passes the chi-square test.\n');
   fprintf('Chi-Square value=%6.5f\n',ql)
end

if qw <=ql & qw <=qr & qw <=qri
   fprintf('\nWeibull distribution passes the chi-square test.\n');
   fprintf('Chi-Square value=%6.5f\n',qw)
end

if qri <=ql & qri <=qw & qri <=qr
   fprintf('\nRice distribution passes the chi-square test.\n');
   fprintf('Chi-Square value=%6.5f\n',qri)
end
```

D.3 The BASIC Control Program

```
10    ! This program, called fastcw2.5, will take CW measurements of
20    ! S21 and write them to memory (size of array to be determined)
```

```
30    ! in less than 1 ms. (milli-second),
40    ! See FASTCW_NOTE for the original program.
50    !
60    ! ASSIGNMENTS
70    !
80    OPTION BASE 0
90    !
100   ASSIGN @Na1 TO 716;FORMAT ON      ! ASCII transfers to 8510
110   ASSIGN @Na2 TO 716;FORMAT OFF     ! Binary transfers to 8510
120   !
130   INTEGER Points
140   !
150   Points=2500
160   !
170   ! You must change both this variable and all the arrays if you
180   ! want to change the number of measurement points.
190   !
200   ! Now, we have the number of points and we are ready for action.
210   !
220   INTEGER Fast_data(2500,0:2)       ! Fast data collection array
230   REAL Data_16bit(2500,0:1)         ! 16 bit data array
240   REAL Magnitude(2500)              ! Magnitude array
250   REAL Phase(2500)                  ! Phase array
260   REAL Exp_tbl(0:255)               ! Exponential table array.
270   INTEGER Fast_correction(1,0:2)
280   REAL Correct_16bit(1,0:1)
290   REAL Correct_mag(1)
300   REAL Correct_phase(1)
310   !
312   GOSUB Calibrate_data
```

```
312   PAUSE
315   !
320   GOSUB Start_measure
330   ! Now we start with the program interface.
340   !
490 Start_measure:  !
500   !
510   ! This routine performs the actual measurement process.  Note
520   ! that it merely calls many other routines.
530   !
540   ABORT 7  ! Ceases HP-IB activity. Causes computer to assume control.
550   CLEAR 7  ! Allows the controller to put devices in dependent state.
560   !
570   GOSUB Clear_scrn      ! Clear the screen before beginning.
580   GOSUB Init_nwa        ! Initialize the 8510B
590   GOSUB Setup_nwa       ! Set up the 8510B
600   !
610   ! Ready for data acquisition and waiting for interrupt service.
620   GOSUB Interrupt
630   !
640   RETURN
650   !
660   ! Interrupt service begins here.
670   !
680 Interrupt:  !
690   Gpio=12               ! Select Gpio code
700   CONTROL Gpio;1        ! Reset Interface
710   !
720   ENABLE INTR Gpio
730   !
```

```
740   ON INTR Gpio GOSUB Gpio_serv   ! Check the state of EIR line for
750                          ! interrupt service: low for interrupt and
760                          ! high for waiting
761   BEEP
770   PRINT "Waiting for the interrupt signal"
780   ENABLE INTR Gpio;1  ! Enable EIR-type only
790   !
800   ! Show concurrent processing.
810   !
820   KEY LABELS PEN 5
830   !
840 Loop:  !
850   ON KEY 1 LABEL "Start      Measure" GOSUB Start_measure
860   ON KEY 2 LABEL "End        Program" GOSUB End_program
870   ON KEY 3 LABEL "Plot       Mag" GOSUB Plot_magnitude
880   ON KEY 4 LABEL "Plot       Phase" GOSUB Plot_phase
890   ON KEY 5 LABEL "Clear      Screen" GOSUB Clear_scrn
900   ON KEY 6 LABEL "Save to    Disk" GOSUB Save_data
910   ON KEY 7 LABEL "CAL.       Analyzer" GOSUB Calibrate_data
920   GOTO Loop
930   !
940   RETURN
950   !
960   !
970 Gpio_serv:  !
971   !
980   PRINT "Begin the data acquisition"
990   GOSUB Trigger_nwa ! Trigger the device. one measurement will be
1000  ! taken every time a falling edge is received on the TTL input
1010  ! at the back of 8510B
```

```
1020  GOSUB Enter_nwa       ! Get the data from the 8510B
1030  GOSUB Stop_data_acq   ! Stop the acquisition of data
1040  GOSUB Convert_data    ! Convert the data to 16 bit format
1050  GOSUB Compute_mag     ! compute the magnitude of the data
1060  GOSUB Compute_phase   ! compute the phase of the data (in DEG)
1070  !
1080  BEEP
1090  !
1100  PRINT "Data acquisition done"
1101  !
1100  RETURN
1120  !
1130 Init_nwa:  !
1140  !
1150  ! This subroutine initializes the network analyzer
1160  !
1170  OUTPUT @Na1;"PRES;"  ! Sends the "PRESET" command"
1180  WAIT 3               ! Waits for 3 seconds
1190  !
1200  RETURN
1210  !
1220 Setup_nwa:  !
1230  !
1240  ! This subroutine sets up the network analyzer (center freq, etc.)
1250  !
1260  OUTPUT @Na1;"POIN51;"          ! Sets the buffer size to 51 points
1270  OUTPUT @Na1;"S21; CENT 14 GHZ;"     ! S21, Center @ 14 GHz
1280  WAIT 3                              ! Wait for 3 seconds
1290  OUTPUT @Na1;"POWE 0"                ! Output power is 0 dBm
1300  OUTPUT @Na1;"FASC;"                 ! Enter "fastcw" mode
```

```
1310  !
1320  RETURN
1330  !
1340 Trigger_nwa: !
1450  !
1360  ! This subroutine provides the HP-IB trigger for data transfer
1370  !
1380  REPEAT          ! Loop until the 8510B is ready
1390  WAIT .01        ! Wait 10 ms
1400  UNTIL BIT(SPOLL(716),2)
1410  TRIGGER @Na1    ! Trigger the analyzer
1420  !
1430  RETURN
1440  !
1450 Enter_nwa: !
1460  !
1470  ! This routine tells the 8510B to send a data point upon
1480  ! external trigger.
1490  ENTER @Na2;Fast_data(*)      ! Puts binary data in the array
1500  !
1510  RETURN
1520  !
1530 Stop_data_acq: !
1540  !
1550  ! This routine stops the acquisition of data from the 8510
1560  !
1570  OUTPUT @Na1;"HOLD; SINP;" ! Hold the 8510B when acquisition is done.
1580  !
1590  RETURN
1600  !
```

```
1610  !
1620 Convert_data: !
1630  !
1640  ! This subroutine calls "Build_table" and converts the binary
1650  ! data to workable 16 bit data
1660  !
1670  GOSUB Build_table
1680  !
1690  INTEGER I      ! This is a local variable, I believe
1700  REAL Exp       ! Same deal here.
1710  !
1720  FOR I=0 TO Points
1730       Exp=Exp_tbl(BINAND(Fast_data(I,2),255))
1740       Data_16bit(I,1)=Fast_data(I,1)*Exp
1750       Data_16bit(I,0)=Fast_data(I,0)*Exp
1760  NEXT I
1770  !
1780  RETURN
1790  !
1800 Build_table: !
1810  !
1820  ! This routine builds the table of results need for converting
1830  ! data.
1840  Exp_tbl(0)=2^(-15)
1850  !
1860  FOR I=0 TO 126
1870       Exp_tbl(I+1)=2*Exp_tbl(I)
1880  NEXT I
1890  !
1900  Exp_tbl(128)=2^(-143)
```

```
1910  !
1920  FOR I=128 TO 254
1930       Exp_tbl(I+1)=2*Exp_tbl(I)
1940  NEXT I
1950  !
1960  RETURN
1970  !
1980 Compute_mag: !
1990  !
2000  ! This routine computes the magnitude of the data
2010  !
2020  FOR I=1 TO Points
2030       Magnitude(I)=20*LGT(SQR((Data_16bit(I,0))^2+(Data_16bit(I,1))^2))
           +ABS(Correct_mag(1))
2040       PRINT Magnitude(I)      ! Just a precautionary measure.
2050  NEXT I
2060  !
2070  RETURN
2080  !
2090 Compute_phase: !
2100  !
2110  ! This routine computes the phase of the data
2120  !
2130  DEG            ! This sets the default mode to Degrees.
2140  !
2150  FOR I=1 TO Points
2160   IF Correct_phase(1)<0 THEN
2170    Phase(I)=ARG(CMPLX(Data_16bit(I,1),Data_16bit(I,0)))
                 -ABS(Correct_phase(1))
2180   ELSE
```

```
2190    Phase(I)=ARG(CMPLX(Data_16bit(I,1),Data_16bit(I,0)))
                +ABS(Correct_phase(1))
2200   END IF
2210    PRINT Phase(I)      ! Just another precaution.
2220  NEXT I
2230  !
2240  RETURN
2250  !
2260 Plot_magnitude: !
2270  !
2280  ! This routine plots the magnitude response of the data
2290  !
2300  PLOTTER IS CRT,"INTERNAL"    ! Sets the plotter to crt
2310  GRAPHICS ON                  ! Turn on screen graphics
2320  GOSUB Clear_scrn             ! Clear the screen
2330  !
2340  CSIZE 3.5                    ! Set aspect ratio to 3.5
2350  !
2360  ! Now I will call for an axis.
2370  !
2380  GOSUB Draw_axis
2390  !
2400  PEN 2                        ! Red pen for magnitude data
2410  !
2420  MOVE 10,95                   ! Move to 10,95
2430  LABEL TIME$(TIMEDATE);"     ";DATE$(TIMEDATE)! Plot date and time
2440  LABEL "Magnitude in dB vs. Points"
2450  !
2460  ! These lines actually plot the data.  Note that it is normalized
2470  ! in the x axis by Points/100 as my screen is 100 X 100.  Note it
```

```
2480  ! is also offset by 50 to put 0 dB at the middle of the screen
2490  !
2500  FOR I=1 TO Points
2510       IF I=1 THEN
2520            MOVE (I/(Points/100)),(Magnitude(I)+50)
2530       ELSE
2540            DRAW (I/(Points/100)),(Magnitude(I)+50)
2550       END IF
2560  NEXT I
2570  !
2580  RETURN
2590  !
2600 Plot_phase: !
2610  !
2620  ! This routine will plot the phase.  Note that magnitude is
2630  ! already computed so it will only have to normalize the data.
2640  !
2650  PLOTTER IS CRT,"INTERNAL"     ! Plotter is internal crt
2660  GRAPHICS ON                   ! Turn on screen graphics
2670  GOSUB Clear_scrn              ! Clear the screen
2680  !
2690  CSIZE 3.5                     ! Set the aspect ration to 3.5
2700  !
2710  ! Now draw the axis.
2720  !
2730  GOSUB Draw_axis
2740  !
2750  PEN 14
2760  !
2770  MOVE 10,95                    ! Move to 10,95
```

```
2780  LABEL TIME$(TIMEDATE);"     ";DATE$(TIMEDATE) ! Plot date and time
2790  LABEL "Phase in Degrees vs. Points"
2800  !
2810  ! This data will be normalized by 3.6 in y - axis and by
2820  ! Points/100 in x direction.  Note it still has + 50 offset, so 0
2830  ! degrees is at the center of the screen with 180 degrees at the edge.
2840  !
2850  FOR J=1 TO Points
2860       IF J=1 THEN
2870            MOVE (J/(Points/100)),((Phase(J)/3.6)+50)
2880       ELSE
2890            DRAW (J/(Points/100)),((Phase(J)/3.6)+50)
2900       END IF
2910  NEXT J
2920  !
2930  RETURN
2940  !
2950 Draw_axis: !
2960  !
2970  ! This routine draws a 10x10 grid in an area 100x100
2980  !
2990  VIEWPORT 10,110,20,90
3000  WINDOW 0,100,0,100
3010  PEN White                ! I want a white grid.
3020  GRID 10,10               ! 10x10 grid
3030  !
3040  RETURN
3050  !
3060 Save_data: !
3070  !
```

```
3080  ! This routine saves the buffered data to a file on disk.
3090  ! NOTE:  File must exist (empty) before program will run correctly.
3100  !
3110  GOSUB Clear_scrn
3120  !
3130  INPUT "What would you like the data file to be called (small
name)",Name$
3140  !
3150  CREATE ASCII Name$,128
3160  ASSIGN @Output TO Name$;FORMAT ON
3170  !
3180  OUTPUT @Output;Data_16bit(*),END
3190  !
3200  RETURN
3210  !
3220 Clear_scrn: !
3230  !
3240  GCLEAR              ! Clear the graphics screen
3250  PRINT USING "@"     ! Clear the text screen
3260  !
3270  RETURN
3280  !
3290 Calibrate_data: !
3300  !
3310  ! This routine will get one data point whose magnitude and phase will
3320  ! be used to perform the correction that is normally done by the 8510B
3330  ! before displaying the results.  Unfortunately, we get the data well
3340  ! before it is displayed, so it's uncorrected.  This measurement
3350  ! should be taken with just a through before any others are taken.
3360  !
```

```
3370  !
3380  DEG                          ! Put this subroutine is degree mode
3390  !
3400  Point=1
3410  GOSUB Init_nwa
3420  GOSUB Setup_nwa
3430  GOSUB Trigger_nwa
3440  !
3450  ! Now I might as well right my own routines for this, as I can't
3460  ! see and easy way to modify the existing ones.
3470  !
3480  ENTER @Na2;Fast_correction(*)
3490  !
3500  ! Now I will stop the one point of data acquisition.
3510  !
3520  OUTPUT @Na1;"HOLD; SINP;" ! Hold the 8510B when acquisition is complete
3530  !
3540  GOSUB Convert_correct
3550  !
3560  ! Now, I compute the magnitude and the phase of the correction
3570  ! data point in one move.
3580  !
3590  FOR I=1 TO Point
3600  Correct_mag(I)=20*LGT(SQR((Correct_16bit(I,0))^2+(Correct_16bit(I,1))^2))
3610  Correct_phase(I)=ARG(CMPLX(Correct_16bit(I,1),Correct_16bit(I,0)))
3620  !If you want to correct the data later, set them to zero.
3630   PRINT Correct_mag(I)
3640   PRINT Correct_phase(I)
3650  !
3660  NEXT I
```

```
3670  !
3680  RETURN
3690  !
3700 Convert_correct: !
3710  !
3720  ! This routine converts the binary data to 16 bit data for the
3730  ! correction.
3740  GOSUB Build_table
3750  !
3760  INTEGER K
3770  REAL Exp_cor
3780  !
3790  FOR K=1 TO Point
3800        Exp_cor=Exp_tbl(BINAND(Fast_correction(K,2),255))
3810        Correct_16bit(K,1)=Fast_correction(K,1)*Exp_cor
3820        Correct_16bit(K,0)=Fast_correction(K,0)*Exp_cor
3830  NEXT K
3840  !
3850  RETURN
3860  !
3870 End_program: !
3880  !
3890  END
```